UNIVERSIDAD DE MURCIA

FACULTAD DE MEDICINA

Influence of Aberrations on Binocular Vision by means of Adaptive Optics Instruments

Influencia de las Aberraciones en Visión Binocular Mediante el uso de Sistemas de Óptica Adaptativa

Dª. Christina Schwarz

2013

Universidad de Murcia

Departamento de Física

Laboratorio de Óptica

INFLUENCE OF ABERRATIONS ON BINOCULAR VISION BY MEANS OF ADAPTIVE OPTICS INSTRUMENTS

INFLUENCIA DE LAS ABERRACIONES EN VISIÓN BINOCULAR MEDIANTE EL USO DE SISTEMAS DE ÓPTICA ADAPTATIVA

Thesis presented at the Faculty of Medicine
of the University of Murcia by:

Christina Schwarz

To attain the degree of PhD from the University of Murcia.

Laboratorio de Óptica. Departamento de Física. Universidad de Murcia.
October 2013

Don Pablo Artal Soriano, Catedrático de Universidad del Área de Óptica en el Departamento de Física, AUTORIZA:

La presentación de la tesis doctoral titulada "**INFLUENCIA DE LAS ABERRACIONES EN VISIÓN BINOCULAR MEDIANTE EL USO DE SISTEMAS DE ÓPTICA ADAPTATIVA**", realizada por D^{a}. Christina Schwarz bajo mi inmediata dirección y supervisión, en el Departamento de Física, y que presenta para la obtención del grado de Doctor por la Universidad de Murcia.

Murcia, 15 de Octubre de 2013

Resumen

Las aberraciones ópticas del ojo limitan la calidad de la visión. Durante los últimos 20 años, se han desarrollado instrumentos basados en tecnología de óptica adaptativa que permiten su medida y corrección (Liang *et al.*, 1994, 1997; Prieto *et al.*, 2000). Después de dos décadas de desarrollo ininterrumpido, en la actualidad los sistemas de óptica adaptativa están disponibles para aplicaciones oftálmicas de laboratorio. En particular, estos instrumentos han permitido allanar el camino para entender cómo afectan las aberraciones a la calidad de la visión (Liang & Williams, 1997; Yoon & Williams, 2002; Artal *et al.*, 2004, 2010).

Hasta el momento, estos estudios se han llevado a cabo de manera monocular. Sin embargo, en condiciones naturales de visión percibimos el mundo a través de los dos ojos. Más aún, la visión binocular es superior a la visión monocular en muchos aspectos. Entre ellos, las ventajas más importantes son la sumación binocular (Campbell & Green, 1965*a*; Cagenello *et al.*, 1993), es decir, la mayor calidad visual en condiciones binoculares en comparación con las monoculares, y la estereopsis (Wheatstone, 1838), que es la manera binocular de percibir profundidad basada en la disparidad de las imágenes retinianas. Para ambos fenómenos, la combinación de las dos imágenes a través de los dos canales monoculares juega un papel esencial, que aún no se conoce en profundidad. No obstante, hay evidencias de que tanto la sumación binocular como la estereopsis pueden depender de diversos factores ópticos (Pardhan & Gilchrist, 1990; Jiménez *et al.*, 2008; Castro *et al.*, 2009).

Recientemente se han desarrollado los primeros prototipos de simuladores visuales de óptica adaptativa binocular (Fernández *et al.*, 2009*a*, 2010). Estos instrumentos posibilitan la simulación visual bajo condiciones binoculares, es decir, permiten medir y manipular las aberraciones de ambos ojos de manera independiente mientras el sujeto realiza pruebas visuales. Estos prototipos pueden servir por un lado para la investigación básica, y por otro, para realizar evaluaciones antes de someter al ojo a cirugías refractivas o de cataratas. Con la ayuda de las versiones binoculares, es posible en la actualidad investigar el impacto de las aberraciones en la visión binocular. Además, estos dispositivos permiten la evaluación, no invasiva, de diferentes tipos de corrección de presbicia.

Objetivos

En este trabajo se pretende investigar diferentes aspectos de la visión binocular, bajo condiciones de laboratorio cuidadosamente controladas mediante el uso de un instrumento de óptica adaptativa. Los objetivos específicos, expresados brevemente, son:

- El desarrollo y montaje de una nueva versión de un simulador visual binocular de óptica adaptativa que permita el control completo de la amplitud y de la fase de la función compleja de pupila de cada ojo, así como la adaptación del instrumento para satisfacer los requisitos particulares de los experimentos con sujetos reales.

- La reevaluación de los modelos existentes de sumación binocular, a partir de la investigación del efecto de diversos factores ópticos en el rendimiento de la visión binocular. En concreto, se investigarán las aberraciones, la calidad óptica retiniana, las condiciones de luminancia y las diferencias de estos factores entre los dos ojos.

- La simulación visual de soluciones binoculares para la presbicia, junto con la evaluación no invasiva de su potencial y de sus limitaciones en medidas con sujetos reales, y por lo tanto, la demonstración de que el simulador visual de óptica adaptativa binocular sirve de instrumento de análisis previo para evaluar métodos de corrección visual binocular.

Métodos

El instrumento de óptica adaptativa desarrollado en este trabajo permite la ejecución de pruebas visuales bajo condiciones binoculares, al mismo tiempo que las aberraciones ópticas de ambos ojos son medidas y manipuladas. De este modo, el sistema es capaz de hacer una simulación visual binocular, por lo que en lo sucesivo se referirá como *simulador visual binocular de óptica adaptativa*. Una propiedad especial del aparato es la capacidad para controlar de manera completa las dos funciones de pupila complejas. Para asegurar la relativa sencillez en la construcción y el manejo del sistema, se empleó un sensor binocular de Hartmann-Shack y el instrumento se diseñó en base a dispositivos de cristal líquido, con el fin de poder modular, de manera independiente, las funciones de amplitud y de fase de ambos ojos. Todos estos componentes son operados en modo binocular. Para ello, un periscopio reúne los dos caminos ópticos (uno para cada ojo) en el sistema.

Las aberraciones se miden tras iluminar los ojos con luz procedente de un diodo láser que emite en 780 nm. La luz reflejada en el fondo de cada ojo entra al sistema por el periscopio. Un primer telescopio conjuga los planos de pupila del sujeto con el plano del modulador espacial de luz de cristal líquido sobre silicio (Pluto-VIS, Holoeye, Berlín, Alemania). Éste dispositivo, que opera en reflexión y contiene 1920 x 1080 pixeles de un tamaño de 8 µm, modula únicamente la fase, de forma que permite manipular las aberraciones de ambos ojos. El dispositivo fue calibrado para inducir un desfase de 2π para una longitud de onda de 543 nm y está implementado en el instrumento de tal manera que permite utilizar pupilas de hasta 7.5 mm de diámetro. En el caso de pupilas de 4 mm, cada una es controlada por más de 195000 píxeles independientes. Un

segundo telescopio, situado entre el modulador y el sensor, con aumento de 0.5, conjuga los dos planos de pupila guiando la luz por un espejo plegable. El sensor de Hartmann-Shack emplea una matriz de microlentes de 200 µm de abertura y 6 mm de focal y una cámara con alta sensibilidad en el rango cercano al infrarrojo (C5999, Hamamatsu Photonics, Hamamatsu, Japón). De esta forma resuelve las dos pupilas espacialmente, una al lado de la otra, y muestrea una pupila de 4 mm de diámetro con aproximadamente 80 microlentes.

Para realizar tests visuales, el sujeto ve el estímulo, presentado en un micromonitor proyectado al infinito, a través del sistema. Las pupilas de entrada se generan con un modulador espacial de luz (LC2002, Holoeye, Berlín, Alemania) operando en transmisión y modulando únicamente la intensidad. El dispositivo tiene 800 x 600 píxeles y ocupa un área activa de 26.6 mm x 20 mm. Una vez implementada en el simulador visual, una pupila de 4 mm se muestrea aproximadamente por 12000 píxeles individuales. La generación de pupilas con un modulador espacial presenta ventajas en cuanto a comodidad y precisión durante el centrado y, sobre todo, permite la creación de pupilas con gradientes de intensidad. Un telescopio sin aumentos conjuga el plano del modulador de intensidad con el plano del modulador de fase y, por lo tanto, con los planos de pupila del ojo del sujeto. Se utilizaron varios tests visuales empleando el método del ajuste o el de estímulos constantes. En este trabajo se usa el test de la *letra E*, el de las *letras Sloan* y el test de sensibilidad al contraste basado en *estímulos de Gabor*. Para realizar el alineamiento de los ojos del sujeto con las pupilas de entrada del sistema, se utilizó una cámara auxiliar de pupila con una alta sensibilidad en el rango del infrarrojo (Manta G-145 NIR, Allied Vision Technologies GmbH, Stadtroda, Alemania), ya que la iluminación de LEDs está centrada en torno a 850 nm.

Previo a la realización de los diversos experimentos se realizaron protocolos de calibración que incluyen el alineamiento preciso de las pupilas en planos conjugados, el calibrado del contraste a través del sistema para los micromonitores empleados, y las adaptaciones del sistema necesarias para usar el instrumento en luz policromática.

Resultados

<u>Rendimiento visual binocular con desenfoque y aberración esférica inducidos unilateralmente o bilateralmente</u>

Bajo condiciones normales de visión, el rendimiento binocular supera ligeramente al monocular. No obstante, la sumación binocular no es una medida fija, puesto que su magnitud depende de numerosos factores. Según estudios previos, el cociente de sumación binocular aumenta cuando se induce desenfoque de manera bilateral; pero su comportamiento difiere si se induce desenfoque unilateralmente, en cuyo caso el cociente experimenta una disminución al inicio seguida por un crecimiento, hasta alcanzar nuevamente unidad.

Este experimento estudió los efectos del desenfoque y de la aberración esférica (AE) sobre la visión binocular, en condiciones de laboratorio altamente controladas. Partiendo de la situación visual en la que la refracción y la AE natural están corregidas, se indujeron el desenfoque y la AE bilateralmente, es decir en ambos ojos y, a continuación, unilateralmente en el ojo no-dominante. Se midió la agudeza visual (AV) monocular en ambos ojos y la AV binocular para un cierto rango de desenfoques y valores de AE, con pupilas limitadas a 4 mm y acomodación paralizada. A continuación, se dedujo el cociente de sumación binocular y la diferencia entre ambos ojos del rendimiento visual para cada condición óptica.

Aunque el desenfoque y la AE tienen en común un perfil de fase con simetría de rotación, se pueden observar diferencias esenciales entre sus efectos sobre la AV binocular y sobre la sumación binocular cuando se inducen bilateralmente. En cuanto al desenfoque inducido, la AV binocular disminuye de una manera parecida a la AV monocular. El cociente de sumación binocular parte de un valor próximo a 1 para la situación de referencia (refracción y AE natural corregidas), disminuye para 0.5 y 1 D de desenfoque, y recupera valores superando la cantidad inicial cuando se generan desenfoques más altos. En cambio, para la AE inducida bilateralmente, la AV binocular disminuye con la mitad de la pendiente que muestra la curva monocular. Por lo tanto, la AE bilateral claramente beneficia a la sumación binocular. Para aberraciones inducidas unilateralmente, la AV binocular tiende a ser ligeramente peor que la AV monocular. Como consecuencia de ello, los cocientes de sumación binocular descienden exponencialmente cuando la diferencia del rendimiento visual en presencia de aberraciones aumenta entre ambos ojos.

<u>Agudeza visual binocular con corrección combinada de aberración esférica y aberración cromática longitudinal</u>

El ojo humano está afectado tanto por las aberraciones monocromáticas como por las aberraciones cromáticas. Su corrección produce, generalmente, una mejora del rendimiento visual monocular. El objetivo de este estudio consistió en investigar el efecto de la corrección combinada de la AE y de la aberración cromática longitudinal (ACL) en visión binocular, así como la estimación del beneficio de una corrección bilateral. La aplicación práctica de este estudio consistió en determinar los beneficios potenciales de estos tipos de corrección en pacientes operados de cataratas e implantados con lentes intraoculares correctoras de AE y ACL. Utilizando el sistema binocular de óptica adaptativa, se indujo y se corrigió la AE promedio de ojos pseudofáquicos implantados con lentes intraoculares esféricas, al tiempo que se eliminó el efecto de la ACL llevando a cabo las medidas en condiciones de luz cuasi-monocromáticas, y se compararon con las condiciones policromáticas. La AV a bajo contraste binocular y monocular del ojo dominante se midieron en cuatro condiciones de aberraciones: 1) AE y ACL presente;

2) AE presente y ACL corregida; 3) AE corregida y ACL presente; y 4) AE y ACL corregidas.

El experimento demostró que la AV mejora cuando se corrigen estas aberraciones. Tanto para medidas binoculares como para medidas monoculares, la agudeza visual más alta se obtiene cuando la AE y la ACL se corrigen conjuntamente. Para todos los niveles de corrección, la AV binocular promediada entre sujetos resulta superior a la AV monocular. Sin embargo, la sumación binocular depende de las condiciones ópticas, y disminuye al aumentar el nivel de corrección de aberraciones.

Profundidad de foco binocular con coma inducido a diferentes orientaciones

Existen lentes intraoculares que extienden la profundidad de foco monocular gracias a perfiles de fase añadidos a la fase refractiva. Aparte de la AE de cuarto y sexto orden, el coma también podría ser una aberración adecuada para esta finalidad. En este estudio se investigó la posible influencia del coma inducido en diferentes orientaciones sobre la AV y la profundidad de foco monocular y binocular.

Para ello, se midió la AV en función del desenfoque para una serie de condiciones. Las condiciones monoculares incluían los casos de 1) aberraciones de alto orden no modificados; 2) coma natural corregido; y 3) el coma inducido en 8 orientaciones diferentes, es decir, a 0°, 45°, 90°, 135°, 180°, 225°, 270°, y 315°, sobre una pupila de 4.8 mm. Las condiciones binoculares comprendían los casos en que: 1) aberraciones no habían sido modificadas en ningún ojo; 2) el coma natural había sido corregido en ambos ojos; y 3) el coma vertical positivo había sido inducido en un ojo y el mismo valor pero con diferentes orientaciones en el otro ojo. Aunque se generaron aberraciones sobre una pupila mayor, la pupila artificial efectiva quedó limitada a 3.5 mm de diámetro, lo que produjo una pupila recortada, generando coma superpuesto con desplazamiento. A partir de las AVs medidas para varios desenfoques, se derivó la profundidad de foco fijando un umbral de AV mínima de 0.8.

El estudio demuestra que el coma negativo y positivo inducido en dirección vertical aumenta la profundidad de foco monocular. En promedio, se logró la extensión de la profundidad de foco en 0.4 D. A pesar de generar disparidad retiniana, la magnitud está dentro del área de Panum, y por tanto, todos los sujetos fusionaron las imágenes sin excepción, mejorándose de igual manera las profundidades de foco monocular y binocular. Sin embargo, la disparidad afecta al cociente de sumación binocular. Al añadir desenfoque, la disparidad entre imágenes retinianas aumenta y el cociente de sumación binocular disminuye. Como consecuencia, la orientación relativa del coma entre los dos ojos debe ser controlada cuidadosamente, puesto que puede causar magnitudes de disparidad que afecten a la visión binocular.

Rendimiento visual binocular con corrección de aberraciones mediante óptica adaptativa en función del nivel de luminancia

La AV disminuye en condiciones de baja luminancia. Por un parte, el rendimiento neuronal de la retina decrece, y por otra, los diámetros de pupila, y con ello, las aberraciones, aumentan bajo luminancias reducidas. Estudios anteriores encontraron que el beneficio visual asociado a corregir las aberraciones con óptica adaptativa (OA), para un tamaño de pupila, aumenta con niveles de luz inferiores.

Con la intención de entender la visión binocular para tamaños de pupila adaptados a la luz ambiental, se investigaron la AV binocular y monocular y la sensibilidad al contraste binocular con y sin corrección de OA en distintos niveles de luminancia. Además, se dedujeron e interpretaron los beneficios de la corrección de las aberraciones y la sumación binocular.

De manera similar a la situación en visión monocular, tanto la AV como la sensibilidad al contraste disminuyen con menores niveles de luz. El rendimiento binocular mejora comparado con el rendimiento monocular, y los rendimientos (monocular y binocular) mejoran con las aberraciones corregidas comparados con los rendimientos sin corrección de OA. Los cocientes entre AV o sensibilidad al contraste con corrección de OA y sin corrección de OA aumentan ambas de 1.2 en la condición de la luminancia más alta a 1.5 para la condición de luminancia más baja. A pesar de que el cociente de sumación binocular promediado entre sujetos no varía significativamente con la luminancia, para dos de los sujetos existe un claro comportamiento lineal entre sumación binocular y AV monocular. Se podría sugerir la hipótesis de que tal relación se debe a la activación de un número mayor de neuronas responsables de una visión bajo ciertas condiciones.

Cambios refractivos a baja luminancia en visión monocular y binocular

En la transición del rango fotópico al rango escotópico de luminancias, el ojo muestra una tendencia hacia la miopización. Habiendo encontrado que la visión binocular se beneficia especialmente en condiciones de baja luminancia, el propósito de este estudio fue la detección de una posible diferencia en el desplazamiento miópico del mejor foco a luminancias más bajas entre visión binocular y visión monocular, así como el efecto de la AE sobre ello.

Los observadores ajustaron el mejor foco para estímulos con diferentes luminancias en visión monocular y binocular. En este experimento no se limitó el tamaño de las pupilas para que pudieran ajustarse a la luminancia del estímulo, y se permitió la acomodación natural. Las medidas se realizaron bajo diferentes condiciones de aberración, en concreto: 1) con aberraciones naturales; 2) con la AE natural corregida; y 3)-5) con AE inducida de 0.3, 0.6 y 0.9 µm sobre pupilas de 7 mm de diámetro.

Para bajas luminancias, se encontró un leve, aunque significativo, desplazamiento miópico del mejor foco tanto en visión monocular como en visión binocular. Debido a su moderada magnitud, este desplazamiento puede ser explicado enteramente por el efecto de Purkinje en combinación con la ACL del ojo humano. Al inducir AE, el desplazamiento relativo del mejor foco aumenta, probablemente a causa de la extensión de la profundidad del foco.

Simulación visual de un implante corneal de abertura pequeña

Una opción de corrección de la presbicia son los implantes corneales de pequeñas aberturas que extienden la profundidad de foco del ojo en el que se implanta. Su diámetro interior mide 1.6 mm, mientras que su diámetro exterior es de 3.8 mm por razones cosméticas y para permitir imágenes del fondo del ojo en caso de necesidad. Aunque los estudios clínicos muestran la eficacia del implante, existen limitaciones que deben ser mejor evaluadas. Las simulaciones por ordenador de la calidad óptica en ojos modelos pueden predecir resultados monoculares, pero debe determinarse cómo se comporta el sistema visual binocular bajo estas condiciones, considerando los diámetros de pupila y las iluminancias retinianas desiguales. Con ayuda del simulador visual binocular se pueden llevar a cabo estudios que aporten esta información, los cuales deben entenderse como complementarios a los estudios clínicos.

En este experimento se estudiaron varios aspectos del implante corneal. En primer lugar, se midió el efecto de la pupila anular que genera el implante corneal en combinación con una pupila natural de mayor tamaño, que sobrepasa al diámetro exterior del implante. En segundo lugar, se comprobó el centrado más favorable en relación a la AV de los sujetos. Por último, se midió la AV binocular en un rango de vergencias y se comparó con la monovisión.

Se encontró que la pupila anular mejora la AV para objetos cercanos con respecto a una pupila circular de 4 mm, mientras que la AV de lejos se reduce menos de una línea. Por otro lado, la AV lejana puede verse reducida por un centrado inadecuado del implante. Las mejores AVs se obtienen para un centrado de entre 0 y 0.5 mm nasal respecto del centro de la pupila. El valor exacto, sin embargo, depende del sujeto. En cuanto al rendimiento binocular con el implante, se pudo comprobar que en condiciones fotópicas el implante en combinación con micro-monovisión de 0.75 D es igual de efectivo que la monovisión tradicional de 1.25 D. No obstante, bajo condiciones mesópicas, las AVs binoculares dependen de cada individuo. Mientras para dos sujetos la monovisión de abertura pequeña extiende la profundidad de foco igual que la monovisión tradicional, para un tercer sujeto, el implante no resultó beneficioso en iluminación mesópica. Por tanto, los resultados sugieren la necesidad de realizar tests de visión en iluminación mesópica, antes de contemplar una cirugía.

Conclusiones

El objetivo de esta tesis ha sido desarrollar herramientas que faciliten una mejor comprensión de la influencia que tienen las aberraciones en la visión binocular. A continuación se resumen los resultados principales y las conclusiones de este trabajo:

1. Se diseñó y construyó un simulador visual binocular de óptica adaptativa capaz de controlar de manera precisa la función pupila compleja en ambos ojos simultáneamente. El sistema se basa en el uso de moduladores espaciales de cristal líquido, lo que permite una alta resolución en planos conjugados de pupila para manipular la amplitud y la fase de ambos ojos de manera independiente.

2. La aberración esférica tiene un impacto favorable en la sumación binocular. En cambio, si se corrige esta aberración, se reduce la sumación binocular.

3. Se simuló el beneficio visual al llevarse a cabo una implantación bilateral en pacientes pseudofáquicos con lentes intraoculares correctoras de aberración esférica y aberración cromática longitudinal. En el caso de la corrección combinada de aberración esférica y aberración cromática longitudinal, se puede esperar un aumento significativo de la agudeza visual binocular, aunque la mejora en condiciones binoculares resulta inferior a la obtenida bajo condiciones monoculares. Con la corrección de aberraciones la sumación binocular disminuye.

4. El coma tiene el potencial de extender la profundidad de foco tanto monocular como binocularmente, en gran parte, sin afectar a la agudeza visual en el mejor foco. Debido a la generación de disparidad retiniana, el efecto depende, sin embargo, de la orientación del coma. La mayor extensión de la profundidad de foco se obtiene si el coma está orientado verticalmente en la misma dirección en ambos ojos.

5. La corrección de aberraciones binoculares y la sumación binocular proporcionan una mayor ventaja en condiciones de baja luminancia. La sumación binocular parece estar correlacionada inversamente con la agudeza monocular alcanzada a esos niveles de iluminación y, por tanto, mitiga el rendimiento visual reducido.

6. La visión binocular incrementa la precisión subjetiva en la determinación del mejor foco en baja luminancia. Se encontró un pequeño, pero consistente, desplazamiento relativo miópico cuando se reduce la iluminación, que puede explicarse mediante el efecto Purkinje junto con la aberración cromática longitudinal del ojo humano. El desplazamiento aumenta si la aberración esférica está presente, probablemente debido a la extensión de la profundidad de foco en combinación con el error acomodativo.

7. La simulación de un implante corneal de abertura pequeña demuestra que en condiciones fotópicas aumenta la profundidad de foco con igual eficacia que la monovisión tradicional. Bajo condiciones de luz mesópicas, el rendimiento depende más del sujeto, lo que destaca la importancia de tener en cuenta la agudeza visual bajo estas condiciones de iluminación durante la selección de pacientes.

8. La evaluación de diversos procedimientos de corrección de presbicia muestran el potencial del simulador visual binocular de óptica adaptativa como instrumento de uso clínico. Se podría usar el aparato para encontrar la corrección visual óptima al tiempo que los pacientes podrían adquirir un rol activo en el proceso de tratamiento.

Índice

Resultados

Conclusiones

Table of contents

Results

List of abbreviations

AO	Adaptive optics
BS	Binocular summation
BSR	Binocular summation ratio
CS	Contrast sensitivity
D	Diopters
DE	Dominant eye
DM	Deformable mirror
DOF	Depth of focus
HOA	Higher-Order Aberrations
HSS	Hartmann-Shack sensor
IOD	Interocular difference
IOL	Intraocular lens
LASER	Light amplification by stimulated emission of radiation
LCA	Longitudinal chromatic aberration
LC	Liquid crystal
LCoS	Liquid crystal on silicon
LED	Light emitting diode
MAR	Minimum angle of resolution
MTF	Modulation transfer function
NDE	Non-dominant eye
OD	Oculus dexter, right eye
OLED	Organic light emitting diode
OS	Oculus sinister, left eye
OU	Oculus uterque, both eyes
PSF	Point Spread Function
RMS	Root Mean Square
rMTF	Radially averaged modulation transfer function
SA	Spherical Aberration
SLM	Spatial light modulator
VA	Visual acuity

Introduction

1 Introduction

In this chapter, the literature that has been published previously on relevant aspects of this research is reviewed. It starts with introducing the principle of adaptive optics (AO) and gives then an overview of the human eye. A detailed description is given of the binocular visual system and of properties which are special to binocular vision, followed by a review on how to study the relationship between visual stimuli and human response. The last section of this chapter presents the scientific justification of this thesis and outlines its organization.

1.1 Adaptive optics

The technique of adaptive optics (AO) was developed to overcome the blurring effects of atmospheric turbulence in astronomy for ground-based telescopes. Around twenty years ago, AO systems were adapted for ophthalmic applications, where the time dependent aberrations of the eye are the counterparts of turbulence in astronomy (Liang *et al.*, 1994). Today, AO constitutes a mature technique in vision research and ophthalmology with applications in fundus imaging, vision correction and visual simulation. This section presents a basic overview of the technique of AO with respect to applications for visual testing and simulation.

Wavefront aberrations and retinal image quality

A graphical explanation of the concept of wavefronts and aberrations (Born & Wolf, 1999) is presented in Figure 1.1. A wavefront is a plane of constant phase; in case of perfect optics, a point source emits a spherical wave indicated by the ideal wavefront. The wavefront aberration is the optical deviation of the wavefront from the ideal reference wavefront.

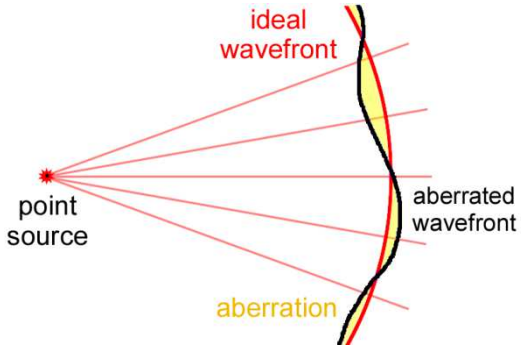

Figure 1.1: Ideal wavefront (red) emitted by a point source and an aberrated wavefront (black). Their optical path difference is referred to as an aberration.

The conventional way to describe ocular wavefront aberrations is the Zernike polynomials. Here, a brief introduction to the American National Standard is given (ANSI, 2010). The Zernike polynomials were first suggested by Frits Zernike in 1934 and constitute a complete, orthogonal set of functions defined over a unit circle (Zernike, 1934). Any wavefront aberration $W(\rho,\theta)$ of optical systems with circular pupils can therefore be expanded by the Zernike circle polynomials in the form

$$W(\rho,\theta)=\sum_{n=0}^{\infty}\sum_{m=-n}^{n} c_n^m Z_n^m(\rho,\theta)\ , \qquad \text{with } m=-n,\ -n+2,\ -n+4,\ \ldots,\ n\ ,$$

where $\rho=\frac{r}{a}$ is a radial variable normalized by the radius a of the pupil, θ is the radial angle, c_n^m are the expansion coefficients, and z_n^m the orthonormal polynomials. The Zernike polynomials up to fourth radial order are listed in Table 1.1 and in Figure 1.2 their corresponding wavefront maps are illustrated. While the zeroth and first radial orders have no relevance for aberrations in the eye, the second order corresponds to the refractive errors. Other terms with radial order higher than 2 are henceforth referred to as higher-order aberrations (HOA).

The Zernike polynomials are defined as

$$Z_n^m(\rho,\theta)=\begin{cases} N_n^m R_n^{|m|}(\rho)\cos(m\theta) & ;\ \text{for } m \geq 0 \\ -N_n^m R_n^{|m|}(\rho)\sin(m\theta) & ;\ \text{for } m < 0 \end{cases},$$

where $R_n^{|m|}(\rho)$ is the radial component given by

$$R_n^{|m|}(\rho)=\sum_{s=0}^{(n-|m|)/2}\frac{(-1)^s(n-s)!}{s!\left[(n+|m|)/2-s\right]!\left[(n-|m|)/2-s\right]!}\rho^{n-2s}\ ,$$

and N_n^m the normalization factor

$$N_n^m=\sqrt{\frac{2(n+1)}{1+\delta_{m0}}}\ .$$

The Kronecker delta function δ_{m0} yields 1 for $m=0$, and 0 otherwise.

Sometimes the Zernike coefficients and polynomials are given in the single indexing scheme. To convert from the double index m and n to the single index j and vice versa, the following relationships can be used:

$$j = \frac{n(n+1)}{2} + \frac{n+m}{2}$$

$$n = \text{roundup}\left[\frac{-3+\sqrt{9+8j}}{2}\right]$$

$$m = 2j - n(n+2).$$

n	m	Zernike polynomial	Aberration name
0	0	1	Piston
1	-1	$2\rho\sin(\theta)$	y-tilt
1	1	$2\rho\cos(\theta)$	x-tilt
2	-2	$\sqrt{6}\rho^2\sin(2\theta)$	y-astigmatism
2	0	$\sqrt{3}(2\rho^2-1)$	Defocus
2	2	$\sqrt{6}\rho^2\cos(2\theta)$	x-astigmatism
3	-3	$\sqrt{8}\rho^3\sin(3\theta)$	y-trefoil
3	-1	$\sqrt{8}(3\rho^3-2\rho)\sin\theta$	y-coma
3	1	$\sqrt{8}(3\rho^3-2\rho)\cos\theta$	x-coma
3	3	$\sqrt{8}\rho^3\cos(3\theta)$	x-trefoil
4	-4	$\sqrt{10}\rho^4\sin(4\theta)$	y-quadrafoil
4	-2	$\sqrt{10}(4\rho^4-3\rho^2)\sin(2\theta)$	y-secondary coma
4	0	$\sqrt{5}(6\rho^4-6\rho^2+1)$	spherical aberration
4	2	$\sqrt{10}(4\rho^4-3\rho^2)\cos(2\theta)$	x-secondary coma
4	4	$\sqrt{10}\rho^4\cos(4\theta)$	x-quadrafoil

Table 1.1: Orthonormal Zernike circle polynomials up to 5th order.

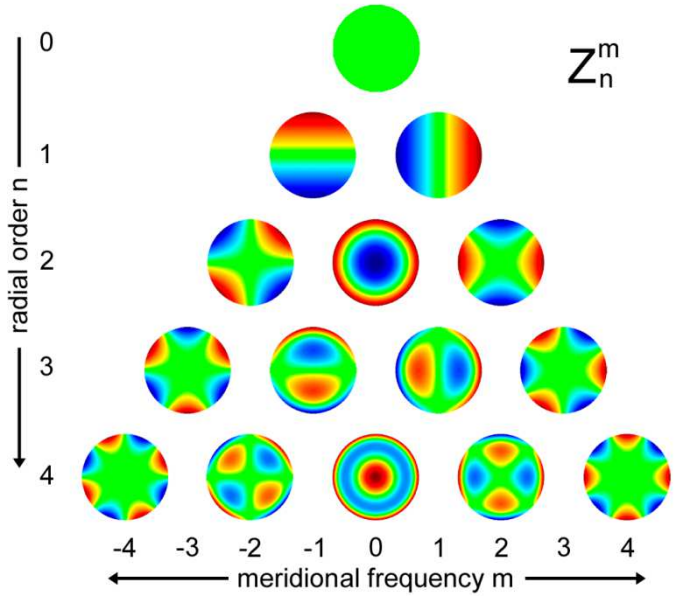

Figure 1.2: Height maps of the first fifteen Zernike polynomials.

To report the detrimental effect optical aberrations have on image quality, many different metrics describing the relationship between the optics of the eye and its visual performance are used (Guirao *et al.*, 2002*a*; Guirao & Williams, 2003; Cheng *et al.*, 2004).

A common pupil plane metric is the root-mean square (RMS) wavefront error. It is defined as the standard deviation of the wave aberration. In case the wave aberration is expressed on the basis of Zernike polynomials, the RMS can be described as

$$\mathrm{RMS} = \sqrt{\sum_{m,n} \left(c_n^m\right)^2} \quad .$$

Usually, only terms with $n \geq 2$ excluding the defocus term c_2^0 are used. To calculate the higher order aberration RMS (HOA-RMS), only terms with $n \geq 3$ are considered.

In order to obtain image plane metrics, it is necessary to make use of Fourier optics (Goodman, 2005). The generalized pupil function is given by

$$P(\rho,\theta) = P(\rho,\theta)\exp\left(-i\frac{2\pi}{\lambda}W(\rho,\theta)\right) \quad ,$$

where λ is the wavelength, $P(\rho,\theta)$ describes the pupil aperture, and $W(\rho,\theta)$ the wave aberration. The point spread function (PSF) is then calculated as

$$\mathrm{PSF}(\rho,\theta) = \left|\mathcal{FT}(P(\rho,\theta))\right|^2 \quad .$$

To simulate how a certain aberration affects the appearance of an object, the PSF can be convolved with an image of this object.

The most common image plane metric is the Strehl ratio. It is defined as the ratio between the maximum of an aberrated PSF and the maximum of a diffraction-limited PSF:

$$\text{Strehl ratio} = \frac{\max(\text{PSF}_{\text{aberrated}})}{\max(\text{PSF}_{\text{diffraction-limited}})} \ .$$

In particular, the Strehl ratio ranges between 1 and 0, where 1 means diffraction limited performance.

The modulation transfer function (MTF) describes the frequency response of a given optical system and is defined as the modulus of the optical transfer function (OTF). The OTF is in turn the Fourier transform of the PSF

$$\text{MTF} = \left|\text{OTF}\right| = \left|\mathcal{FT}(\text{PSF})\right| \ .$$

The MTF also takes values between 1 and 0. Therefore, an MTF of 1 means that no contrast is lost when imaging through the evaluated optical system. Here, we mostly make use of the radially averaged MTF (rMTF).

Adaptive optical systems

AO can be combined with optical systems in order to improve the performance in the presence of aberration fluctuations. Figure 1.3 shows a sketch of such a system. Its basic elements are a wavefront sensor, a wavefront modulator, and a control system addressing the two devices (Porter *et al.*, 2006).

The incoming ideal wavefront is distorted by an aberrating medium. The wavefront sensor detects the aberration. Upon detection, the control system computes the required correction and sends the information to the wavefront modulator. Finally, the wavefront modulator cancels out the aberration and in this way optimizes the performance of the optical system. The most common type of wavefront sensors in vision research and ophthalmology are Hartmann-Shack sensors (Porter *et al.*, 2006). Their principle will be explained in detail in the course of this section. Wavefront modulators can be divided into those that change their surface shape in order to alter the phase profile of the incoming light after reflection, and those that alter their refractive index to modify the optical path of the traversing light. The working principle of both types of wavefront modulator are explained and discussed below.

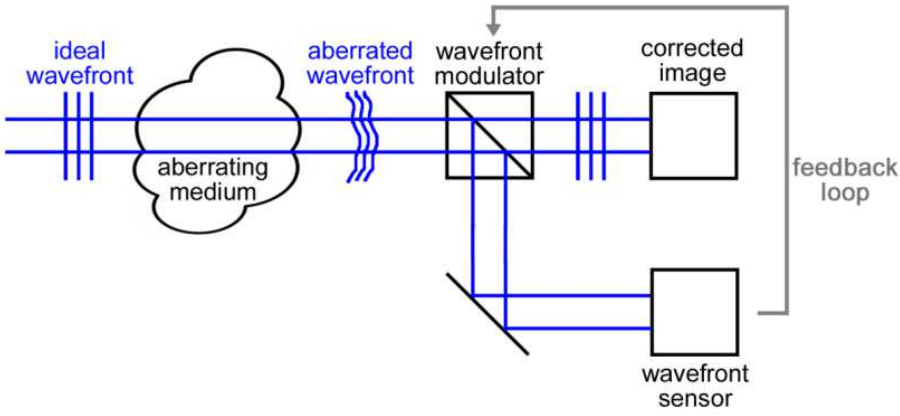

Figure 1.3: Schematic diagram of an adaptive optical system. The essential parts for an adaptive optics control system are the wavefront modulator, the wavefront sensor, and the intercommunicating feedback loop.

AO systems can be set up to operate in open-loop or in closed-loop. In open-loop control, the aberration is merely measured once and corrected once. In general, the wavefront sensor is then located between the aberrating medium and the wavefront modulator. For closed-loop control, aberration measurement and correction are performed repeatedly in a feedback loop. For this purpose, the wavefront sensor has to be located after the wavefront modulator in order to detect remaining aberrations.

Aberration measurements

The Hartmann-Shack sensor (HSS) originates from the Hartmann test, the first objective aberration test which was presented as early as 1900 (Hartmann, 1900). Hartmann divided a light ray in the exit pupil of an optical system into many sub-rays with the help of a mask which has precisely placed holes. By determining the slope of each sub-ray, he could infer the aberrations of the system. The initial design was improved by Shack (Shack & Platt, 1971) using a microlens array instead of a perforated mask. Some 20 years ago, the HSS was first applied to the human eye (Liang *et al.*, 1994). Due to the simple operating principle and easy handling, this sensor type has become very popular in the field of vision research. The device, together with an efficient algorithm, is able to measure the aberration of the whole eye in an objective manner (Prieto *et al.*, 2000).

Figure 1.4 graphically explains the principle of wavefront sensing with an HSS. A light source – usually a laser diode emitting light in the near-infrared range – illuminates the eye and the light is focused on the retina by the optics of the eye. Back-reflected light exits the pupil and falls upon a lenslet array which is located in a conjugate pupil plane. The lenslet array consists of several hundred microlenses with the same diameter and focal length. The wavefront of the eye is sampled by a set of lenses. In case of a perfect plane wavefront (illustrated in blue), every lens focuses the light onto the theoretical focal point on the optical axis. A CCD camera placed at one focal length from the

lenslet array records this spot pattern. In case the wavefront is distorted (illustrated in red), focal spots are formed at a location displaced from the optical axis of each microlens. The displacement $(\Delta x_i, \Delta y_i)$ of each spot from the optical axis of the associated microlens is related to the average slope of the sampled wavefront area in the following way:

$$\frac{(\Delta x_i, \Delta y_i)}{f} = \left(\frac{\partial W(x,y)_i}{\partial x}, \frac{\partial W(x,y)_i}{\partial y} \right) .$$

Taking into account the whole set of displacements, it is possible to reconstruct the wavefront aberration of the eye with a suitable algorithm.

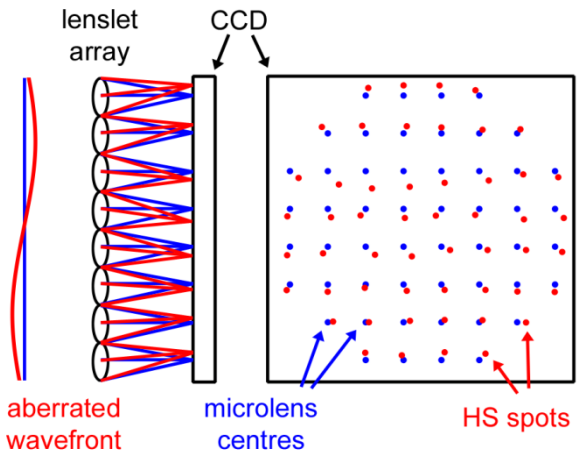

Figure 1.4: Principle of the Hartmann-Shack sensor. The incident wavefront is sampled by an array of microlenses. Using the displacements of the Hartmann-Shack (HS) spots from the respective lenslet centers on the CCD detector, the wavefront can be reconstructed.

Aberration modulation

Wavefront modulators are devices that are capable of altering the phase profile of light over a certain area by modifying the optical path length the light travels along (Porter *et al.*, 2006). Since this research makes use of liquid crystal spatial light modulators (LC-SLM) as wavefront modulators, only these devices are explained in detail. For completeness, a discussion of the pros and cons of using deformable mirrors and liquid crystal (LC) devices is included.

Well-established wavefront modulating devices are deformable mirrors of different makes. Based on mirror technology they adjust their surface shape to impart phase changes. However, devices based on LC technology are of both common and scientific interest. Mainly because the LC technology finds application in the continuously-growing display industry, rapid improvements and decreasing manufacturing costs can be expected.

Liquid crystal spatial light modulators (LC-SLMs) do not contain physically moving parts but alter the optical path by modifying the refractive index of the LC (Saleh *et al.*, 1991). As the name suggests, the LC state is an intermediate state between that of crystallines and liquids. The LC's elongated molecules do have orientational order like crystals but lack complete positional order like liquids (Saleh *et al.*, 1991). Most LC modulators for vision science employ nematic or twisted nematic LCs. Molecular orientations of both types of LCs are illustrated in the left and right panel of Figure 1.5. In a nematic LC, the long axes of the molecules tend to align parallel. An important measure for LCs is the director axis, defined as the vector that points along the direction of the molecules' preferred orientation. For the nematic LC illustrated on the left of Figure 1.5, the director axis points along the x-axis.

Twisted nematic LCs are nematic LCs on which a twist is imposed by external mechanical or electrical forces. A 90°-twisted nematic LC is sketched in Figure 1.5 on the right. The director axis' orientation rotates along the z-axis from its untwisted orientation along the x-axis for z=0 resulting in an orientation along the y-axis for z=d. Twisted nematic LCs are optically inhomogeneous anisotropic media that act locally as uniaxial crystals, with the optic axis parallel to the molecular direction. In case light travels along the z-axis of the twisted nematic LC illustrated on the right of Figure 1.5, and the incident light is linearly-polarized in the x-direction, the plane of polarization rotates around the z-axis, so that the total rotation equals the twist angle Θ=90°.

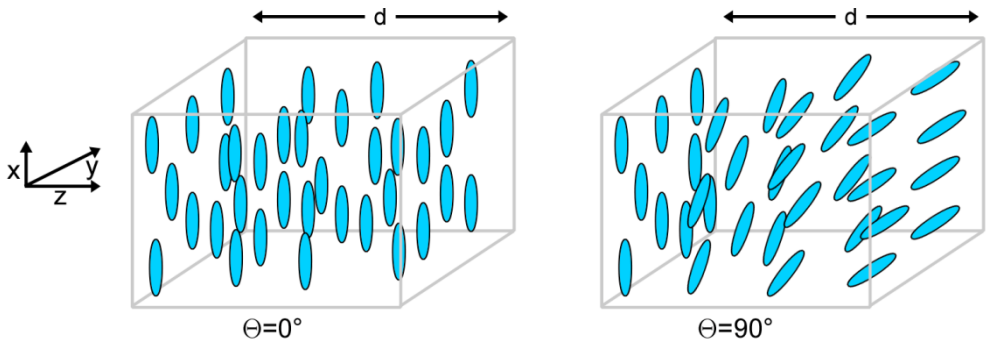

Figure 1.5: Molecular orientations of a nematic liquid crystal and a 90°-twisted nematic liquid crystal.

Under certain conditions, a twisted nematic LC can act as a phase modulator. Therefore, the LC is placed between transparent electrodes. This configuration is illustrated in Figure 1.6. When a sufficiently large electric field is applied, most of the molecules tilt toward the electric field, except those adjacent to the surface of the LC. The cell can then modulate the phase of incoming light linearly-polarized in x-direction. For waves polarized at 45° to this orientation, the cell serves as a voltage-controlled wave-retarder. When placed between two crossed polarizers (at ±45°), a half-wave-retarder becomes a voltage-controlled intensity modulator.

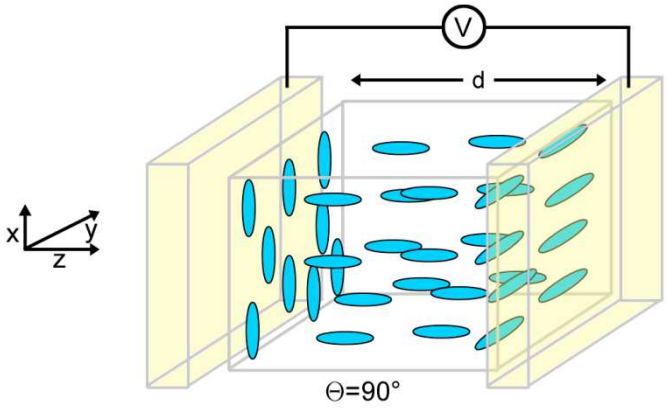

Figure 1.6: Twisted nematic liquid crystal spatial light modulator. An applied electric field in the twist-direction causes the molecules to align with the electric field. The electro-optical effect de-activates the polarization rotary power of the liquid crystal.

Currently, most AO instruments employ DMs as wavefront modulators. However, in recent years, intense research has been performed on LC-SLMs (Vargas-Martín *et al.*, 1998; Prieto *et al.*, 2004; Fernández *et al.*, 2009*b*). Nowadays, with the design of liquid crystal on silicon (LCoS) devices, many of their long-criticized drawbacks have been overcome. In the following paragraphs, DMs and LCoS-SLMs operating as wavefront modulating devices with respect to ophthalmic applications are objectively compared.

Traditionally, the main criticism of LC modulators has been their slow operation rate. While DMs easily keep up with the eye's temporal dynamics of about 5-10 Hz (Hofer *et al.*, 2001) showing response times in the range of milliseconds, LCoS-SLMs exhibit response times depending on the thickness of the LC layer, the viscosity of the material, the ambient temperature, and the nature of the applied drive voltage. Yet, with certain restrictions, current LCoS technology permits modulation at up to 60 Hz which is still far from the temporal performance of DMs but sufficient for real-time correction of ocular aberrations. A second drawback is related to the one previously mentioned. In order to optimize the response time of LCoS devices, the LC layer has to be thin. The LC layer's thickness in turn limits the effective stroke of the device. This can be easily overcome by *2π phase wrapping*. This method makes use of the periodic phase properties of light, implying, however, commitment to a working wavelength for accurate wavefront modulation. Another point of critique for LCoS devices as wavefront modulators is the restriction to linearly-polarized light. While this might be relevant for other applications, the polarization state of light has no practical implications for optical aberration measurement and correction (Prieto *et al.*, 2002).

A first advantage of LCoS-SLMs is their convenience. Handling is straightforward since most devices are optically addressable and controlled by low voltages. In addition, the devices are generally small in size and can easily be fit in optical setups limited in space. A clear plus regarding performance of LCoS modulators is their high fidelity. While DMs are known to be affected by cross-talking, LCoS modulator pixels can be

controlled individually, so that residual wavefront errors are negligible. Hence, after careful calibration, LCoS-SLMs can reliably be used in open-loop AO systems without any supporting feedback. Furthermore, in contrast to DMs, LCoS devices do not present any continuity constrains. Discontinuous phase maps can be created without any problem which allows for a wide variety of new applications. The strongest reason in favor of LCoS-SLMs, however, is the amount of independent elements available for phase control. Compared to the number of actuators a conventional DM depends on, independent LCoS-SLM pixels exceed this number by four orders of magnitude while occupying the same area. Additionally, they are achievable at relatively low cost and prices are continuously falling, driven by the display industry.

Adaptive optics visual simulators

The intention of applying AO to the eye was in first instance to correct for static ocular aberrations to achieve improved resolution for retinal imaging (Dreher *et al.*, 1989). However, with the first HSS measurements of ocular aberrations (Liang *et al.*, 1994) the use of AO in vision science started to develop more quickly and opened up new possibilities. Having achieved static HOA correction (Liang *et al.*, 1997), an important next step was real-time closed-loop aberration correction (Hofer *et al.*, 2001; Fernández *et al.*, 2001). Finally, AO led to the exploration of vision with simulated perfect optics, and evidence was gained that visual performance generally increases when aberrations are corrected (Yoon & Williams, 2002; Artal *et al.*, 2010).

Apart from aberration correction, AO also provides the capacity to induce well-controlled amounts of aberrations. Being of great value for both basic researchers and ophthalmic companies, monocular AO visual simulators were introduced in 2002 (Fernández *et al.*, 2002). These instruments basically exist of an AO system combined with a visual testing unit where visual stimuli can be presented. Figure 1.7 shows a schematic drawing of a monocular AO visual simulator. By virtually altering the optics of a subjects' eye, an AO visual simulator permits to study the relationship between amplitude and phase of the complex pupil function and visual quality on real test persons.

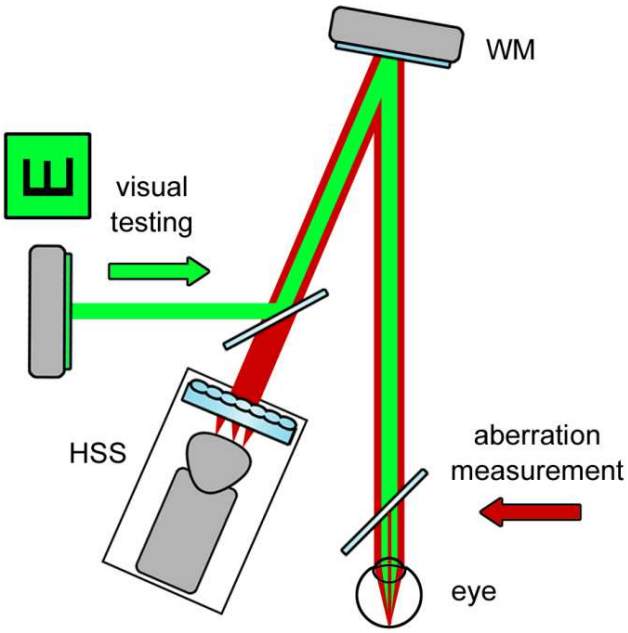

Figure 1.7: Sketch of a monocular adaptive optics visual simulator. Relay telescopes conjugating the pupil planes of the eye, the wavefront modulator (WM), and the Hartmann-Shack-sensor (HSS) were omitted in this drawing.

Basic researchers find in AO visual simulators a convenient way to study how certain aberration patterns affect vision. A path breaking experiment in this aspect was the comparison of visual performance in a group of subjects with their natural ocular aberration patterns to that when their natural aberrations pattern were replaced by a rotated version (Artal *et al.*, 2004). The experiment proved that the subjects experienced images seen with their natural aberration patterns as less blurred and provided thus knowledge about neural adaptation to one's natural aberrations.

Ophthalmic companies benefit from AO visual simulators insofar as the instruments enable interactive design of new ophthalmic products, such as lenses with different phase profiles. Traditionally, following the theoretical design of ophthalmic products, test samples had to be produced which were then iteratively improved. AO visual simulation permits the testing of phase profiles without actually producing test samples, and in this way accelerates the whole process of development and optimization. So far many phase profiles have proven to extend the depth of focus of the pseudophakic eye and are a potential basis for new ophthalmic elements (Piers *et al.*, 2004; Rocha *et al.*, 2009; Artal *et al.*, 2010; Yi *et al.*, 2011).

Over the years, AO visual simulators have been further developed (Manzanera *et al.*, 2007; Cánovas *et al.*, 2010) and are now even commercially available. In the near future, these instruments may be of clinical benefit when determining the best possible correction for individual patients before customized treatment.

1.2 The human eye

The human eye is a relatively simple optical system with two not exactly centered elements, the cornea and the crystalline lens (Artal & Tabernero, 2008). Figure 1.8 shows a horizontal section where the visual and the optical axis are marked. The eye is roughly spherical with a sagittal diameter of about 24 mm in the adult. In the relaxed eye, the cornea is responsible for approximately two-thirds, that is 43 D, of the eye's refractive power (Atchison & Smith, 2000). Both refractive elements project the images onto the retina, the light detector of the eye. Thereby, the iris constitutes the diaphragm which limits the pupil of the eye.

A special region within the retina, located temporally to the optic nerve, is the fovea. The retina is thinner here since it does not contain any blood vessels. In the center of the fovea, the cone photoreceptors are densely packed, whereas rods are lacking. This particular physiology provides high spatial acuity at this part of the retina.

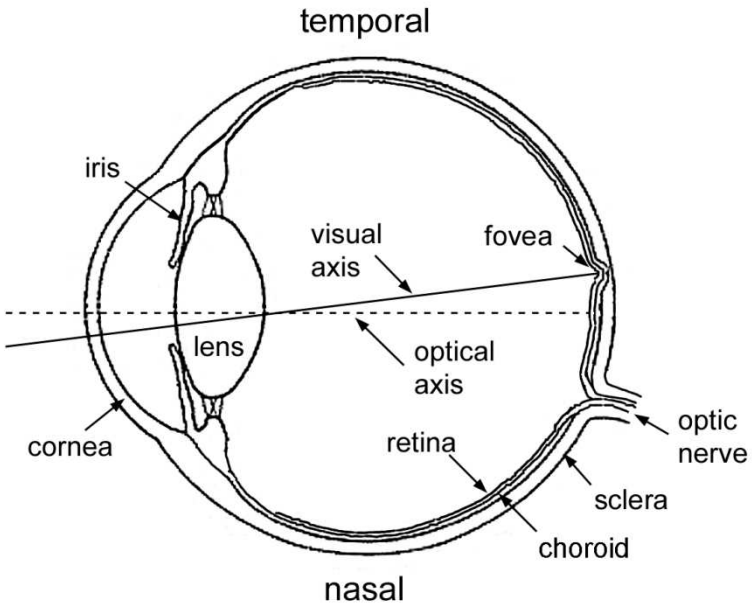

Figure 1.8: Schematic drawing of the human eye. Figure adapted from Atchison & Smith, 2000.

Compared to other optical systems, the human eye is far from being perfect. Apart from diffraction, two different classes of aberrations affect the image quality of the eye: chromatic and monochromatic aberrations. However, the eye is much more flexible than most optical systems. On the one hand, it is able to adapt to different light levels and in this way shows good performance over a large range of luminances. On the other hand, the crystalline lens provides the ability to accommodate to objects located at different distances. The latter capacity is however lost with age. An overview of the different aspects is given in the following sections.

1.2.1 Chromatic aberrations

Due to a wavelength dependent refractive index of its components, the human eye is not able to focus all wavelengths onto one single spot. This phenomenon is referred to as chromatic aberration and can be classified into a transverse and a longitudinal type. While transverse chromatic aberration is the change of magnification with wavelength, in longitudinal chromatic aberration (LCA), different wavelengths focus at different distances from the lens. The refractive index of the human eye is higher for shorter than for the longer wavelengths, and so the eye is more myopic for shorter wavelengths than for the longer ones. Figure 1.9 shows this behavior graphically. If the eye is emmetropic in green light, blue light is focused in front of the retina, whereas red light is focused behind the retina. This is especially important for AO visual simulation, since aberration measurement is performed in near infrared light, in contrast to stimulus presentation. It is therefore common practice to readjust the best-focus position according the subject's personal judgment.

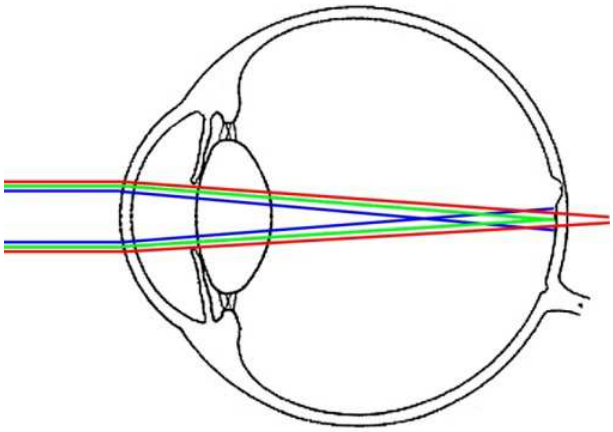

Figure 1.9: Longitudinal chromatic aberration of the human eye. Depending on the wavelength, light is focused at different distances to the retina.

It has been known since Newton that the eye is affected by LCA (Newton, 1730). Young measured the difference in refractive power of his own eye to be 1.3 D when accommodating for objects in red and violet light, respectively (Young, 1802), which could be widely confirmed by Helmholtz's theoretical calculations of the chromatic aberration for an eye model entirely composed of distilled water and possessing a single refractive surface (Helmholtz, 1909). Wald and Griffin measured the LCA in 14 subjects and observed a myopic shift of 2.10 D for a wavelength change from 691 nm to 405 nm (Wald & Griffin, 1947).

Since then, many subjective and objective measurements of LCA have been performed for different wavelengths (Bedford & Wyszecki, 1957; Howarth *et al.*, 1988; Rynders *et al.*, 1998; Marcos *et al.*, 1999), including the near infrared range (Fernández *et al.*, 2006). On the basis of their own measurements, Thibos et al. developed a chromatic-

eye model (Thibos *et al.*, 1992) which gives the LCA of the human eye. The eye model is emmetropic for 589 nm, the sodium D-line. To calculate the refractive error in diopters, the following formula is given

$$\Delta R_x = p - \frac{q}{\lambda - c},$$

where p=1.68524, q=0.63346, c=0.21410, and λ is in introduced in micrometers.

Figure 1.10 shows results of a collection of publications and the prediction of the chromatic-eye model. The total LCA of the photopic human eye is about 2.1 D over the visible range from 400 to 700 nm.

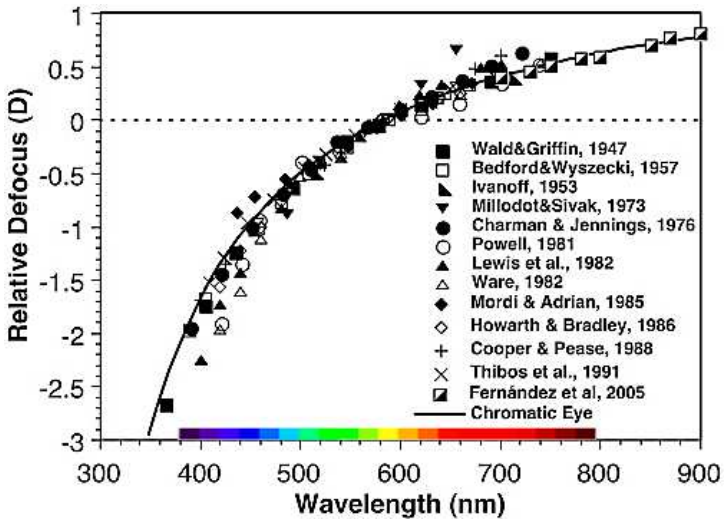

Figure 1.10: Published measurements of adult ocular chromatic aberration, compared with the Indiana chromatic-eye model (Thibos *et al.*, 1992). The data was normalized to the defocus measured at 589 nm. Figure adapted from Wang *et al.*, 2008.

1.2.2 Monochromatic aberrations

Like all optical system, the human eye is affected by aberrations (see Figure 1.11). Monochromatic aberrations mostly arise from the cornea and the crystalline lens and have a detrimental effect on retinal image quality. While defocus and astigmatism can be corrected with spectacles or contact lenses, HOAs remain.

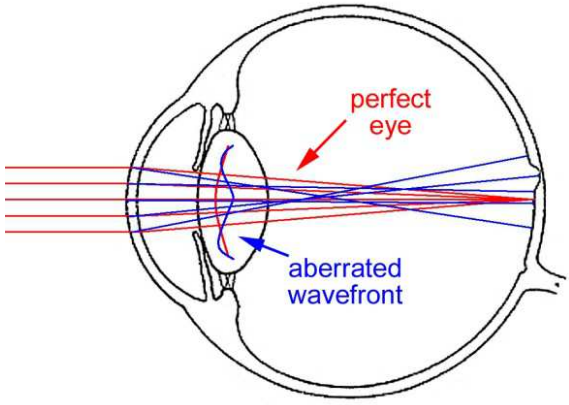

Figure 1.11: Monochromatic aberrations of the human eye.

In recent years, monochromatic aberrations have been extensively studied (Porter *et al.*, 2001; Castejón-Mochón *et al.*, 2002). In Figure 1.12, averaged data from HSS measurements on more than 2500 eyes obtained by several research sites are presented. The data was collected and scaled to the different pupil sizes by Salmon and Van de Pol (Salmon & van de Pol, 2006). The two most prominent Zernike modes for a 6 mm pupil are coma (0.14 µm) and spherical aberration (0.13 µm). In general, coma coefficients tend to be negative, while the SA coefficient is positive. Both aberrations will be explained below. As can be seen in Figure 1.12, the amount of HOAs increases with pupil size. As a consequence, they affect vision more dramatically under low luminance conditions where the pupil dilates.

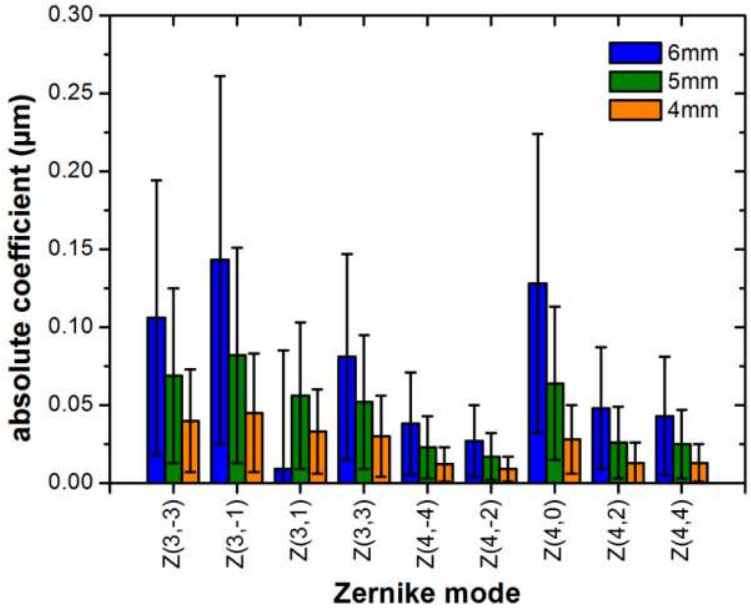

Figure 1.12: Mean absolute Zernike coefficients for pupil diameters of 6 mm (n=2205), 5 mm, and 4 mm (n=2560). Error bars represent standard deviations. Data collected from Salmon & Van de Pol, 2006.

Spherical aberration

Spherical aberration (SA) is an on-axis rotationally symmetric aberration. For optics exhibiting SA, peripheral rays do not meet at the on-axis focus. The further eccentric the rays are, the further in front of the on-axis focus point they meet in case of positive SA (Atchison & Smith, 2000). Figure 1.13 shows ray tracing in a lens affected by positive SA, the wavefront map, and the PSF in log gray scale.

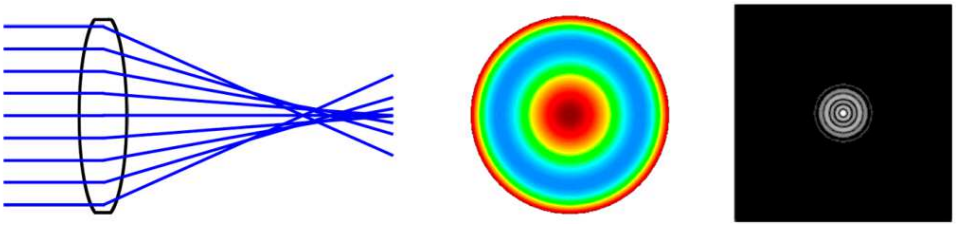

Figure 1.13: Ray tracing in a lens affected by positive spherical aberration, the associated wave aberration, and point-spread function in log gray scale.

Coma

An optical system only affected by coma distorts off-axis rays in a way that the image presents a comet-like tail directed either towards or away from the optical axis (Atchison & Smith, 2000). In the case of negative coma, marginal rays arrive at the image plane closer to the axis than central rays, generating the comet-like tail. The further off-axis the rays are, the worse the effect. In Figure 1.14, ray tracing of a lens only affected by negative coma, the aberration map, and the PSF in log gray scale are shown. For the PSF, light distribution is highest at the pointed end.

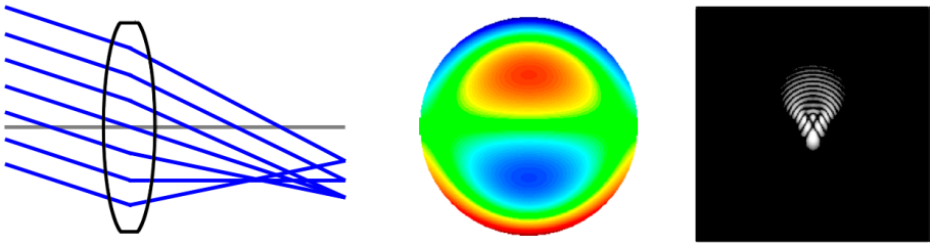

Figure 1.14: Ray tracing in a lens only affected by negative coma, the corresponding wave aberration, and point-spread function in log gray scale.

Coma can also be present in a rotationally symmetric system merely affected by SA in case the pupil is decentered. This effect is made use of during the fine alignment of the system's pupil planes described in section 2.7.1.

1.2.3 Light adaptation

The eye operates over a luminance range from 10^{-4} cd/m^2 in a starry night to 10^5 cd/m^2 in bright sunlight (Atchison & Smith, 2000). In order to achieve efficient functioning under extremely unequal conditions, several mechanisms act in concert (see Figure 1.15).

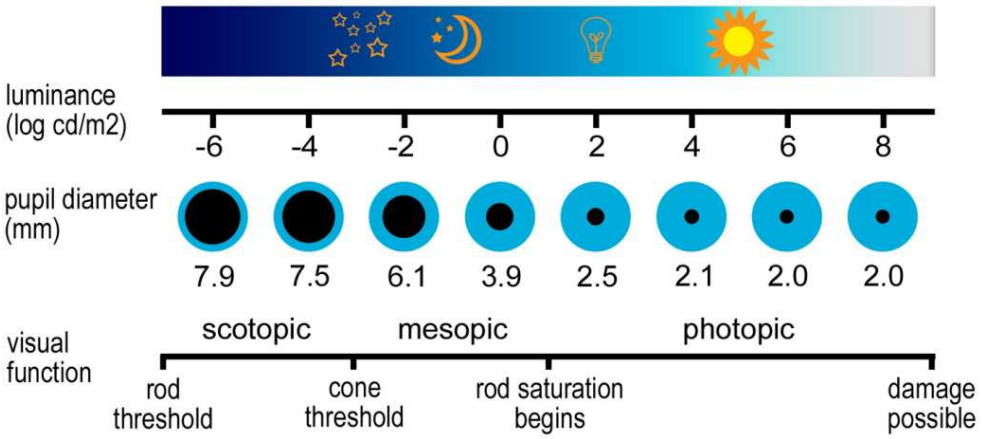

Figure 1.15: Illustration of the visual function of the human eye. Typical ambient light levels are compared to pupil sizes and receptor type operation (based on the design of Stockman & Sharpe, 2006).

First of all, the pupil constricts under bright light conditions to regulate the amount of light reaching the retina. For young subjects, pupils can easily dilate to a diameter of 8 mm in low light (Winn *et al.*, 1994), whereas in bright sun light the pupils constricts to approximately 2 mm in diameter. As the eye ages, pupil diameters become smaller, so that a fully dilated pupil of the average eighty-year-old measures approximately 5 mm in diameter.

Secondly, the visual system of the human eye is able to work in two completely different manners. At high luminance levels (>3 cd/m^2), the cone photoreceptors operate alone and photopic vision occurs. At low luminance levels (<10^{-3} cd/m^2), in contrast, exclusively the rod photoreceptors work which is referred to as scotopic vision. In the intermediate or mesopic range both receptor types work together.

While cones are most efficient for light of 555 nm (yellow), rods are most sensitive to light of 507 nm (green-blue). Figure 1.16 shows the spectral luminous efficiency for photopic and scotopic light defined by the Commission Internationale de l'Eclairage (CIE). The photopic spectral luminous efficiency function varies among subjects. Considering that three types of cones sensitive to different wavelengths (S-, M-, and L-cones) are responsible for photopic vision, this is evident for people with abnormal color vision, such as people in whose retina one cone type is absent or has an altered spectral sensitivity. However, the efficiency also varies among people with normal color vision due to a subject-dependent ratio between S-, M-, and L-cones (Hofer *et al.*,

2005). In addition, sensitivity changes as people age, because the spectral transmittance of ocular media changes. As photopic vision gives way to scotopic vision, a shift in relative spectral sensitivity occurs, which is referred to as the Purkinje shift. Taking into account the chromatic aberration, a defocus shift goes hand in hand with the Purkinje shift (Wald & Griffin, 1947).

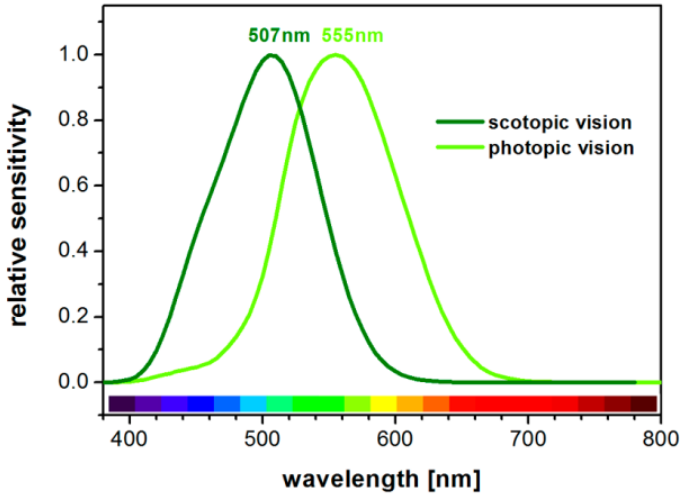

Figure 1.16: Spectral sensitivity functions for scotopic vision (rod vision) and photopic vision (cone vision) with their respective peaks at 507 nm and 555 nm.

Finally, the last mechanism that makes vision efficient over several log units of luminance changes is due to adaptation of the photoreceptors. Therefore, photoreceptors receive continuously feedback form horizontal cells averaging the input over a certain receptive field. Receptive field sizes seem to work best under a certain light level, with increasing receptive filed areas for decreasing illuminance (Hubel & Wiesel, 1962). Dark adaptation occurs rather slowly and full dark adaptation is only achieved after 45 minutes, approximately. In Figure 1.17 dark adaptation is illustrated graphically. The dark adaptation curve, that is, absolute intensity threshold versus time, also reveals the two-receptor nature of the visual system as it proceeds in two stages. At first, a rapid decrease in threshold can be observed which, at about 5 minutes, shows a first plateau. It is the cones that are responsible for this part of the adaptation curve. After 7-9 minutes of adaptation, again, a rapid decrease occurs which, at about 20 minutes, gives way to another plateau. This second stage corresponds to the rod adaptation. The abrupt change in slope of the dark adaptation curve is known as the rod-cone break. In contrast to dark adaptation, light adaptation is a fast process and comes about within seconds.

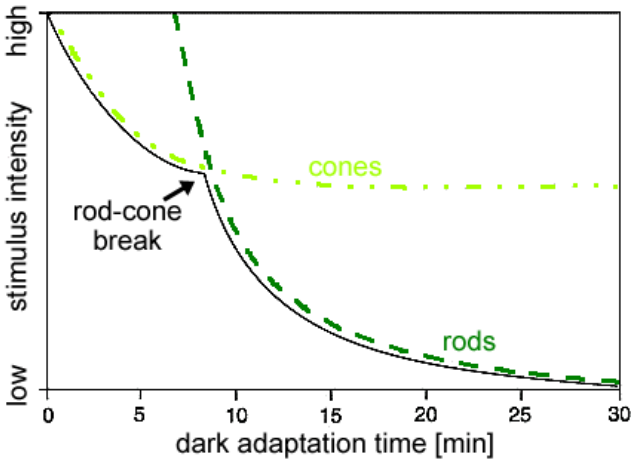

Figure 1.17: Dark adaptation threshold as a function of time.

Form our daily experience we know that visual performance worsens as light levels decrease. Figure 1.18 shows visual acuity as a function of the logarithm of background luminance. Data for a broad range of luminances was provided by Koenig (Koenig, 1897) and has become classic. The relationship between visual performance and background luminance is sigmoid. For very low light levels where the rods are active, a moderate increase of VA with background luminance was observed. Over the intermediate range of luminances from -2 to 1 log mL (-2.5 to 0.5 log cd/m^2) where the cones are active, the increase is greater. For high light levels, the function levels off and VA no longer improves with increasing luminance.

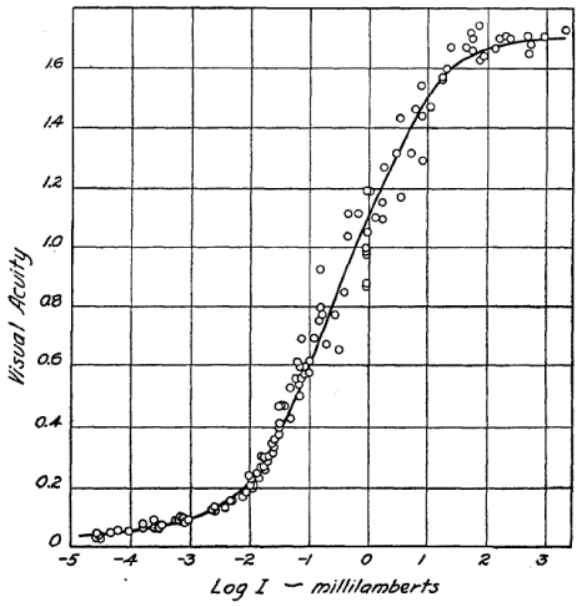

Figure 1.18: Visual acuity as a function of background luminance. Data from Koenig, 1897, figure taken from Hecht, 1928.

1.2.4 Presbyopia

Presbyopia is known as the loss of accommodative amplitude with age. The accommodative mechanism is generally accepted to occur largely according Helmholtz' theory (Helmholtz, 1909). When the emmetropic eye is at rest and a distant object is focused, the ciliary muscle is relaxed, whereas when a close object is focused and accommodation occurs, the ciliary muscle contracts. As a consequence, the resting zonular tension around the lens equator is released and allows the lens to change its shape owing to its inherent forces. The lens diameter decreases and the crystalline lens becomes more rounded. The optical power of the eye increases thus due to increased anterior and posterior lens curvatures and increased lens thickness (compare Figure 1.19) caused by a single active element, the ciliary muscle.

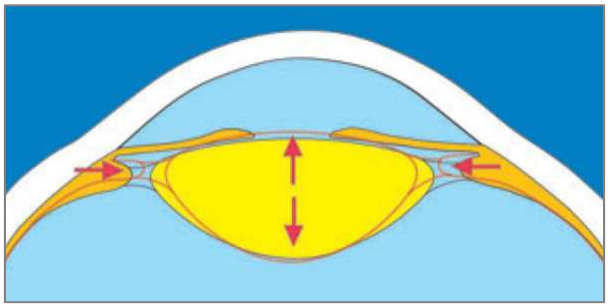

Figure 1.19: Schematic diagram of the accommodative mechanism. Figure taken from Glasser, 2008.

Prevention from accommodation (cycloplegia) can be caused pharmacologically by paralyzing the ciliary muscle. Typically used cycloplegic drugs are cyclopentolate, homatropine and tropicamide. Apart from paralysis of the ciliary muscle, they also induce mydriasis (dilation of the pupil).

While the young eye is able to dynamically increase its optical power to focus at close objects by about 10 D to 15 D, this ability gets almost completely lost by the age of 50. Historical measurement were performed by Donders (Donders, 1864) and Duane (Duane, 1912). The decline proceeds approximately linear and is in the order of 3 D per decade (see Figure 1.20).

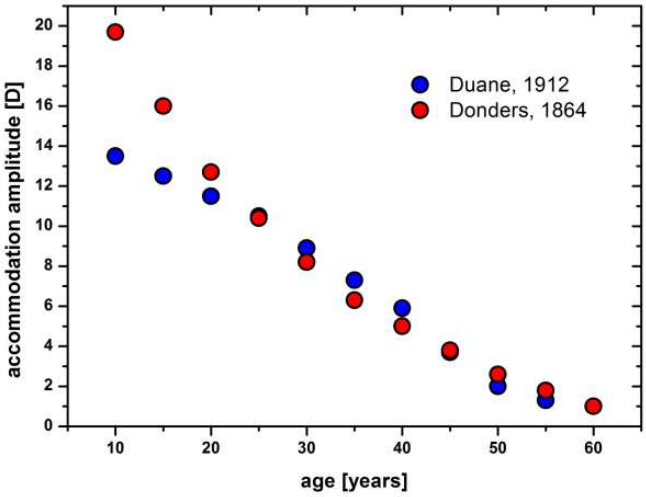

Figure 1.20: Maximum accommodative amplitudes as a function of age measured by Donders (Donders, 1864) and Duane (Duane, 1912). Figure adapted from Benjamin, 2006.

Many different components, i.e. the ciliary muscle, the zonule fibers, the lens capsule, and the crystalline lens, interact during accommodation and, therefore, all of them could play a role in presbyopia. However, it is nowadays well established that presbyopia is to a large extent – if not entirely – due to stiffening of the crystalline lens. Glasser and Campbell found that if no other aspect of the accommodative apparatus changed with age but the lens stiffness increased progressively as it does, this would ultimately lead to a lens that is too stiff to undergo the changes in shape required for accommodation (Glasser & Campbell, 1998, 1999). Since accommodation loss is universal, presbyopia treatment is of common interest.

Though femtosecond laser treatment of the crystalline lens in order to regain the flexibility of the lens seems to be promising (Krueger *et al.*, 2005; Schumacher *et al.*, 2009), the method is still immature. Contemporary clinical practice is it, to treat presbyopia without actually restoring accommodation by providing patients with pseudo-accommodation. Non-surgical techniques include spectacles or multi-focal contact lenses with profiles extending the monocular DOF. IOLs and surgeries modifying the shape of the cornea, in contrast, present surgical techniques. Another alternative is to increase the binocular DOF. Thereby, every procedure exhibits intrinsic advantages and disadvantages which should be weighed carefully before treatment.

1.3 Binocular vision

Binocular vision literally means vision with two eyes, though it is clearly more than that. The fact that adaptation to a stimulus viewed monocularly biases perception when viewing the stimulus with the fellow eye proofs this statement. An example to experience interocular transfer of the tilt-aftereffect is presented in Figure 1.21.

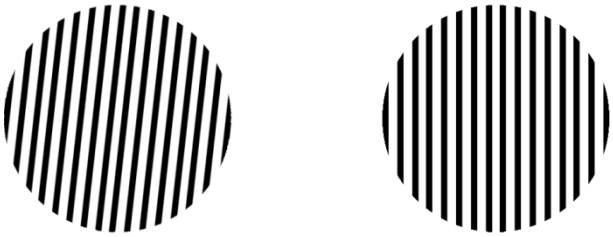

Figure 1.21: When adapting to the left stimulus with one eye for 2 minutes and subsequently observing the right stimulus with the other eye, the line orientation is perceived as rotated due to interocular transfer of the tilt-aftereffect.

The term binocular vision is commonly used for those species who have "a large area of binocular overlap" (Howard & Rogers, 1995). For humans, the total field of view is about 210° with a binocular overlap of 120°. Under normal conditions, people are not aware that their vision is binocular. Within Panum's fusional area binocular vision is single and can be described by vision with a cyclopean eye located midway between the two eyes, the egocenter (Panum, 1858). The fusional range is larger for stimuli separated horizontally than for stimuli separated vertically thus making fusional areas elliptical (Ogle, 1952). Additionally, fusion limits decrease with spatial frequency and increase with eccentricity. To attain binocular fusion a series of sensory and motor processes have to effectively operate. In case any of these processes fails, binocular vision is impaired to some extent.

Although during binocular vision images seen by both eyes are perceived as single, binocular vision is superior to monocular vision in many aspects (Fielder & Moseley, 1996; Steinman *et al.*, 2000). Apart from having a spare eye in case of disease or damage, binocular vision enlarges the field of view. Furthermore, it gives an advantage in performance, which is known as binocular summation. The major advantage of binocular vision is that depth perception is much more accurate due to stereopsis.

Following an explication of how the binocular visual system is organized, the advantage of binocular summation is explained in detail. In the course of this thesis, mainly this benefit is investigated. For completeness, an introduction to stereopsis is given, followed by a short comment on ocular dominance.

Although a visual stimulus is translated into a neural response already in the retina of the eyes, it is the brain that eventually combines the input from both eyes to a single visual percept and interprets the information (Schwartz, 2009). Figure 1.22 shows a schematic drawing of the retinal projections in the human brain.

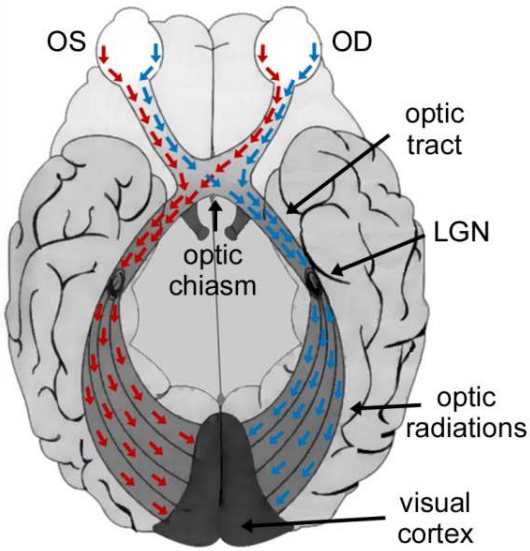

Figure 1.22: Schematic drawing of the human visual pathway. The optic nerves of each eye meet at the optic chiasm and neurons containing information from the nasal retina cross over to the contralateral side. The left side of the brain receives input from the right field of view (left hemiretina), whereas the right side of the brain receives input from the left field of view (right hemiretina).

Nerve fibers leave the eye over the optic nerve and project to the optic chiasm where monocular information is reorganized. Axons from the nasal retina cross over and project to the contralateral lateral geniculate nucleus (LGN) whereas axons from the temporal retina project to that at the ipsilateral side. In this way neurons containing information from corresponding retinal points of the two eyes terminate in close proximity in the LGN. In this part of the brain, however, only some inhibitory binocular interactions have been observed, probably playing a role in binocular suppression and binocular rivalry (Sanderson *et al.*, 1969; Haynes *et al.*, 2005). Neurons emanating from the LGN project to the visual cortex where the first true binocular cells are located in the visual system. In particular, about 50% of the simple and complex cortical cells are binocular.

1.3.1 Binocular summation

A special feature of binocular cells in the striate cortex is that cells increase their firing rate under binocular viewing conditions compared to monocular viewing when an appropriate stimulus lies within corresponding receptive field of both eyes (Hubel & Wiesel, 1962). However, increased binocular response (binocular summation) only occurs if the stimuli presented to both eyes match in many of their properties. If low level binocular vision is developed adequately, visual acuity (VA) and contrast sensitivity (CS), for instance, are greater with binocular viewing than with either the left eye or the right eye individually (Blake & Fox, 1973), a phenomenon called binocular summation. However, the degree of such improvement is variable with the visual tasks.

To quantify and compare binocular summation it is common practice to make use of the binocular summation ratio (BSR) which is defined for VA and CS in the following way:

$$\mathrm{BSR} = \frac{\text{binocular performance}}{\text{monocular performance}_{\text{better eye}}} .$$

If not explicitly stated otherwise, BSRs in this thesis uses the definition given above.

BSR is known to be larger for supra-threshold stimuli than for stimuli at threshold. Binocular CS is improved by a factor of 1.4 over monocular CS of the better eye (Campbell & Green, 1965*a*). However, this is only true when refractive errors are corrected. Binocular visual outcome also seems to depend on the interocular difference of visual quality (Pardhan & Gilchrist, 1990; Castro *et al.*, 2009). In contrast, binocular summation provides only a small gain when measured by threshold stimuli, such as VA. Binocular VA is known to be improved by a factor of approximately 1.1 over monocular VA of the better eye (Horowitz, 1949; Cagenello *et al.*, 1993).

Being CS and VA two different measures to assess visual quality, the natural difference in both binocular summation factors is obvious. The relationship between CS and VA, the high spatial frequency cut-off of the CS curve, is illustrated in Figure 1.23 together with CS data obtained by Campbell and Green (Campbell & Green, 1965*a*).

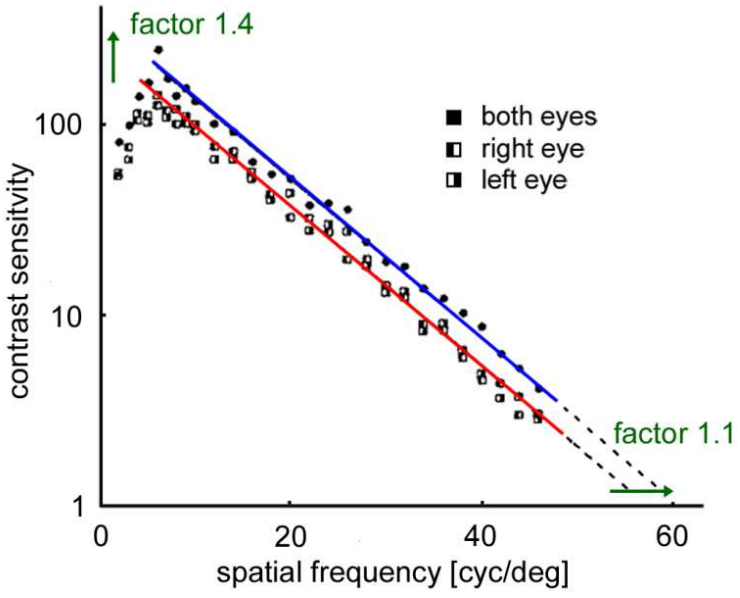

Figure 1.23: Monocular and binocular contrast sensitivity measured by Campbell and Green (Campbell & Green, 1965*a*). Binocular contrast sensitivity exceeds monocular contrast sensitivity by a factor of 1.4. Visual acuity, the upper cut-off of the curve, only improves by a factor 1.1, approximately. Figure adapted form Schwartz, 2009.

1.3.2 Stereopsis

If binocular vision works normally, stereopsis, the most accurate form of depth perception (Wheatstone, 1838; Barlow *et al.*, 1967), occurs. Especially for tasks requiring complex hand-eye coordination, stereopsis is of functional benefit. Although monocular cues can be used to judge distances, depth can be seen much better with two eyes together.

Due to the fact that we see the central visual field with both eyes which are at a certain distance from each other, roughly 59-67 mm (Dodgson, 2004), an object is viewed from two slightly different angles at a time. The subtle differences between the images in each eye produce retinal disparity. Retinal disparity is defined as the difference in the convergence angles. Figure 1.24 explains this graphically, when a subject fixates objects A and C which are located in one plane, while object B is located farther away. Retinal disparity in radians can be approximated by the relationship

$$\eta = \alpha - \beta \approx \frac{ID}{d} - \frac{ID}{d + \Delta d} \approx ID \cdot \frac{\Delta d}{d^2} \ ,$$

where ID is the interpupillary distance, d the viewing distance, and Δd the distance between the plane of fixation and the disparate object, assuming that both angles α and β are small, and $\Delta d \cdot d \approx 0$. Stereoacuity is the smallest perceptible retinal disparity. Under ideal experimental conditions, stereoacuity thresholds may reach 2-3 arcsec (Westheimer, 1994), in clinical practice values of around 30-40 arcsec are regarded as normal. While stereopsis is a very important binocular depth cue at near, it is of less importance at greater distances.

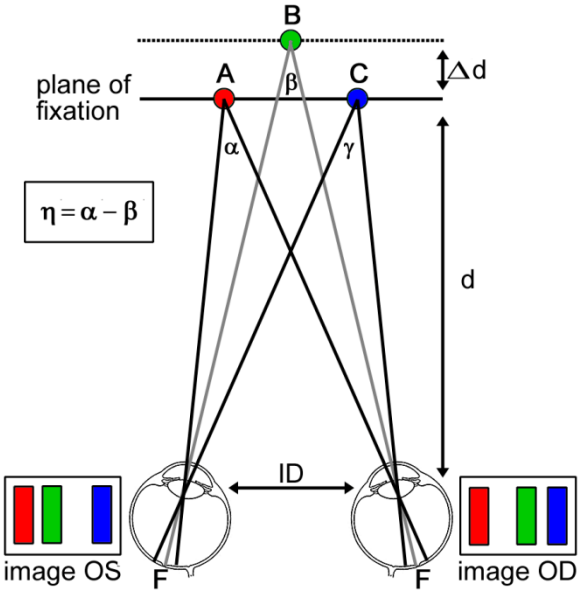

Figure 1.24: Binocular disparity of an object B with respect to fixated objects A and C.

1.3.3 Ocular dominance

Ocular dominance is the tendency to prefer visual input from one eye to the other (Porac & Coren, 1976). Theory regarding eye dominance is still controversial and up to now not sure if of major importance (Mapp *et al.*, 2003). So far, ocular dominance in most patients does not seem to be fixed, but rather depending on the visual situation (Evans, 2007). When gaze is fixed straight ahead, approximately two thirds of the population is right-eye dominant, one third is left-eye dominant, and in a small portion of the population neither eye is dominant. Furthermore, ocular dominance depends on horizontal gaze (Khan & Crawford, 2001) and switches due to relative image size (Banks *et al.*, 2004).

The most common criteria by which the dominant eye is identified, is the eye used for sighting when fixating a distant object. A suitable test is the Miles test (Miles, 1929) illustrated in Figure 1.25. Subjects are asked to fixate a distant object binocularly through a small hole formed by both hands partially superimposed at arm's length. When either closing the left or the right eye, the object moves out of the formed opening. The eye that is used for sighting when the object can be seen in the opening is the dominant eye (DE), the other eye is the non-dominant eye (NDE). Throughout this thesis, the DE refers to the sighting DE and is determined by the Miles test.

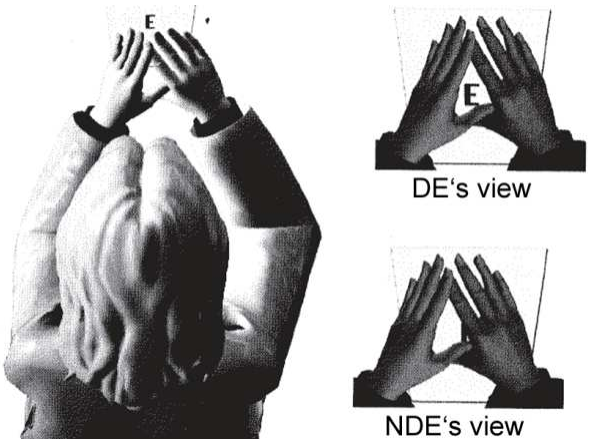

Figure 1.25: Determination of the sighting dominant eye (DE) and sighting non-dominant eye (NDE) with the Miles test. Figure taken from Steinman *et al.*, 2000.

1.4 Psychophysical measurement of visual responses

Psychophysical methods are useful when determining thresholds, that is, the minimum quantity of a stimulus that can be detected (Ehrenstein & Ehrenstein, 1966; Schwartz, 2009). For a perfect observer, a threshold does not change from measurement to measurement. However, humans are not perfect observers, and thresholds are prone to statistical errors. As the stimulus intensity increases, the probability of detecting the

stimulus is increased as well. Apart from random neural noise which is always present in the visual system, attention, motivation, and fatigue can also affect thresholds.

Measurement of visual responses can be achieved through several methods, of which the *method of adjustment* and the *method of constant stimuli* are applied in this work. Both methods are explained in the following.

The *method of adjustment* involves asking the subject to either increase the stimulus intensity until the stimulus can just be seen or to decrease the stimulus intensity until the stimulus has just disappeared. Typically, thresholds are obtained several times in both ways and results are averaged. Although this method is the simplest and quickest way to determine absolute thresholds, it suffers in particular from habituation and anticipation. By starting consecutive trials at different stimulus intensities, this can be mitigated. In this thesis, the *method of adjustment* is only applied in experiments with experienced subjects.

The *method of constant stimuli* involves repeated presentation of a number of stimulus values with the threshold value lying somewhere within this range. To ensure this, the threshold should be explored previously, for instance by employing the *method of adjustment*. Stimuli are then presented in quasi-random order, so that each stimulus intensity occurs equally often. If necessary, the number of total trials can be organized in several series. The subject responds after each presentation whether the stimulus was detected or not. Once completed the series, the proportion of "detected"-responses is calculated for each stimulus level and is then plotted against stimulus intensity. The resulting sigmoidal curve represents the psychometric function. As an example, data for a tumbling E test in form of a 4 alternative forced choice test is shown in Figure 1.26. For every stimulus size the illiterate letter E was presented randomly at four different orientations. Each measurement point represents an average of 18 trials. For small stimuli, the subject was forced to guess and the probability for a correct response was 25%. By convention, the absolute threshold measured with the *method of constant stimuli* is defined as the intensity value that provokes "detected"-responses on 50% of the trials. For the *method of constant stimuli*, subjects cannot anticipate the visibility of an upcoming presentation. Although this method provides the most reliable threshold estimates, its major drawback is that it is time-consuming and requires a patient, attentive subject.

The psychometric function is usually fit by a sigmoidal function, such as the Weibull function or the Boltzmann function (Wichmann & Hill, 2001*a*, 2001*b*). A general form of this function is

$$\Psi(x;\alpha,\beta,\gamma,\lambda) = \gamma + (1-\gamma-\lambda)\cdot F(x;\alpha,\beta) \ .$$

The lower bound γ can be interpreted as the performance when no perception occurs. In n-alternative forced-choice tests, γ will usually be fixed at the reciprocal of the number of alternatives per trial (1/n). In yes/no paradigms, it is often taken as corresponding to the guess rate, which depends on the subject and the experimental conditions. The upper bound 1-λ is correlated with the lapse rate λ. For trained subjects, a lapse rate (the rate at which subjects respond incorrectly, no matter how big the stimulus intensity) between 0% and 5% seems standard. Between the two bounds, the shape of the curve is determined by α and β, with the exact meaning of α and β depending on the form of the chosen function. As a fit function for the example illustrated in Figure 1.26, we chose a Boltzmann function of the form

$$\Psi(x) = A_1 + (A_2 - A_1 - \lambda) \cdot \frac{1}{1 + \exp(\frac{x - x_0}{d})},$$

in which A_1 is the guess rate of 25% and the upper bound is 100%-25%-λ. For big stimuli, the subject could detect all the presented stimuli, that is, the subject showed a lapse rate λ of 0%. x_0 represents the stimulus intensity where 50% of the answers were correct and d is related via $\Psi'(x_0) = 75/(4 \cdot d)$ to the slope of the fit curve in x_0.

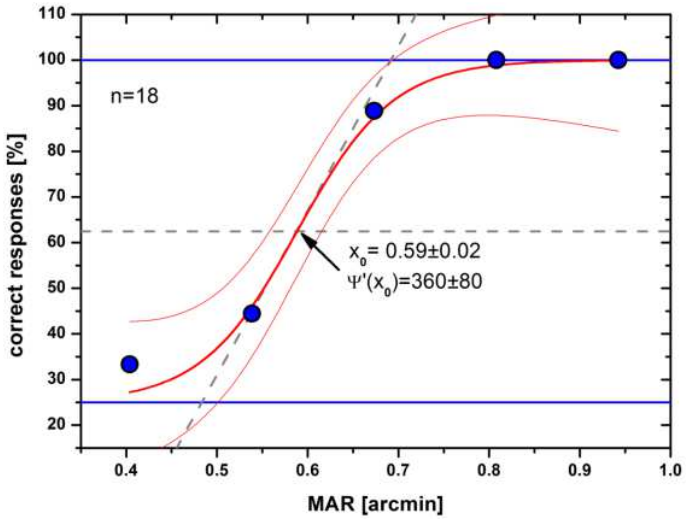

Figure 1.26: Psychometric curve for a tumbling E test. The measurement points represent the percentage of correctly detected stimuli at each stimulus intensity. The bold red curve is a Boltzmann function fit to the measurement points. Thin red curves mark the 95% intervals. Blue horizontal lines mark the lower and upper bound, respectively. The horizontal dashed gray line marks the threshold where 50% of the stimuli were detected.

1.5 Justification and scope of the thesis

1.5.1 Motivation and objectives

Optical aberrations of the human eye degrade the retinal image quality and, therefore, limit spatial vision. During the last 20 years, instruments have been developed which are based on the technology of adaptive optics and are able to measure and to manipulate ocular aberrations (Liang *et al.*, 1994, 1997; Prieto *et al.*, 2000). After two decades of maturation, adaptive optics systems are now well understood and engineered. These instruments have paved the way to intensive investigation of how aberrations affect vision (Liang & Williams, 1997; Yoon & Williams, 2002; Artal *et al.*, 2004, 2010).

All these studies have been performed monocularly, that is, for one eye only while the other eye was generally covered. However, under normal circumstances and in everyday life our vision is binocular. Binocular visual performance is superior to that of monocular vision in many aspects. The two most important advantages are binocular summation (Campbell & Green, 1965*a*; Cagenello *et al.*, 1993), improved binocular performance compared to monocular performance, and stereopsis (Wheatstone, 1838), the binocular form of depth perception. In both phenomena, the combination of the two images via two monocular channels plays a fundamental, yet to a large extent unacquainted role. However, evidence exists that both binocular summation and stereopsis depend on a variety of optical factors (Pardhan & Gilchrist, 1990; Jiménez *et al.*, 2008; Castro *et al.*, 2009).

Recently, first prototypes of binocular adaptive optics vision simulators have been developed (Fernández *et al.*, 2009*a*, 2010). These instruments permit visual simulation under actual binocular vision, that is to say, measurement and manipulation of the aberrations of both eyes independently while the subject undergoes binocular visual testing. These prototypes show a great potential in many aspects. Regarding basic research, the devices provide the possibility to investigate the impact of aberrations on binocular vision and to reveal potential interactions of aberrations with the binocular visual system. Ophthalmic companies might use the instruments to test profiles for contact lenses or intraocular lenses without the need to produce test samples and in this way accelerate the process of developing new products. Finally, in a clinical environment, binocular visual simulators could serve as pre-screening devices for programmed surgical interventions and to personalize treatment plans and predict post-surgical visual outcomes in a non-invasive manner.

The aim of this research is to develop an instrument in order to investigate different aspects of binocular vision under carefully controlled optical conditions by means of a binocular adaptive optics instrument. The individual objectives of this research can be summarized as follows:

- To design and construct a binocular adaptive optics visual analyzer which permits full control over the two complex pupil functions (amplitude and phase) and adapt the instrument to meet the particular requirements for experiments with human subjects.
- To investigate the effect of optical factors, such as aberrations, retinal image quality and lighting conditions, on binocular visual performance, and to reassess existing binocular summation models.
- To optically simulate binocular solutions to presbyopia and to non-invasively evaluate their potential and limitations in accordance with measurements on real subjects. To demonstrate that the binocular AO system can be utilized as a pre-screening device for binocular vision correction methods.

1.5.2 Outline of the thesis

The research covered in this dissertation is organized in 9 chapters. An overview of each chapter is given below:

Chapter 1 is intended to establish the background for the work presented here.

Chapter 2 describes the experimental system that is used in this work. It explains the optical layout of the binocular adaptive optics visual simulator and specifies the major components of the instrument and calibration procedures. Programs developed for the electronic devices are explained up to a user based level. At last, the procedure to obtain measurements on human subjects is explained.

Chapter 3 is dedicated to investigating the impact of defocus and spherical aberration on binocular vision. Aberrations were either induced only in the non-dominant eye or in both eyes and visual performance was assessed as visual acuity and contrast sensitivity. From the obtained data, binocular summation was derived.

In **Chapter 4**, binocular visual performance was tested after correcting spherical and longitudinal chromatic aberrations. Therefore, spherical and longitudinal chromatic aberrations were either corrected separately or in combination. Benefits for individual levels of aberration correction and binocular summation factors were determined.

Chapter 5 describes the influence of induced coma at different orientations on monocular and binocular through-focus visual acuity. Binocular summation and depth of focus was derived from the measurements, and results were related to the induced disparity between both eyes.

Chapter 6 investigates binocular performance at different light levels with best-corrected refraction or with full adaptive optics correction.

In **Chapter 7**, we examine the relative best-focus shift for low light levels under monocular and binocular visual conditions. In particular, we study the effect spherical aberration has thereby.

In **Chapter 8**, a corneal small aperture inlay is simulated. Performance with the device is measured by means of monocular and binocular through-focus visual acuity and is then directly compared to that achieved with pure-defocus monovision.

Chapter 9 concludes this dissertation, summarizing the main contributions of this research.

METHODS

2 Methods

This chapter describes the AO instrument which is used in the presented research. The system permits binocular visual testing on real subjects, while optical aberrations of both eyes can be measured and manipulated. Thus, it is capable of binocular visual simulation, and therefore referred to as binocular adaptive optics visual simulator (BAOVS). A special feature of this device is the ability to fully control the two complex pupil functions. To ensure the relative simplicity of the setup, a binocular HSS is employed and the optical system is based on LC devices to independently modulate both pupils' amplitude and phase functions. The BAOVS is able to simulate and to evaluate a large variety of binocular optical conditions. Previous versions of this instrument have been reported before (Fernández *et al.*, 2009*a*, 2010).

The following sections start by describing essential components of the system identified in Figure 2.1: the binocular wavefront sensor, the binocular wavefront modulator, the artificial pupil generator, the pupil monitoring channel (the pupil camera together with the periscope), and the visual testing unit. That followed, the optical setup of the complete BAOVS is explained together with the elaborated optimization and calibration protocols (Schwarz *et al.*, 2011). Finally, information is given on how to operate the instrument.

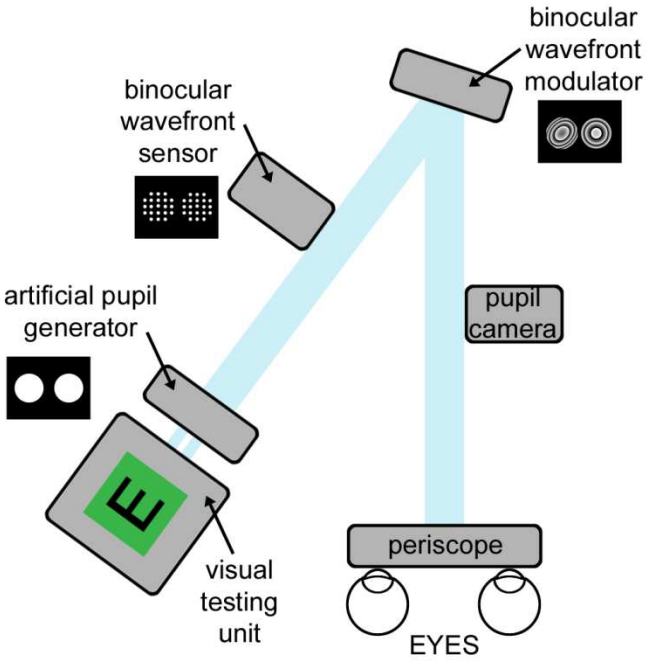

Figure 2.1: Simplified schematic setup of the binocular adaptive optics visual simulator.

2.1 Binocular wavefront sensor

To obtain the wave aberration of both eyes at a time, one possibility would be the use of two separated but synchronized HSSs, one for each eye (Kobayashi *et al.*, 2008). Due to the advantages of reduced cost and less complexity, a configuration is employed where the pupils of both eyes are projected onto one HSS instead. This method was first reported by Chin et al. (Chin *et al.*, 2008) who were interested in the correlation of aberration dynamics between the two eyes.

In the setup presented here, a binocular periscope and a demagnifying telescope (2:1) between the subject's eyes and the microlens array permit spatial resolution of both pupils on a 2/3" sensor. Consequently, aberrations from both eyes can be measured simultaneously. The eyes are illuminated with a 780 nm laser diode; the lenslets' pitch and focal length were chosen as 200 µm and 6 mm, respectively. The CCD camera located in the focal plane of the lenslet array (C5999, Hamamatsu Photonics, Hamamatsu, Japan) exhibits high sensitivity in the near infrared range. With this configuration, pupils of 4 mm in diameter are sampled by approximately 78 microlenses each.

The software to obtain the aberrations out of the spot images, named *BinoCamWin*, was written under Matlab (Matlab, Mathworks, Natick, MA, USA). It is based on the former monocular version programmed in C and was developed further to serve binocular applications. Its graphical user interface is displayed in Figure 2.2 showing the HSS spot image when measuring a subject's aberrations. In a separate pop up window, all system and alignment parameters can be introduced. The program employs a robust spot finding algorithm. From the HSS-spot displacements, wavefront slopes are computed and aberrations are reconstructed.

Taking into account the second order coefficients, the subject's objective refraction is also determined. Since aberration measurement is performed with near infrared light but visual testing in visible light, the average chromatic aberration of the human eye has to be taken into account. Based on published measurements (see section 1.2.1), a myopic shift of 0.8 D is added for the chromatic aberration between 780 nm and the central visual testing wavelength of 543 nm.

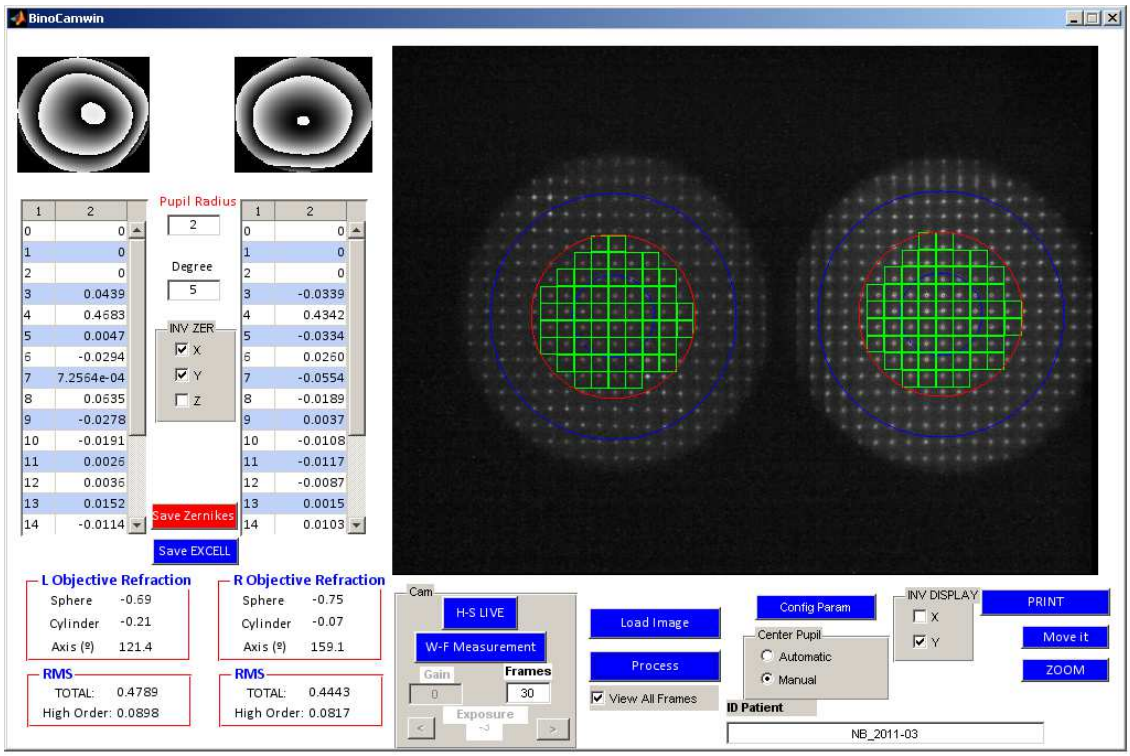

Figure 2.2: Both pupils appear spatially resolved on the HSS, so that *BinoCamwin* permits simultaneous measurement of both eyes' aberrations.

2.2 Binocular wavefront modulator

The wavefront modulator is also operated in binocular mode. Therefore, phase profiles of both pupils are projected side by side onto the device. The LCoS-SLM which is used to correct or induce aberrations (Pluto-VIS, Holoeye, Berlin, Germany) is a reflective phase only device with a broadband antireflection coating for the visible range. A photo is shown in Figure 2.3. The silicon array has 1920 x 1080 pixel resolution with 8 µm pixel pitch. The fill factor is given by the manufacturer as 87 % resulting in high light efficiency.

Figure 2.3: Photo of the reflective liquid crystal on silicon spatial light modulator.

The device is optically-addressed as an external monitor with 8 bit gray-level images (see Figure 2.4) with a frame rate of 60 Hz. Phase modulation is achieved in a very ac-

curate manner enabling open-loop high-resolution wavefront control. The LCoS-SLM was calibrated to perform a phase shift of 2π at a wavelength of 543 nm (Prieto *et al.*, 2004).

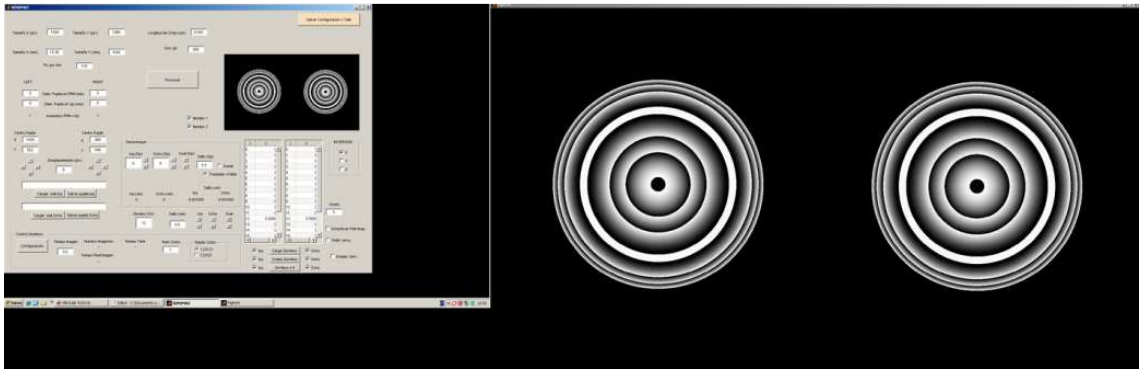

Figure 2.4: Screenshot of the extended display configuration for wavefront control.

In the optical setup, it is the wavefront modulator that limits the maximum possible pupil size to about 7.5 mm in diameter. In case of 4 mm pupils, the wavefront of every pupil is controlled by more than 195,000 independent pixels.

The wavefront modulator's control software *Binomat* was developed in Matlab and allows for user-friendly input via the graphical user interface illustrated in Figure 2.5 and a high degree of versatility. After system magnification, system inversions, and the LCoS-SLM's hardware parameters (pixel array resolution and pixel size) are introduced, calibration values such as the dominating wavelength to be modulated and the relation gray value level versus 2π phase change have to be set. Additionally, the pupil positions and diameters have to be inserted. Based on these settings, the control software computes phase images for aberration control from the single-indexed Zernike coefficients which can be introduced either manually or by loading a previously saved file.

The software allows for fine alignment of the optical system insofar as it enables precise positioning of the modulator pupils. With respect to visual simulation, a number of special functions have been included in the software. An essential capacity is the possibility to load previously generated phase images and superimpose them with aberrations. This feature is especially beneficial when simulating refractive elements such as intraocular lenses or contact lenses. Any phase image that is created by the software can be saved and recalled later on. Furthermore, the wavefront modulator software permits to use the LCoS-SLM as a virtual Badal optometer. Therefore, the subject is given control to adjust his or her optimum defocus for the optical condition set.

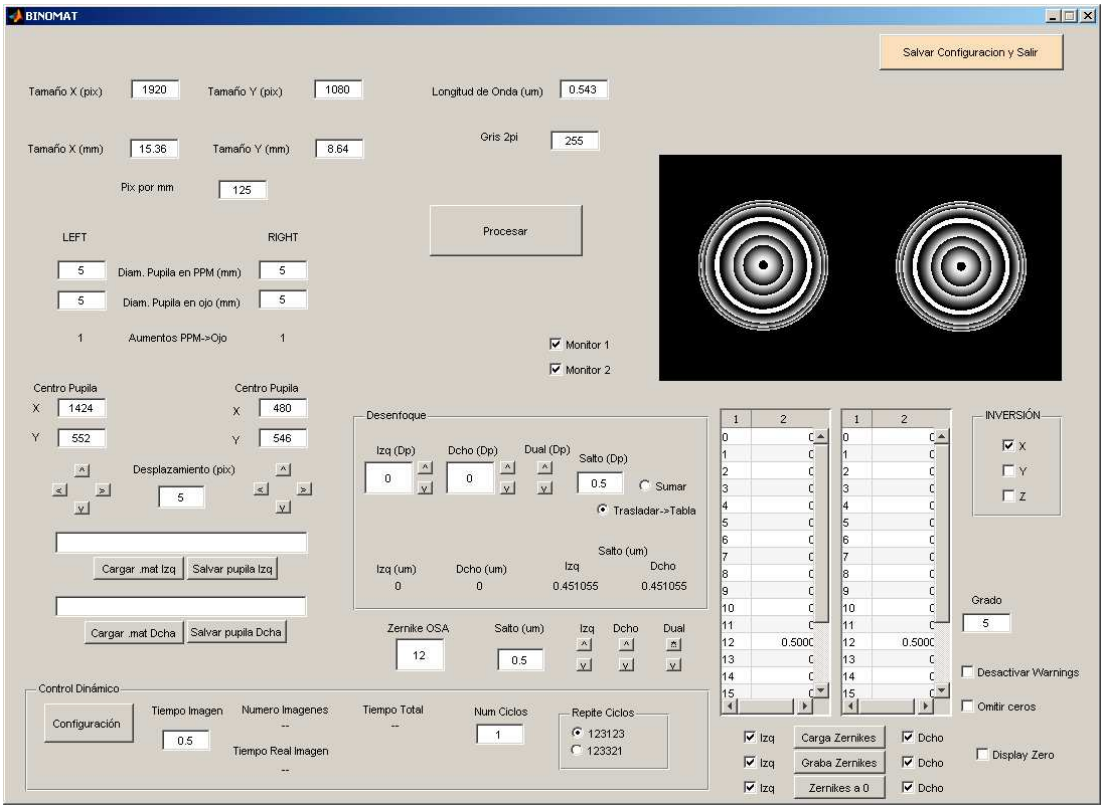

Figure 2.5: Graphical user interface of *Binomat*, the program that controls the wavefront modulator. On the upper right, the phasemap that is sent to the wavefront modulator can be seen.

2.3 Artificial pupil generator

Since the prospect of the BAOVS was the full control over the two general pupil functions, apart from phase modulation, intensity has to be efficiently controlled. While artificial pupils are habitually generated with manufactured pupil masks, an alternative are transmissive LC-SLMs operating in pure intensity modulation. In this way, pupil apertures become fully computer-controlled.

Generating artificial pupils by an intensity modulator has several advantages over the milled pupil masks typically used in optical setups. First of all, the alignment procedure is facilitated to a great extent. The modulator roughly has to be placed in the required position and fine adjustment can be performed by moving the generated pupils on the LC array via software. Second, the milled pupil masks have to be replaced and realigned every time the pupil diameter is changed, either by hand or via motorized stages. Finally, the LC-SLM in pure intensity configuration permits generating pupils that are extremely challenging to create by manufactured masks.

The LC-SLM that was chosen to generate the artificial pupils in the BAOVS works in transmission and is optically-addressed (LC2002, Holoeye, Berlin, Germany). It is based on a 90° twisted nematic LC. The active area is controlled by 800 x 600 pixels and

measures 26.6 mm x 20 mm. The manufacturer specifies a maximum refresh frame rate of 60 Hz. A photo of the LC-SLM is shown in Figure 2.6.

Figure 2.6: Image of the transmissive liquid crystal spatial light modulator.

The input director orientation Ψ_D was found to be at 45°, approximately. Placed in between crossed polarizers, the device operates in pure intensity modulation. To ensure for a high contrast ratio after implementation of the LC-SLM, the polarizers have to be carefully set to avoid light to be transmitted through intended blocking areas.

The calibration procedure consisted of determination of the transmitted intensity for displayed flat images of distinct 8 bit gray values, once the analyzer angle was correctly set. The calibration curve presented in Figure 2.7 showed that an intensity difference of 80% is achieved by a gray-level difference of about 60, so that the device permits rough transmittance control.

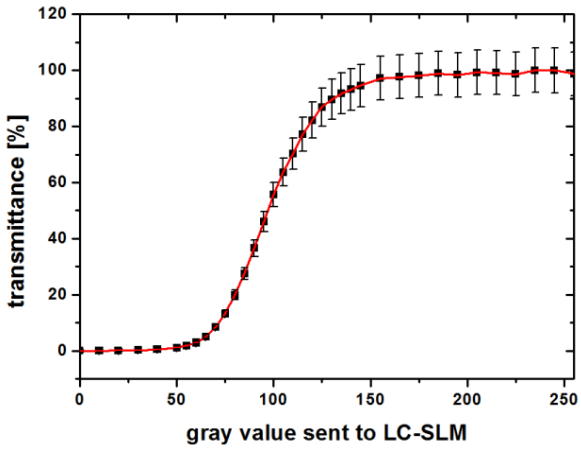

Figure 2.7: Here the light transmittance in dependence of the gray value sent to the LC-SLM is shown for a polarizer-analyzer setup in 532 nm light.

Additionally, we measured induced phase changes with the help of a HSS when the modulator was in pure intensity configuration. Phase maps were compared for binary intensity pupils and intensity gradient pupils with a quadratic profile of different diameters. The RMS changes in the induced wavefronts were smaller than 20 nm for pupils up to 8 mm in diameter (see Figure 2.8). Second order RMS (RMS2) was most affected,

for third and fourth order RMS (RMS3 and RMS4, respectively) only a minor change was observed.

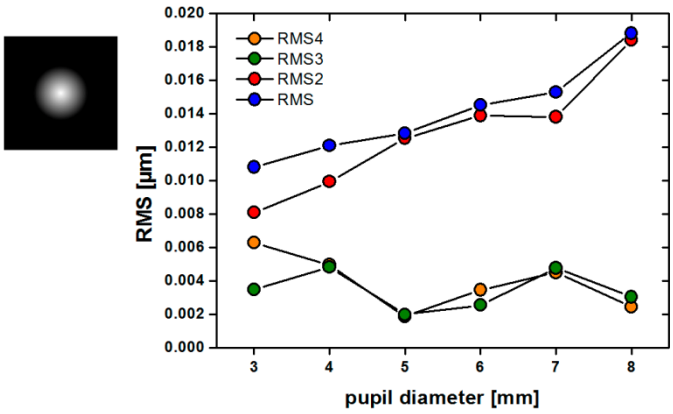

Figure 2.8: Induced RMS wavefront aberrations when generating gradient pupils with quadratic profiles for several pupil sizes compared to conventional binary pupils.

For convenience, the LC-SLM was implemented in the optical setup in such a way that the input director axis coincided with the vertical axis. Because of this configuration and the fact that the microdisplay used for visual testing emits linearly polarized light, merely an analyzer is required. Since the relay telescopes between the subject's pupil plane and the transmissive modulator's pupil plane are of unity magnification, a 4 mm pupil is sampled by about 12,000 individual pixels.

A drawback of the device is the observed diffraction effect because the pixel array of the LC acts as an optical grid. First-order diffraction images appear at a visual angle of 0.96°. Diffraction images are observed to be more intense in one direction, probably due to electrodes' layout. To avoid the first order image to interfere with the zero order image we had to restrict the visual testing field to a circular region of 0.95° in diameter and additionally block higher-order images by means of a diaphragm in the conjugate image plane next to the intensity modulator. Figure 2.9 shows images as seen through the instrument without and with correcting diffraction effects. This will also be mentioned in the section describing the complete optical setup (section 2.6).

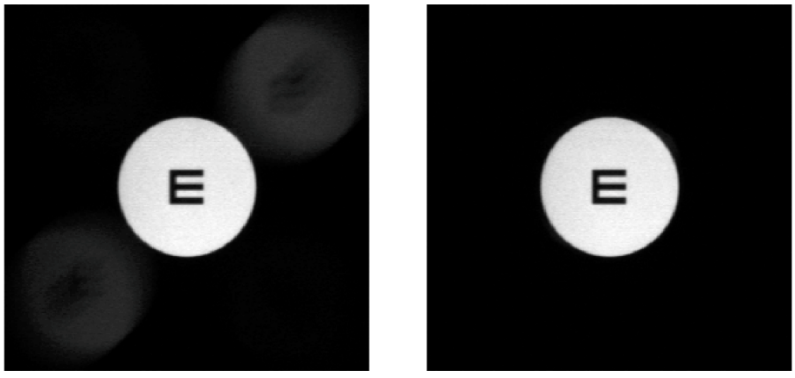

Figure 2.9: Diffraction effects arising from the transmissive LC-SLM and correction.

The software to control the LC-SLM was written in Matlab and enabled pupil positioning, transmittance control, and setting aperture diameters of differently shaped pupils after including the calibration curve mentioned above. A screenshot of the graphical user interface is shown in Figure 2.10.

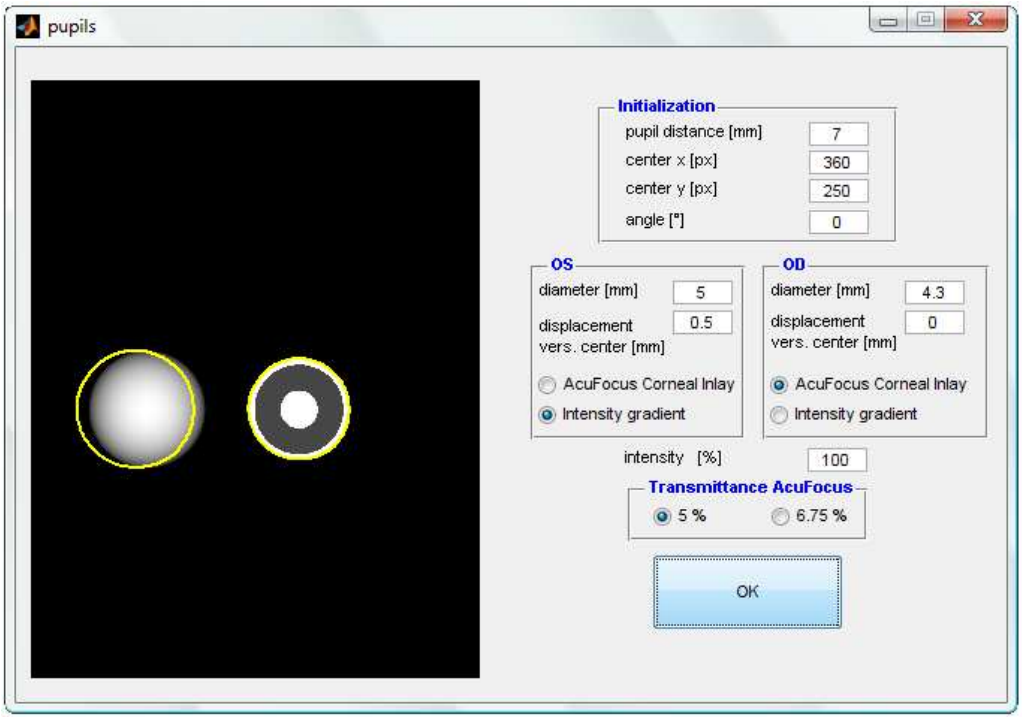

Figure 2.10: Graphical user interface for the software controlling the artificial pupil generator.

The LC-SLM is conjugated with the eyes' pupil plane, so that many desired pupil masks as to size, location, shape, and transmittance can be created. Examples of different intensity profiles taken by a camera directly focusing at the modulator's LC are presented in Figure 2.11. In particular, the device generates binary pupils, no matter if conventional contiguous or discontiguous ones like the one illustrated in the left, and all kind of gradient pupils similar to the profile on the right.

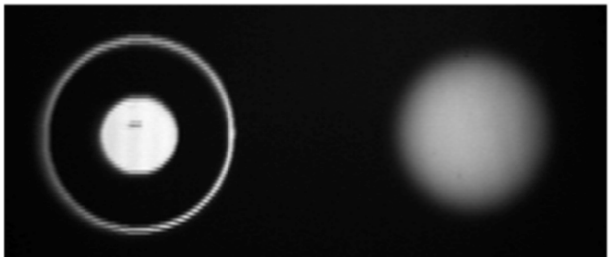

Figure 2.11: Examples of artificial pupils that can be realized with the transmissive liquid crystal spatial light modulator. Apart from conventional pupils that could be easily realized with diaphragms, it enables discontiguous pupils or gradient pupils.

2.4 Pupil monitoring channel

Alignment of the subject's eyes with the optical system is performed with the aid of the pupil monitoring channel. A schematic drawing is presented in Figure 2.12. The subject's pupils are illuminated with near-infrared LEDs emitting light of around 850 nm. The LEDs (LED1 and LED2) are connected via goosenecks to the periscope mirrors M1 and M2. The reflection of the two eyes is then recorded by one single pupil camera which features enhanced sensitivity in the near infrared range (PC; Manta G-145 NIR, Allied Vision Technologies GmbH, Stadtroda, Germany). Therefore, the periscope system composed of a right-angle mirror prism P1 and two mirrors M1 and M2 brings together the two light paths and allows them to travel side by side trough the optics of the system. A hot mirror (HM) with a cutoff wavelength of 805 nm but high transmission (>90%) up to 780 nm leads infrared light towards the pupil camera. To adjust for the subject's interpupillary distance, the periscope prism P1 is mounted onto a microtranslation stage. By moving P1 away from the subject, the periscope matches a smaller interpupillary distance, whereas movement towards the subject has the opposite effect.

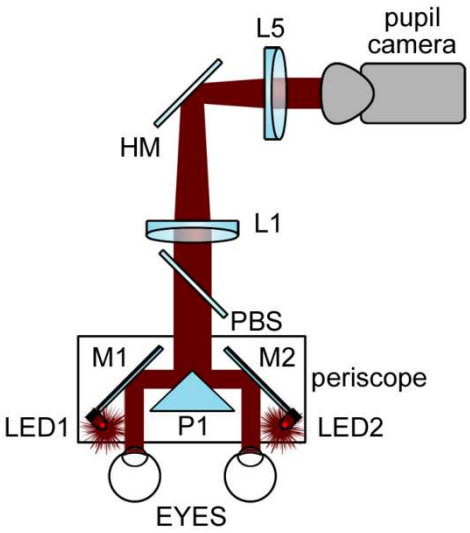

Figure 2.12: Schematic drawing of the pupil monitoring channel imaging the pupils of both eyes onto one single sensor.

The sub-system allows for continuous pupil monitoring assuring the subject's proper position regarding the system's entrance pupils. Additionally, it permits the experimenter to get knowledge about the natural pupil diameter in case no mydriatic drugs are used. A screenshot of the software's graphical user interface is provided in Figure 2.13, while a subject is looking through the AO system.

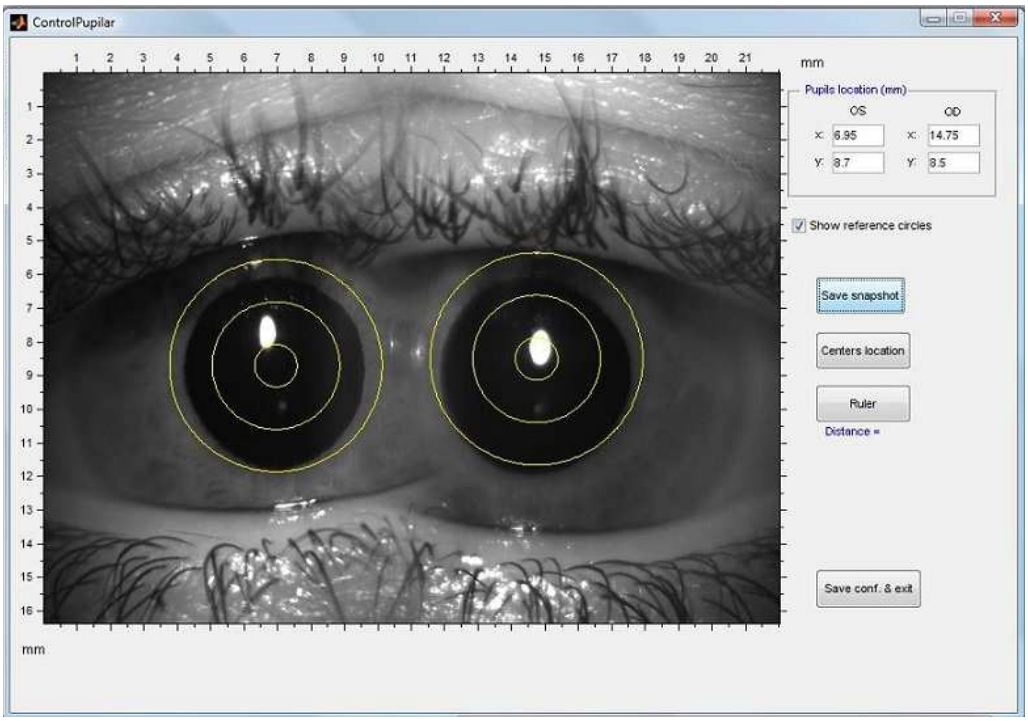

Figure 2.13: The pupil camera permits continuous monitoring of the subject's pupils positions with reference to the entrance pupils of the adaptive optics system and of the pupil size. The bright spots in the subject's pupils are corneal reflexes.

2.5 Visual testing unit

The general layout of the visual testing unit used for experiments in this work is illustrated in the left panel of Figure 2.14. Here, this configuration is referred to as *phoropter-type setup* since the subject views the same object through modified optics similar to the situation when looking through a phoropter at a visual test chart. An important difference to be mentioned, however, is the fact that natural vergence is optically eliminated here. For the standard *phoropter-type setup*, the visual testing unit comprises the collimating lens L and the microdisplay MP1 to be used located at the focal length of L. In this way, the image that is presented appears to the observer at optical infinity. For stimulus presentation, two different types of microdisplays were used. In an earlier version of the BAOVS an LC display was implemented and in the most recent an OLED display. The properties of both displays are described below.

The experimental system can easily be transformed into a stereoscope by merely changing the position of prism P2 (see Figure 2.14, right versus left panel). Although this configuration is not used in the experiments included in this thesis, it is mentioned here for completeness. The visual testing unit then consists of lens L, a periscope (composed of prism P2, mirror M4 and mirror M5) and two microprojectors (MP2 and MP3). To guarantee for a smooth transition between both setups, prism P2 is mounted onto a rail and can be slid into the beam path. By doing this, one pupil receives light

emitted by microprojector MP2 via mirror M4 and prism P2, the other pupil receives light that is emitted by microprojector MP3 via mirror M5 and prism P2. An external multi-display adapter (Matrox TripleHead2go Digital, Matrox Graphics Inc., Dorval, Canada) that is interconnected between both microdisplays and the notebook running the visual testing software, permits their synchronous control. The *stereoscope setup* is of use if unequal images are presented to both eyes in order to test binocular rivalry or stereopsis, for instance.

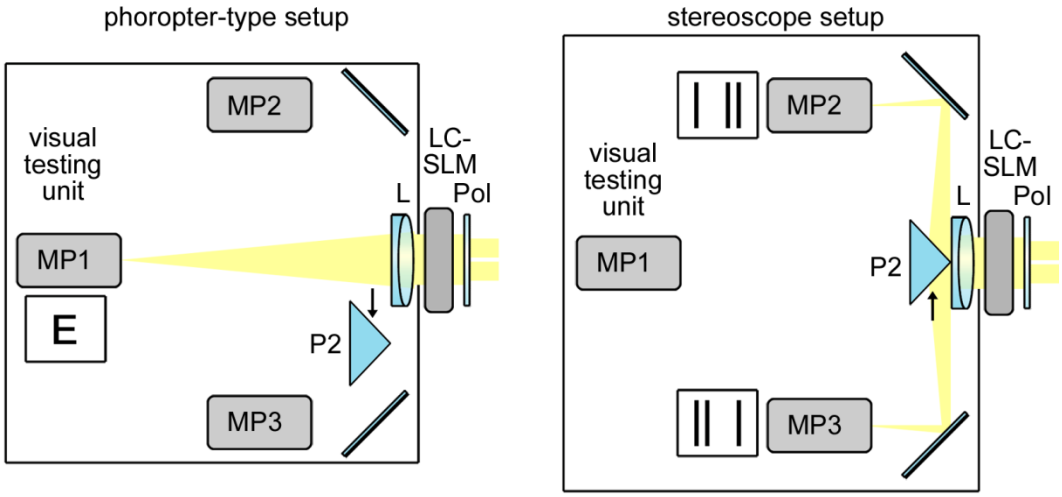

Figure 2.14: Visual testing unit in the *phoropter-type setup* on the left and in *stereoscope setup* on the right. To change in between setups, only the mirror prism P2 is moved.

Liquid crystal microdisplay

The LC microdisplay is a modified pocket projector (MPro120, 3M Projecting Systems, St. Paul, MN, USA). A photo of the off-the-shelf device is shown in Figure 2.15. Before incorporation of the projector into the setup, the adjustable microlens was removed and several layers of diffusing paper were placed in front of the LED array.

Figure 2.15: Pocket projector which was converted into a microdisplay by removing the zoom lens.

The measured spectrum for this type of microprojector is shown in Figure 2.16. It shows peaks at 458 nm, 522 nm, and 631 nm, respectively. The dominant wavelength locating a bandpass filter with central wavelength 550 nm and full width at half maximum of 40 nm (Thorlabs FB550-40) is calculated as 543 nm.

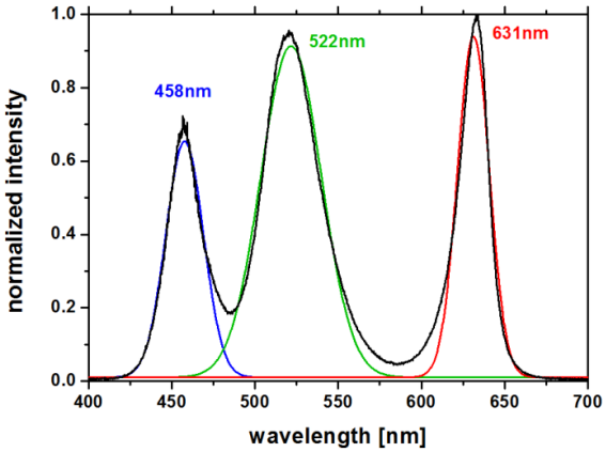

Figure 2.16: The spectrum of the LC microdisplay shows peaks at 458 nm, 522 nm and 631 nm.

Regarding the LCoS display size, the manufacturer gives a diagonal of 9.4 mm and VGA (640 x 480) as native resolution which results in a pixel size of 11.75 µm. However, we used an external display resolution of 600 x 800 pixels (SVGA), for which the microprojector calculates the image by a default anti-aliasing technique. The device's polarizing beam splitting cube, reflecting illuminating light towards the LCoS display and transmitting reflected light from there, magnifies the apparent pixel size by a factor of approximately 1.25, resulting in 11.75 µm per pixel for SVGA resolution. The microprojector output polarization is horizontally orientated. Together with the collimating lens of 300 mm focal length, one pixel subtends about 0.1346 arcmin.

Before the microdisplay can be used for visual testing its innate gamma-factor has to be corrected for. A decoding gamma of 2.72 was measured when comparing measured intensity to intended intensity. After correction, proper linearization was achieved (R^2=0.998). Intensity measurements before and after gamma correction are illustrated in Figure 2.17.

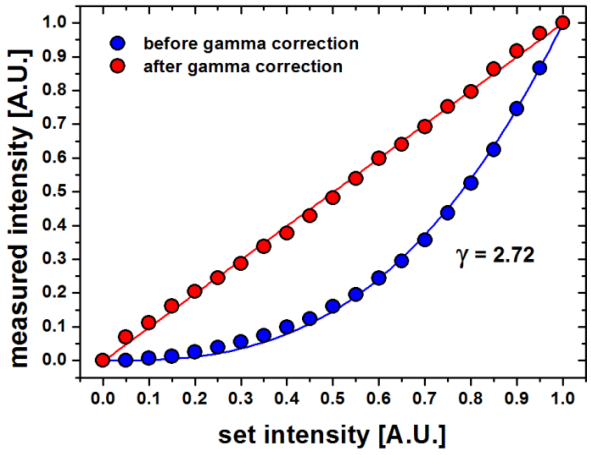

Figure 2.17: Determining the microprojector's gamma factor and consecutive linearization.

OLED display

An organic light emitting diode (OLED) consists of a minimum of two layers of organic material which makes a minimum of five essential layers in total: the substrate, the anode, the two organic layers (emissive and conductive layer), and the cathode. A schematic sketch is shown in Figure 2.18. The substrate merely serves as a supporting base for the organic material. While the anode is in general transparent, the cathode may or may not be transparent depending on the type of the device. In case current flows through the OLED, electron holes from the conductive layer jump to the emissive layer and recombine with the electrons, which results in energy release in form of photons. With respect to other displays, OLEDs provide improved image quality with superior brightness and contrast and reduced display dimensions.

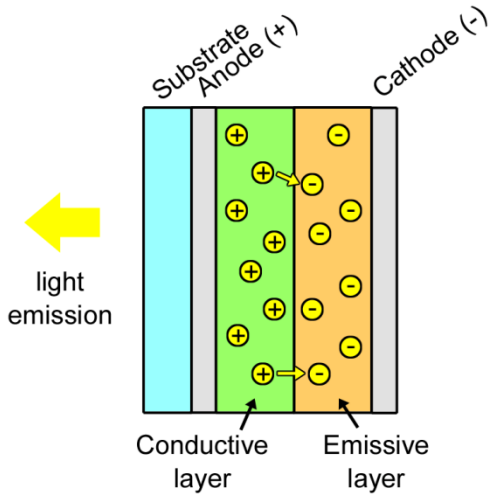

Figure 2.18: OLED principle. Energy is released in form of photons due to electron hole recombination.

The OLED that was used in this setup (SVGA+ Rev3 XL OLED, eMagin, Bellevue, WA, USA) provides a resolution of 852 x 600 pixels with 15 µm pixel pitch and can be used in full-color or monochromatic mode. In contrast to the LC microdisplay, the OLED display emits unpolarized light. The measured spectrum is represented for use in white light or in quasi-monochromatic modes, i.e. red, green and blue, in Figure 2.19. It shows four peaks at 480 nm, 505 nm, 568 nm and 614 nm. For quasi-monochromatic operation in red and blue, the spectrum shows single peaks. However, when operating in green light, the spectrum is composed of two wavelengths, 505 nm and 568 nm.

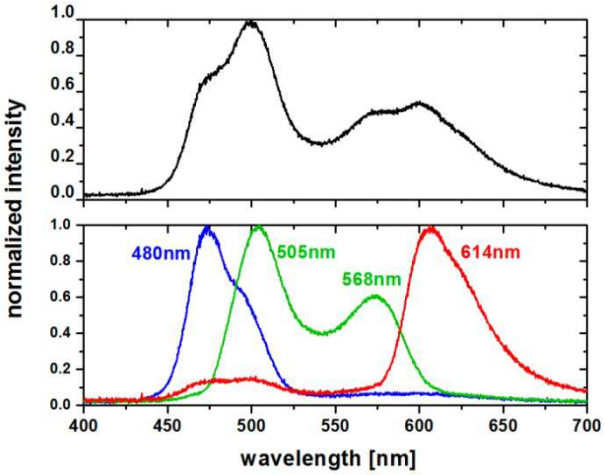

Figure 2.19: Measured spectrum of the OLED microdisplay in polychromatic (upper graph) and quasi-monochromatic (lower graph) mode showing peaks at 480 nm, 505 nm, 568 nm and 614 nm.

Due to the bigger pixel pitch and reduced light output compared with the LC microdisplay, the system magnification had to be optimized. By adding a demagnifying lens in front of the OLED display and changing the collimating lens an effective pixel size of 3.86 µm was obtained which corresponds to an angle of 0.088 arcmin in the setup.

In contrast to the LC microdisplay's decoding gamma, the OLED monitor manifests an encoding gamma. Measured intensity versus set intensity can be well fit (R^2=0.998) with a sigmoidal function of the form $f(x)=\frac{1}{1+\left(\frac{x_0}{x}\right)^{\gamma}}$. The exponent results $\gamma=2.90$.

Measured data and the fit function are illustrated in Figure 2.20. By applying the inverse function to the gray values being sent to the microdisplay, linearization is achieved.

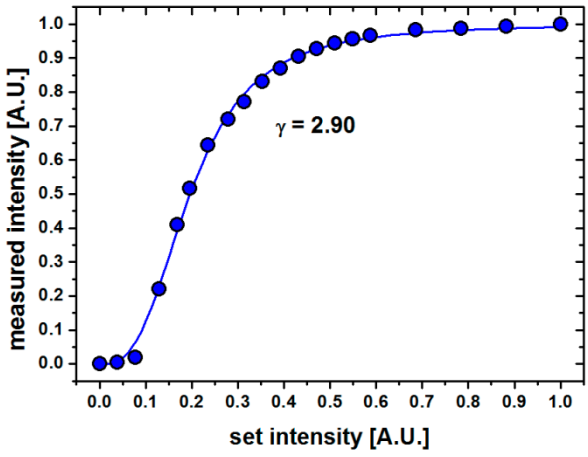

Figure 2.20: Encoding gamma measured for the OLED microdisplay.

Spatial vision tests

A set of different vision tests was developed under Matlab employing the *Psychtoolbox* (Pelli, 1997; Brainard, 1997). A screenshot of the graphical user interface is provided in Figure 2.21. The program permits input of system parameters such as magnification, inversions and rotations, the pixel size of the used microdisplay, and the focal length of the collimating lens. Available tests which were relevant for the experimental part of this work are described in the following subsections. Tests can be realized by adjustment or constant stimuli. Due to the diffraction effects in the LC device noted in section 2.3, the visual test field is limited to 0.95°. Microdisplay pixels exceeding this area were always set to black. Stimulus contrast was computed as Michelson contrast $C = \frac{I_{max} - I_{min}}{I_{max} + I_{min}}$, where I_{max} and I_{min} are the maximum and minimum luminance, respectively.

Figure 2.21: Graphical user interface of the vision test package.

Tumbling E test

The tumbling E test is based on the illiterate optotype E (Snellen, 1862) illustrated in Figure 2.22. Optotypes possess special design properties, in particular, their details (lines and gaps) measure one fifth of their overall size L. During testing, the tumbling E appears such that the legs of the optotype alternately point in one of the four orientations 0°, 90°, 80° or 270°, hence the name. Since the subject's task is it to identify the presented orientation, the test is particularly useful if test persons are not familiar with the Latin alphabet. Although the test is usually performed with maximum contrast, it is possible to reduce this measure. In this case, only the letter's gray value is modified, whereas the background gray level stays at maximum.

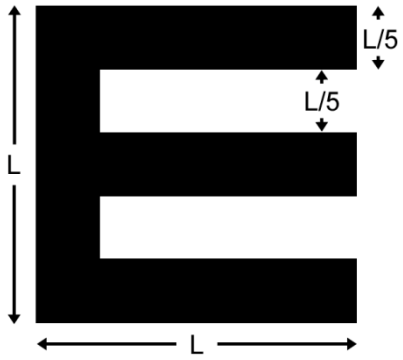

Figure 2.22: Construction of the tumbling E optotype. Overall size is five times its detail.

The optotype is composed of several spatial frequencies (the carrier frequency and its harmonics). This can be seen by Fourier decomposition of a square wave grating, which the legs of the letter E can be thought of as:

$$F(x) = \frac{1}{2} + \frac{2}{\pi}\left(1 \cdot \cos(2\pi fx) - \frac{1}{3}\cos(3 \cdot 2\pi fx) + \frac{1}{5}\cos(5 \cdot 2\pi fx) - \ldots\right)$$

Sloan letters test

Another test was based on the ten Sloan optotypes (Sloane, 1959) illustrated in Figure 2.23. Therefore, the program employs the Sloan font provided by Pelli (Pelli *et al.*, 1988; Pelli, 2013). During testing, one of the letters is chosen by chance and presented on the microdisplay. Subjects subsequently have to identify the letter. Compared to the tumbling E test, the Sloan letters test is more reliable, especially if astigmatism is present. Again, for low contrast letters, only the letter's gray value is increased, the background gray value is kept at maximum.

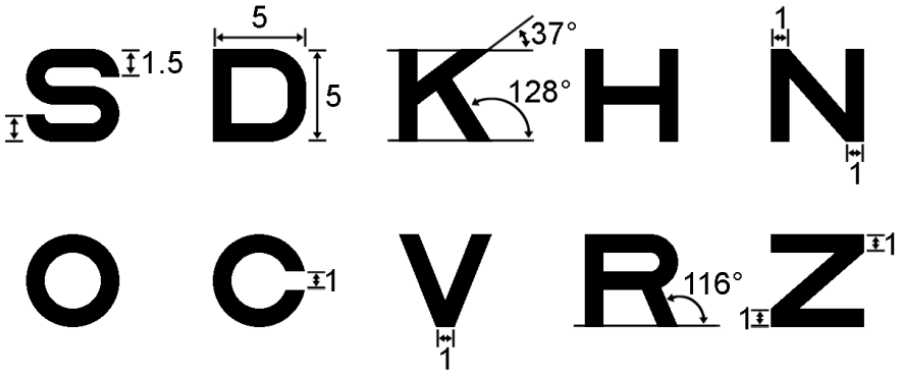

Figure 2.23: Geometrical design of the Sloan letters.

Contrast sensitivity test

Contrast sensitivity (CS) can be measured by means of sinusoidal gratings (Gabor patch). An example is shown in Figure 2.24 along with its luminance profile. Our stimuli present a constant envelope in the center and a Gaussian drop-off. At the border the envelope approaches the mean luminance $I_{mean} = \frac{I_{max} + I_{min}}{2}$. Gabor patches can be fully described by stating the carrier frequency, contrast, phase, orientation, diameter d and Gaussian standard deviation σ of the envelope. In the experiments in this work, Gabor patches were presented horizontally and vertically.

In contrast to optotypes, a Gabor patch is composed of merely one spatial frequency, and is thus more difficult to identify than, for example, a tumbling E of the same carrier frequency.

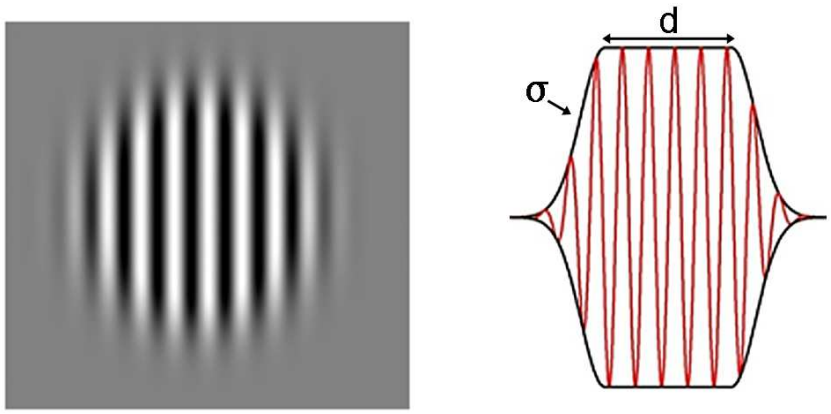

Figure 2.24 Gabor grating and its luminance profile.

2.6 Binocular adaptive optics visual simulator

Having explained the BAOVS' individual components as illustrated in Figure 2.1 at the beginning of this chapter, here a description of the complete optical setup is given. An important feature of the instrument consists in the use of merely one wavefront sensor, one wavefront modulator, one artificial pupil generator, one visual testing unit, and one pupil camera, all of them operated in binocular mode. A schematic sketch of the experimental apparatus together with the alignment laser is shown in Figure 2.25. Additionally, Figure 2.26 presents a photo of the system in which the most important components were labeled and beam paths included.

The whole setup occupies an area of about 1 x 1.5 m on an optical table. For convenience and flexibility, its electronic components are controlled by three individual computers, although control with a single computer would be possible. A personal computer runs the AO software for aberration measurement and modulation, one laptop is responsible for visual testing and a second laptop controls the artificial pupil generator and the pupil camera.

2.6.1 Adaptive optics channel

When measuring ocular aberrations by means of the binocular wavefront sensor, the subject's two eyes are illuminated by a near-infrared laser emitting light at 780 nm. The collimated laser beam is divided into two narrow beams by an opaque mask (D2) with two milled pinholes separated by 10 mm. A pellicle beam splitter (PBS) reflects either beam towards the respective eye via the periscope system composed of a right-angle mirror prism P1 and two conventional mirrors M1 and M2, respectively. Thereby, measurement beams enter the eyes slightly off-axis to avoid corneal reflections. Light reflected on either retina is guided back into the system via the periscope. The first relay telescope consisting of L1 and L2 (f_{L1}=f_{L2}=250 mm) conjugates the subject's pupil plane with the wavefront modulator's (LCoS-SLM) pupil plane. Although aberrations are measured in near-infrared light, the LCoS-SLM is calibrated for accurate phase modulation at a central wavelength of 550 nm, which is why no phase profile can be set during aberration measurement. A second telescope consisting of L3 and L6 (f_{L3}=200 mm, f_{L6}=100 mm) relays the modulator plane onto the Hartmann-Shack sensor's (HSS) lenslet array after passing a flip mirror (FM). Magnification between the pupils and the HSS is of 0.5.

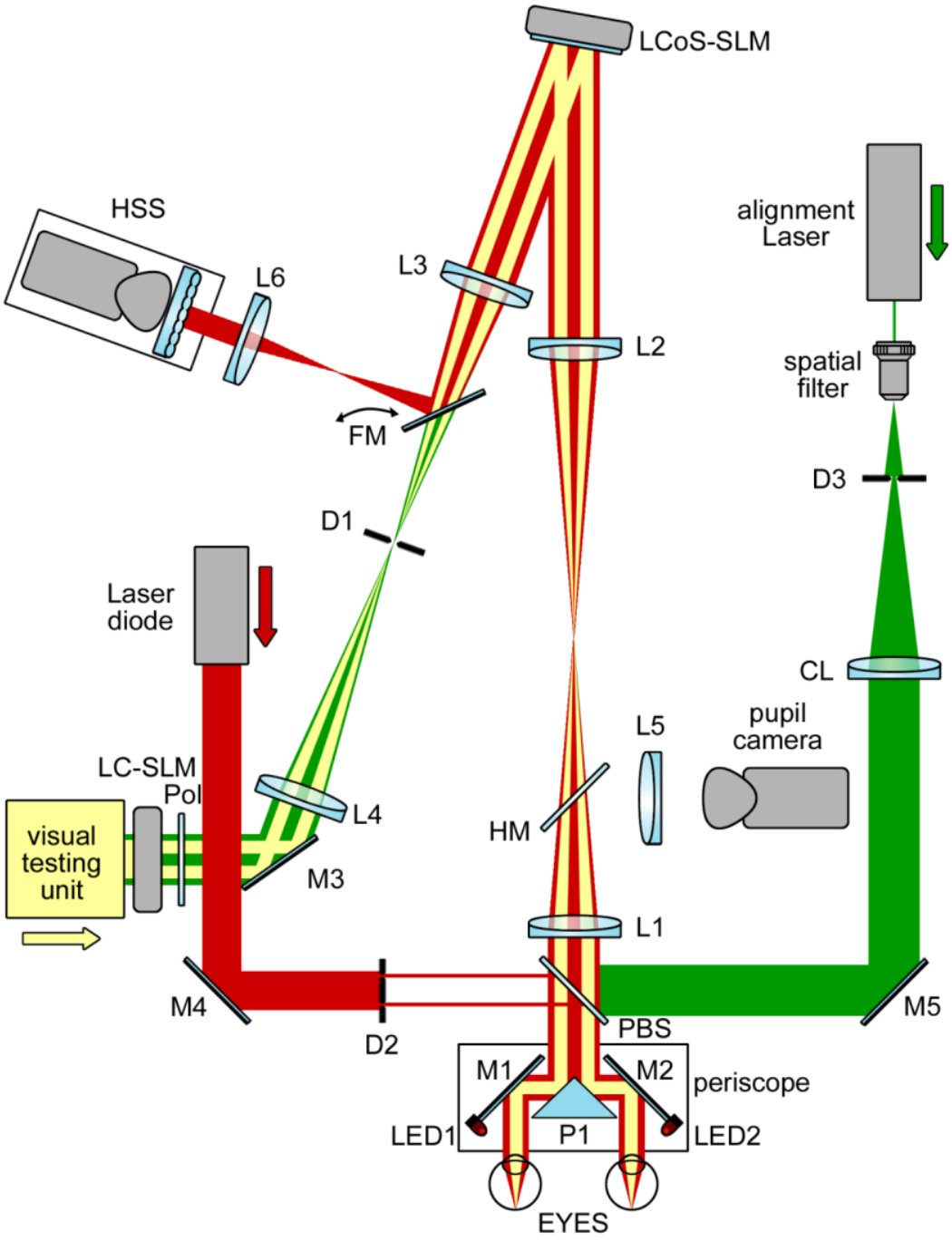

Figure 2.25: Schematic diagram of the adaptive optics system. A near infrared beacon illuminates both eyes at a time (red). Relay lenses image the eyes' pupil planes onto the wavefront modulator (LCoS-SLM), the Hartmann-Shack sensor (HSS), and the pupil generator (LC-SLM). The subject can perform visual tests presented via the visual testing unit with modified aberrations and through artificial pupils (light yellow). The accurate position of the subject's eyes is monitored by the pupil camera. The system's main components are aligned with a HeNe-Laser emitting at 550 nm (green).

2.6.2 Visual testing channel

Once aberrations are obtained, mirror FM is flipped out of the beam. The subject is then able to see the visual stimulus through the system. Entrance pupils are created by means of a transmissive LC-SLM in combination with a polarizer (Pol). The artificial pupils are then projected onto the wavefront modulator (LCoS-SLM) by means of lens L4 and L3 (f_{L4}=f_{L3}=200 mm), respectively. In the retinal plane between these two lenses a diaphragm blocks higher order images originating from diffraction at the LC-SLM's pixel grid. The relay telescope between the subject's pupil plane and the reflective modulator's pupil plane (L2 and L1) is of unity magnification. Minimizing the reflection angle at the LCoS-SLM provides accurate operation of the device. In our setup the angle was smaller than 15°.

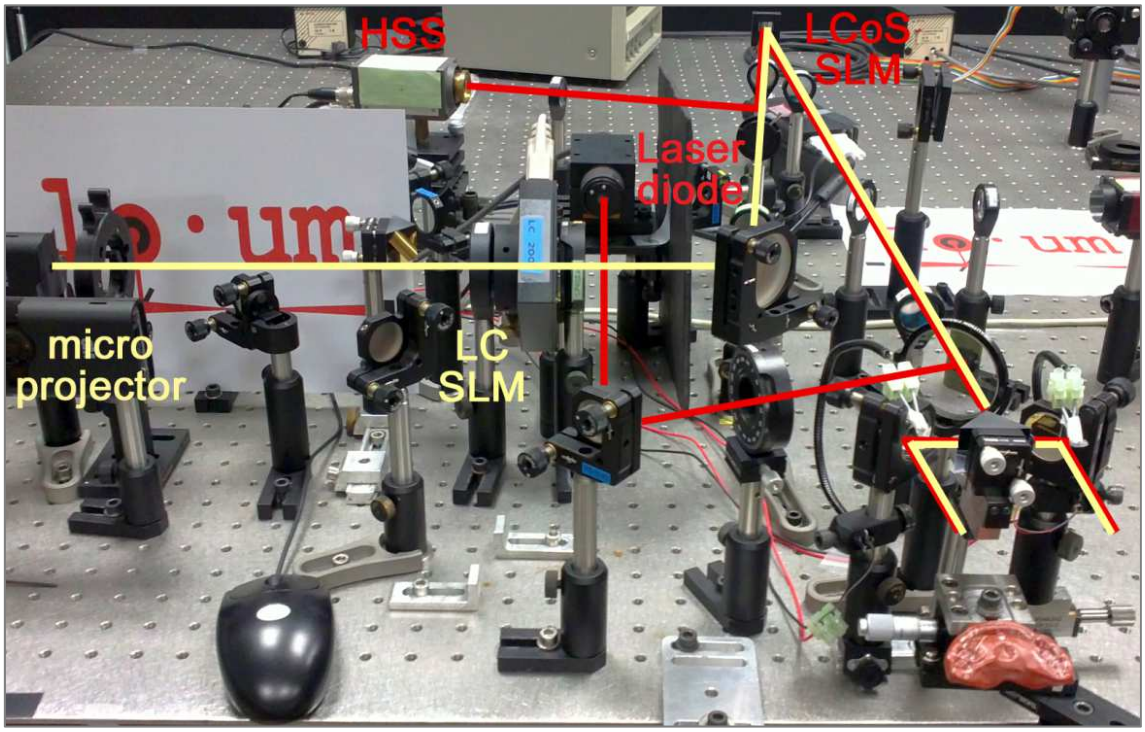

Figure 2.26: Photo of the BAOVS laboratory setup with its labeled main components. The second microprojector belonging to the stereoscope setup is blocked.

2.7 Calibration procedures

2.7.1 Fine alignment of conjugate pupils

Accurate alignment is essential for AO to ensure successful operation. Coarse alignment of the optical components is performed with help of an alignment laser defining the optical axis of the system. In general, the geometrical center of each optical element employed is centered on the optical axis. Once construction of the optical setup

is completed, it is important to perform the fine alignment of the pupils in the individual conjugate pupil planes. For this purpose, the following protocol has been developed.

Wavefront modulator and Hartmann-Shack sensor pupils

Taking into account magnifications of the optical setup, maximum pupil diameters were restricted to approximately 7.5 mm. Initial optimum centration of the left and right pupil was at pixel (480,540) and (1440,540), respectively, corresponding to ¼ and ¾ the width of the LC and ½ the height.

In a first step, the HSS pupils have to be determined to match the WM pupils. For this purpose, SA was induced in both pupils. As aforementioned in section 1.2.2, a system only affected by SA exhibits coma aberration in case of decentered pupils. The HSS pupils, thus, were located correctly when the HSS sensor measured aberrations with minimum amount of coma and maximum amount of SA (i.e. the amount of SA that was induced by the WM). This can be achieved with a simple trial and error method illustrated in Figure 2.27. After some repetitions of pupil refinement and consecutive aberration measurement, the locations with minimum amount of coma are found.

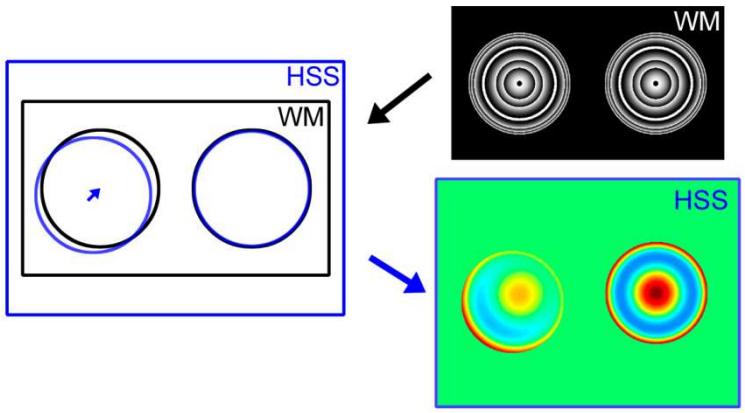

Figure 2.27: Pupil alignment procedure measuring coma due to decentered spherical aberration. In case spherical aberration is induced via the wavefront modulator but Hartmann-Shack sensor pupils are decentered, the wavefront sensor measures coma apart from spherical aberration.

These locations, however, are not the final HSS pupil positions, since we preferred the WM pupil centers to coincide with single microlenses. Once the pupil center with minimum coma aberration is found, the HSS pupil is centered onto the closest neighbor HSS spot.

Now, in turn, the WM pupils have to be aligned with the HSS pupils. Therefore, the modulator's pupil diameters are set to the dimension of one lenslet pitch. By inducing pure tilt in x- or y-direction, in general, several HSS spots become affected. Suppose the WM pupil's center is located somewhere between four microlenses as illustrated in Figure 2.28, then all the four HSS spot of these microlenses become affected to a

certain degree. Moving the center of the WM pupil to match the center of the micro-lens, only one single HSS spot becomes affected when inducing tilt. With reference to these WM positions the pupils in conjugate pupil planes were aligned.

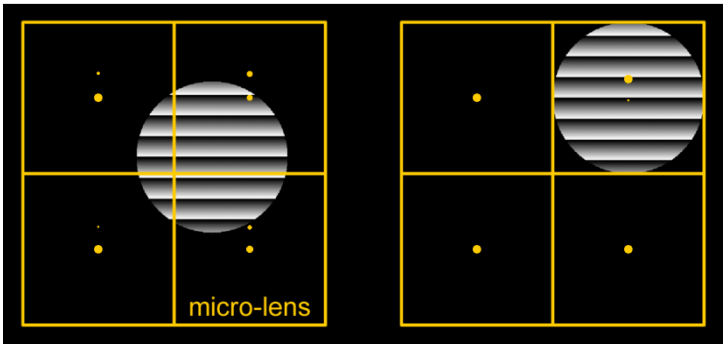

Figure 2.28: Centering the modulator pupils onto one single lenslet, only the Hartmann-Shack spot of this microlens is affected. In general the spots split due to discontiguous phase profiles.

Artificial pupils and wavefront modulator pupils

In a next step, the artificial pupils produced by the transmissive LC-SLM have to be centered onto the WM pupils. For this purpose, again, SA is induced via the WM. This time, however, the LCoS-SLM is switched to operation in pure intensity modulation. In consequence, the intensity image as shown in Figure 2.29 for one of the pupils can be examined when an alignment camera is focused on the transmissive SLM's LC surface. By visual judgment, the artificial pupils are centered onto the WM pupils.

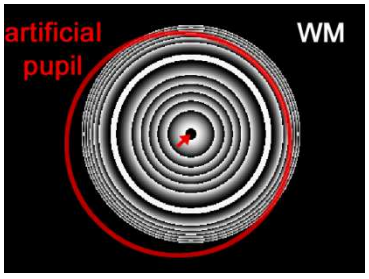

Figure 2.29: Centration of the artificial pupil (red) with respect to the wavefront modulator (WM) pupil.

Pupil camera and artificial pupils

While artificial pupils, modulator pupils and wavefront sensor pupils are situated in conjugate pupil planes, the pupil camera does not necessarily have to be positioned in a conjugate pupil plane. Here, maximum resolution was considered more important in order to provide more precision when aligning the subject later on. Therefore, magnification between the two planes was matched so that a pupil diameter of 8 mm occupied half the pupil camera's sensor size.

Since artificial pupils cannot directly be seen with the pupil camera, the alignment has to be performed in two steps using a pair of simple model eyes (see Figure 2.30). Each

model eye consists of doublet lens with short focal length which simulates both, cornea and crystalline lens, and some diffusive material, i.e. a piece of paper, located in its focal plane representing the retina. The eyes' pupils are mimicked by paper pinholes. Located next to each other with an interpupillary distance of about 60 mm, both model eyes simulate the optics of a human subject.

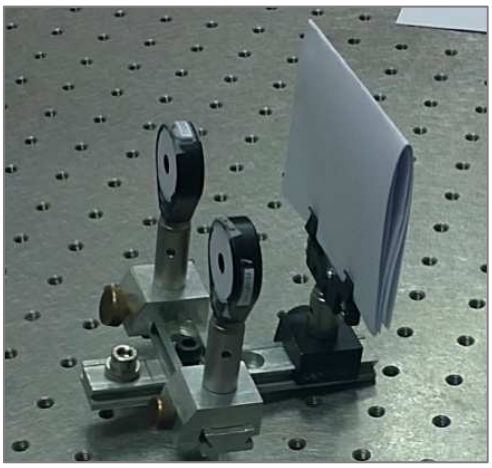

Figure 2.30: Model eyes simulating the optics of a human subject.

As a first step, both model eye pupils are aligned with the artificial pupils. Therefore, the alignment camera is placed in between visual testing unit and artificial pupil generator and focused onto the LC surface of the artificial pupil generator. Apart from artificial pupils, model eye pupils are also visible in case they are illuminated and artificial pupil diameters are set as sufficiently large. Since every subject has an individual interpupillary distance, the center between both model eye pupils and the center between both artificial pupils are matched. That followed, adjustment of the periscope translates the model eyes interpupillary distance to the interpupillary distance of 8 mm in pupil conjugate planes within the optical system. Thereafter, the model eyes' pupil planes are imaged with the pupil camera and the correct pupil centers are fixed with the help of the pupil monitoring software and saved as a reference.

Having followed the described procedure, conjugate pupil planes are perfectly matched and human observers can be aligned with the system in an uncomplicated and efficient manner.

Visual testing unit and artificial pupils

As a final step, the microdisplay has to be carefully aligned with artificial pupils, such that exactly the same image appears no matter through which pupil imaging is performed. A convenient way is it to focus a camera on the retinal plane between artificial pupil generator and wavefront modulator. Alternately closing the left and the right artificial pupil should not affect the image recorded by the camera. Additionally, the

camera is particularly helpful to accurately place diaphragm D (illustrated in Figure 2.25) for blocking higher order images arising from diffraction effects.

2.7.2 Contrast calibration and performance testing

Contrast of projected stimuli is likely to be affected mainly by diffractive elements. This could have important practical implications. We measured actual contrast by means of an external CCD-camera which took images of letters or gratings presented by the stimulus generator. The following sections summarize calibrations for both kinds of displays and present images taken through the AO system for a variety of pupil functions. Contrast calibrations presented here were taken into account in the visual testing software.

Liquid crystal microdisplay

Contrast was measured for square wave gratings of different frequencies and as a function of theoretical contrast when presenting a black E on a white background, a white E on a black background, or Gabor gratings with a fixed carrier frequency of 6 cpd. Results are presented in Figure 2.31. As for square wave gratings (left panel), contrast decreased linearly with increasing frequencies when maintaining theoretical contrast at 100%. The tested frequency range was chosen according to the range typically used for visual testing. In case theoretical contrast was reduced for different types of stimuli, measured contrast was also found to be linearly reduced (right panel).

Using the LC-display with its native resolution should improve the effective image contrast because of the microprojector's anti-aliasing technique. Here, the balance is considered to strike in favor of improved pixel resolution.

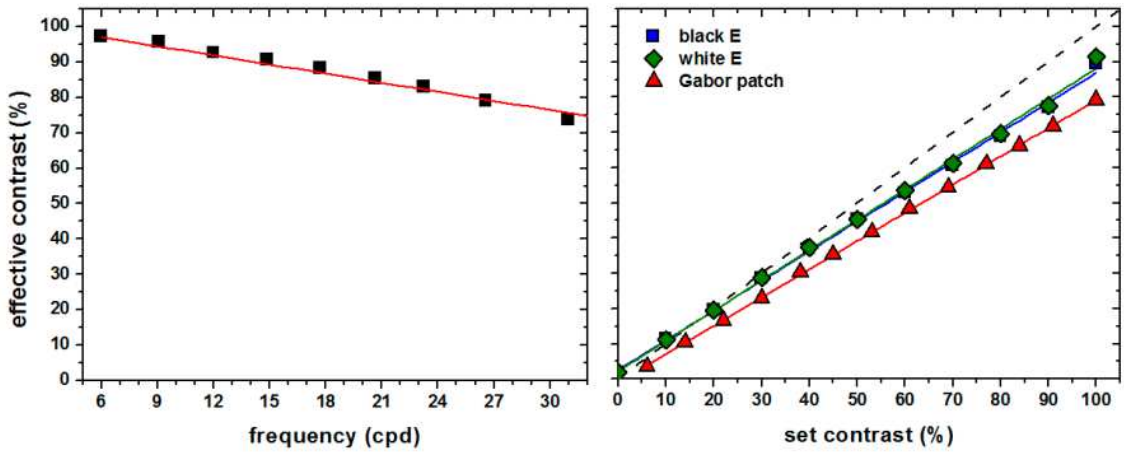

Figure 2.31: Contrast calibration of the liquid crystal display for square wave gratings and different vision tests.

OLED display

Effective contrast as a function of theoretical contrast was measured for square wave gratings characterized by nominal frequencies of 3, 6, and 12 cpd. Results are shown in Figure 2.32. In case theoretical contrast was reduced, measured contrast was also found to be linearly reduced. For a frequency of 6 cpd, a slope of 0.93 was found by linear regression (R^2>0.99). Compared to slope for the LC display of 0.84 (R^2>0.99), effective contrast was closer to the intended value here. Furthermore, contrast presented with the OLED display decreased considerably less when increasing spatial frequency of the square wave gratings (0.33 %/cpd versus 0.859 %/cpd with R^2>0.98 and R^2>0.99, respectively).

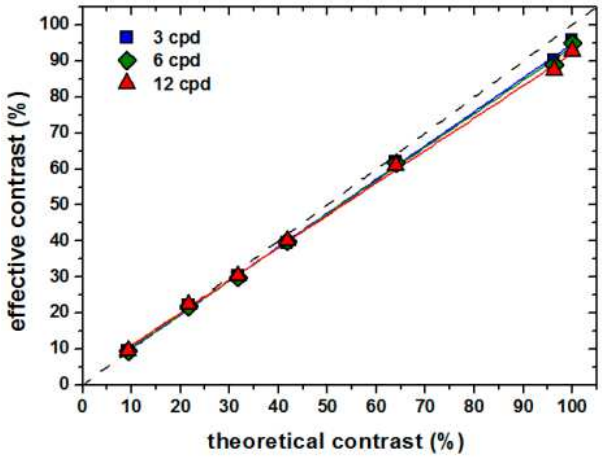

Figure 2.32: Contrast calibration of the OLED display for square wave gratings of different carrier frequencies.

Images formed through the system

Finally, to better illustrate system performance, we placed a CCD camera with a 28 mm objective (relative aperture f⁄3.5) at one of the exit pupils of the simulator. In Figure 2.33, images of presented stimuli for different combinations of pupil shapes and aberration patterns are shown as they are formed through the system. Details of the letter E measure 5 arcmin. The first line gives through-focus images for a binary circular pupil in absence of any higher-order aberrations, whereas the lines underneath show stimuli when SA is present (0.5 µm induced over a 5-mm pupil) and the pupil takes a conventional binary circular profile, a Gaussian intensity profile, or a binary annulus profile, respectively. Although the intensity profile has a minor impact on images compared with SA, changes in contrast and blur can be observed.

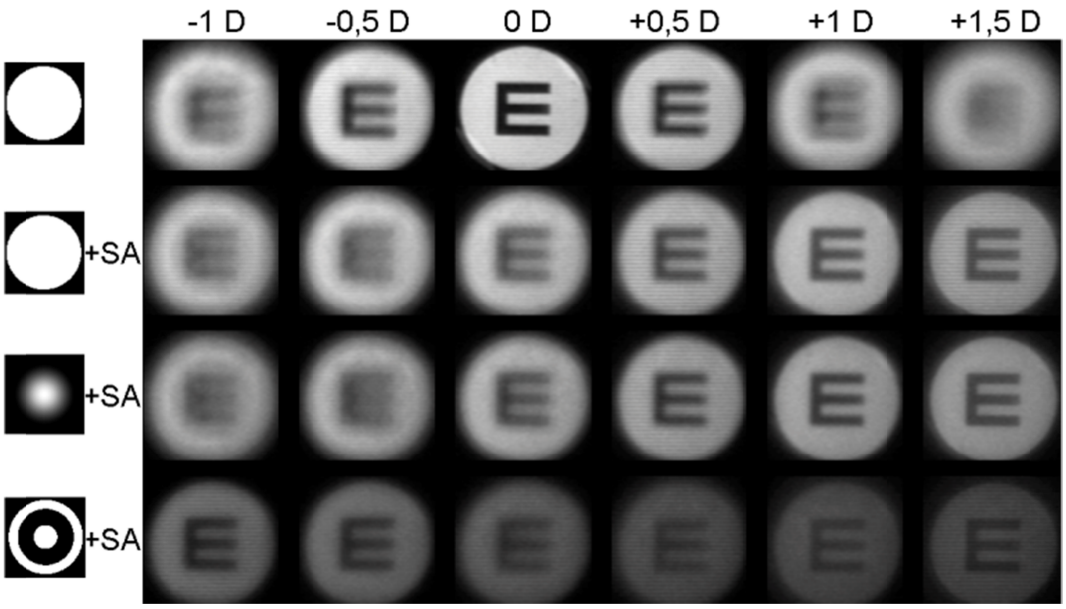

Figure 2.33: Images taken with a camera through the adaptive optics system of the letter E subtending 0.4 degrees for different pupil profiles (marked on the left) with or without spherical aberration (SA). Stimuli are presented with the liquid crystal display.

2.7.3 Use of polychromatic light

The employed method of *2π phase wrapping* in combination with pixelation effects of the LC device restricts the range of efficient aberration generation. In case that the slope of the phase map to be produced approaches λ/pixelsize, the modulator does not provide sufficient sampling. If the slope of the phase map is too steep over a significant region, an unaberrated ghost image appears paraxially together with an aberrated image of the object. This could have important implications for visual simulations as the ghost image would distort visual outcomes.

Upper limits for reliable generation of pure Zernike modes were previously measured with another LCOS-SLM of a different manufacturer (Fernández *et al.*, 2009*b*). Using their criterion, we estimated that with the current system settings defocus induction was efficient over a range of ±2.5 µm for an effective pupil diameter of 4 mm and over a range of ±3.8 µm for a pupil of 6 mm in diameter.

In general, efficient phase modulation with LC devices restricts their use to monochromatic light due to the dispersive characteristics of the LC itself and the application of *phase wrapping*. However, Fernandez et al. showed that by setting the modulating wavefront of the LC to the central wavefront of the used spectrum (here 543 nm), induced *phase wrapping* errors can be minimized to 6% for the extreme wavelengths to either side of the spectrum (Fernández *et al.*, 2012). In comparison with the natural chromatic aberration of the human eye, the chromatic aberration of the LCoS-SLM is

considerably smaller. This relationship is illustrated in Figure 2.34. Additionally, the spectral luminous efficiency of the eye even reduces the effect on visual performance.

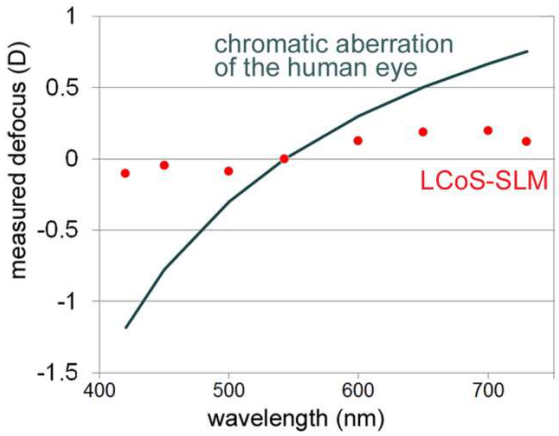

Figure 2.34: Range of defocus that can be reliably induced via the LCOS-SLM and chromatic aberration caused by the modulator when inducing pure defocus of 2 D in comparison to the natural chromatic aberration of the human eye (courtesy of Enrique J. Fernández).

Parts of the presented optical setup were composed of achromatic doublets optimized for the infrared range. Furthermore, reflecting surfaces of the first mirror prisms used in binocular periscopes were gold-coated. As a consequence, light transmittance is perceptibly wavelength dependent. Color compositions when setting the display all white were measured before and after passing the optical system. Results are presented in Figure 2.35. While a white image is composed of a color ratio of 0.62:1:0.45 before passing the system, the transmitted ratio was measured as 0.09:0.53:1. To provide white color appearance, wavelength dependent transmittance has to be compensated for by setting the background to light blue color (RGB 65,153,255). This calibration was included in the visual testing software.

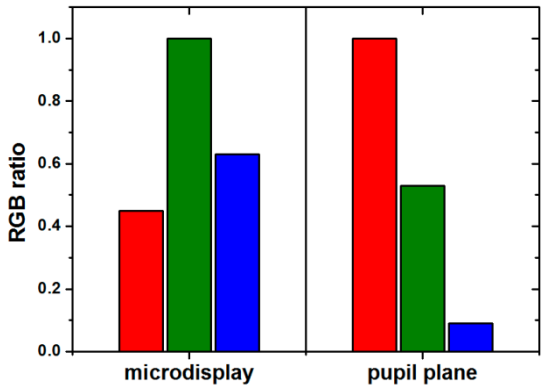

Figure 2.35: Color composition when setting the microdisplay all white measured before and after passing the system.

2.8 Aberration measurement of artificial eyes

Before taking measurements in real eyes, the system performance has to be evaluated. Therefore, we measured the pair of artificial eyes illustrated in Figure 2.30. Defocus and astigmatism were induced by trial lenses attached to the doublet lenses simulating cornea and lens of the eyes. Experimental results for the right artificial eye are given in Figure 2.36. Results for the left eye were very similar. Close to perfect correspondence was found between measured and nominal values.

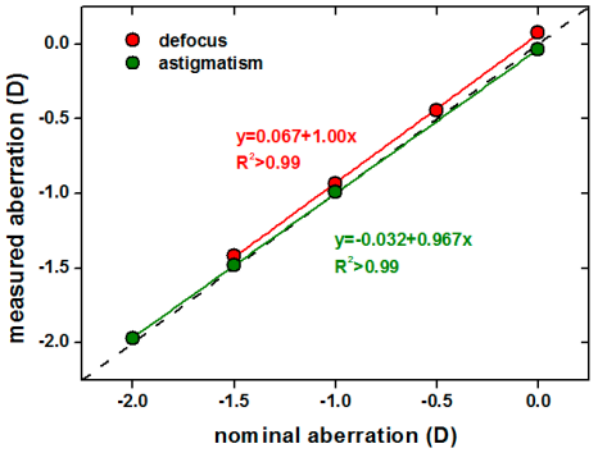

Figure 2.36: Comparison between nominal defocus and astigmatism of an artificial eye and measured aberrations.

2.9 System operation

The ultimate goal of the BAOVS is measurement and manipulation of aberrations in human eyes. It is important to consider, that aberration measurements are obtained at a wavelength of 780 nm, but aberration modulation and visual testing is performed for a central wavelength of 543 nm. Therefore, closed-loop measurements without modifying the modulator's calibration wavelength do not realistically reflect system performance. However, in contrast to deformable mirrors, the modulator's high fidelity permits aberrations modification in merely one step. In the following, the typical experimental procedure is explained when psychophysical measurements are obtained in a subject with modified natural aberrations.

All subjects involved in experiments described in this thesis were experienced with visual testing under modified optics and aberrations. All studies presented here adhere to the tenets of the Declaration of Helsinki. Participating subjects gave their informed consent, after the nature and possible consequences of the experiment had been explained.

Most experiments were performed under mydriasis and cycloplegia induced by 1% Tropicamide. About 20 minutes prior to starting the experiment, one drop of the solution was instilled in either eye followed by a second one 10 minutes after. Once one hour had passed, the effect was replenished.

For alignment of the subject's pupils with the entrance pupils of the BAOVS, the subject's head was stabilized by means of dental impressions attached to a xyz-translation stage in combination with a goniometer. The latter stage permitted fine rotation of the subject's head, in case his or her pupils were not leveled when the head position was fixed by dental impressions. The binocular periscope was adjusted to meet the subject's interpupillay distance. Continuous monitoring of the subjects' pupils ensures alignment with the system.

The next step was binocular aberration measurement. In general, three video-sequences consisting of 30 frames each were taken with the HSS and then averaged to obtain three HSS spot images. Wave aberrations were fit by Zernike polynomials and subsequently averaged. Astigmatism and HOA were corrected statically according objective HSS measurements. Best-focus position, however, was determined subjectively by the subjects themselves, once artificial pupils were set. Therefore, the subjects were given control over the virtual Badal optometer and changed the defocus until a target letter whose details measured 1 arcmin was judged to be in focus. This procedure was always repeated for both eyes separately while the fellow eye was occluded by an eye patch.

Having completed the described procedure, the psychophysical experiment under modified aberrations can be initiated. An example is given below. Monocular visual acuity was measured for one subject with natural and corrected aberrations at best focus. During monocular measurements, the fellow eye is occluded by an eye patch. Figure 2.37 gives aberration maps for 4 mm pupils and achieved VAs.

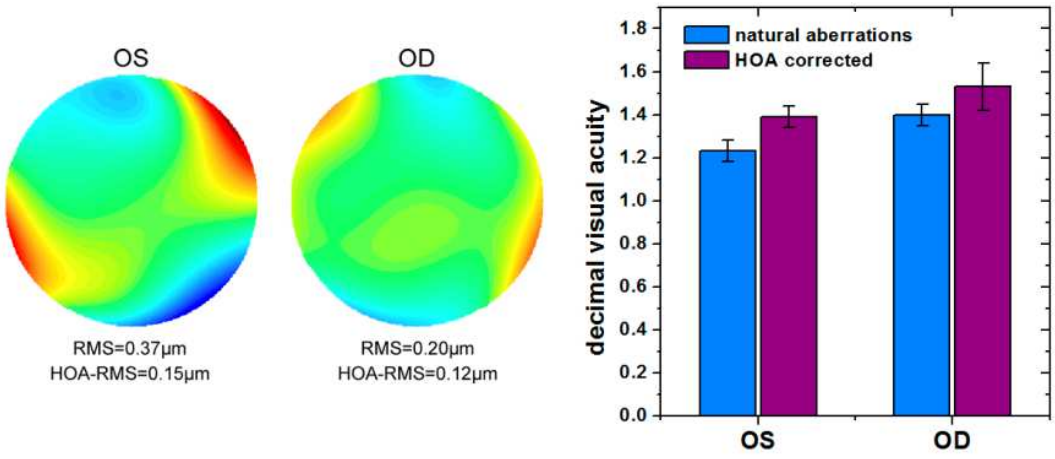

Figure 2.37: Aberration maps for the subject's left and right eye (OS and OD) and measured visual acuity at best focus.

To assess through-focus visual performance, visual quality is measured over a range of vergences. Unless explicitly stated otherwise, a defocus of 0 D means the object is located at distance and spherical refractive errors are corrected while positive defocus values refer to closer objects.

In all experiments, the visual test field measured 0.95°. Background luminance depends thereby on the employed microdisplay. In polychromatic mode, standard luminance measured through the AO system is approximately 5 cd/m^2 in case visual stimuli are presented via the LC display, and 0.6 cd/m^2 in case the OLED display is used.

RESULTS

3 Binocular performance with unilaterally or bilaterally induced defocus and spherical aberration

It is well known that for normal vision and visual conditions, binocular performance is slightly better than monocular performance. Binocular summation (BS) is however not a fixed measure but its magnitude depends on many factors. While for best corrected refraction, binocular CS summation is approximately 1.4 (Campbell & Green, 1965*a*) and binocular VA summation around 1.1 (Cagenello *et al.*, 1993), more recent studies showed that BS is negatively correlated with the visual quality difference between both eyes (Jiménez *et al.*, 2008; Castro *et al.*, 2009). An important question is whether this is also the case when optical aberrations are modified. So far, experiments have mainly addressed defocus. For unilaterally induced defocus, BS was also shown to be diminished (Pardhan & Gilchrist, 1990). In the experiment performed with trial lenses, binocular CS was shown to decrease, reaching worse CS with respect to best corrected monocular performance with monocular defocus beyond 1.5 D. Binocular CS recovered to monocular performance at about 3.5 D. An essentially different behavior was found for bilaterally induced defocus, where the difference between binocular and monocular logMAR VA was found to be greater than that for best corrected defocus (Plainis *et al.*, 2011). A recent study investigating the role of HOA was in line with previous observations as binocular CS summation slightly decreased (1.4 versus 1.3) when HOA were corrected with a BAOVS (Sabesan *et al.*, 2012).

With BS showing such a strong dependence on best monocular visual performance and interocular differences (IOD) in visual quality, this could have important implications with respect to normal binocular visual quality of aging eyes and current presbyopia correction. It is known that overall SA of the average human eye shifts to more positive values with age (Artal *et al.*, 2002; Berrio *et al.*, 2010) since aberration balancing between the cornea and internal media becomes disrupted (Artal *et al.*, 2001). The increased amount of aberrations leads to reduced visual performance of both eyes. However, aberrations increase in both eyes to a similar extent and thus IOD in performance is kept small. The influence of these changes on binocular vision are therefore of common interest.

In contrast, a commonly used binocular method to overcome presbyopia is artificially generated anisometropia referred to as monovision (Evans, 2007). This can be achieved with the help of refractive devices optimizing one eye, usually the NDE, for near vision, while the fellow eye stays corrected for distance. The procedure, thus, is to strongly alter IOD in visual performance. Anisometropia can be generated by inducing either pure defocus or a certain combination of defocus and SA. While pure defocus

merely shifts the best-focus position, SA additionally extends monocular DOF. In both cases, however, IOD in visual performance is increased with respect to normal binocular vision. Taking into consideration the findings of previous studies, a detrimental effect on BS should be inevitable. Estimation of a maximum interocular VA difference that is tolerated by the visual system could thus be of interest.

To our knowledge, the effect of unilaterally and bilaterally induced SA on binocular visual performance has not yet been studied. In the experiment presented here, we induced non-invasively defocus and SA by means of AO either unilaterally in the NDE, or bilaterally in both eyes of three subjects under well-controlled laboratory conditions. BSRs were determined from VA measurements and related to best monocular visual performance and IOD in visual performance.

3.1 Subjects

Three male subjects with normal eye health and binocular vision participated in the study. Their ages were 25, 31 and 39 years and all of them are right eye-dominant. Accommodation was paralyzed by Tropicamide 1%. Two observers are nearly emmetropes; one subject is a mild myope of 3D. Table 3.1 gives refraction and aberration data for 4 mm pupils after induced cycloplegia.

Subject	Age (y)	Eye	Objective refraction (D)	RMS (µm)	HOA-RMS (µm)	SA (µm)
#1	31	OS	+0.29 -0.57 x 175°	0.25	0.10	0.00
		OD*	+0.46 -0.23 x 6°	0.15	0.12	-0.01
#2	39	OS	-2.36 -0.79 x 62°	0.34	0.10	0.02
		OD*	-2.72 -0.4 x 98°	0.18	0.08	0.01
#3	25	OS	+0.55 -0.30 x 15°	0.16	0.10	0.04
		OD*	+0.29 -0.19 x 148°	0.12	0.10	0.05

Table 3.1: Refractive errors of the three subjects. Aberrations are given for 4 mm pupils. The asterisk marks the dominant eye.

3.2 Visual performance testing and data analysis

Astigmatism and SA were corrected on the basis of objective aberration measurements for all subjects throughout the study. Defocus was corrected as the subject carried out monocular best focus searches for either eye. Astigmatism and defocus were induced by the wavefront modulator and remained static during the experiment. Natural HOA other than SA were not corrected.

A tumbling E test was performed with artificial pupils of 4 mm in diameter in quasi-monochromatic light (543 nm). High contrast VA was tested monocularly and binocularly by adjustment. The average of three thresholds was taken as a measurement value.

VA decreases were established by fitting linear regression models to the data. BSR was defined as ratio between binocular and best monocular measures of decimal VA (or $10^{(\text{best monocular logMAR VA - binocular logMAR VA})}$). Statistical significance was tested performing one-sided student's t-tests. In case of p-values smaller than 0.05, difference between data was assumed to be statistically significant.

Defocus and SA were then induced either bilaterally in both eyes or unilaterally in the NDE of the subject by means of an LCoS-SLM wavefront modulator. VA was assessed over a defocus range from 0 D to 2 D in steps of 0.5 D and for induced SA between 0 µm and -0.2 µm in increments of 0.05 µm. Subjects were not told which aberration was induced. Neighboring points on presented VA/induced aberration curves were measured consecutively.

3.3 Binocular performance

Figure 3.1 shows monocular VA for the DE and NDE and binocular VA averaged across subjects. Graphs in the upper row show data for bilaterally induced aberrations, graphs in the lower row for unilaterally induced aberrations. In the left column, defocus was induced, whereas in the right column negative spherical aberration was induced. Typical standard errors were 0.12 logMAR and 0.07 logMAR for defocus and SA induction cases, respectively.

For bilaterally induced aberrations, binocular VA stayed close to best monocular VA. In the case of bilaterally induced defocus, VA decreased by 0.25, 0.20, and 0.21 logMAR/D of induced defocus in the DE, the NDE, and binocular, respectively. For bilaterally induced SA, monocular VA decreased by 0.79 and 0.84 logMAR/µm in the DE and NDE, respectively. The binocular slope of 0.36 logMAR/µm was significantly shallower. Slopes and according R^2 determination coefficients for linear regression fits are listed in Table 3.2.

Visual condition	VA decrease (logMAR/D)	VA decrease (logMAR/µm)
DE	0.25 (R^2=0.97)	0.79 (R^2=0.97)
NDE	0.20 (R^2=0.99)	0.84 (R^2=0.85)
binocular	0.21 (R^2=0.98)	0.36 (R^2=0.94)

Table 3.2: Visual performance decreases for bilaterally induced defocus (left) and spherical aberration (right). R^2 coefficients of determination when fitting straight lines to the data are given in parentheses.

For unilaterally induced aberrations, binocular VA was slightly worse than best monocular VA for all the measurements. However, the difference was only statistically significant for 2 D of induced defocus (p=0.023) and -0.10 µm and -0.15 µm of induced SA (p=0.038 in both cases).

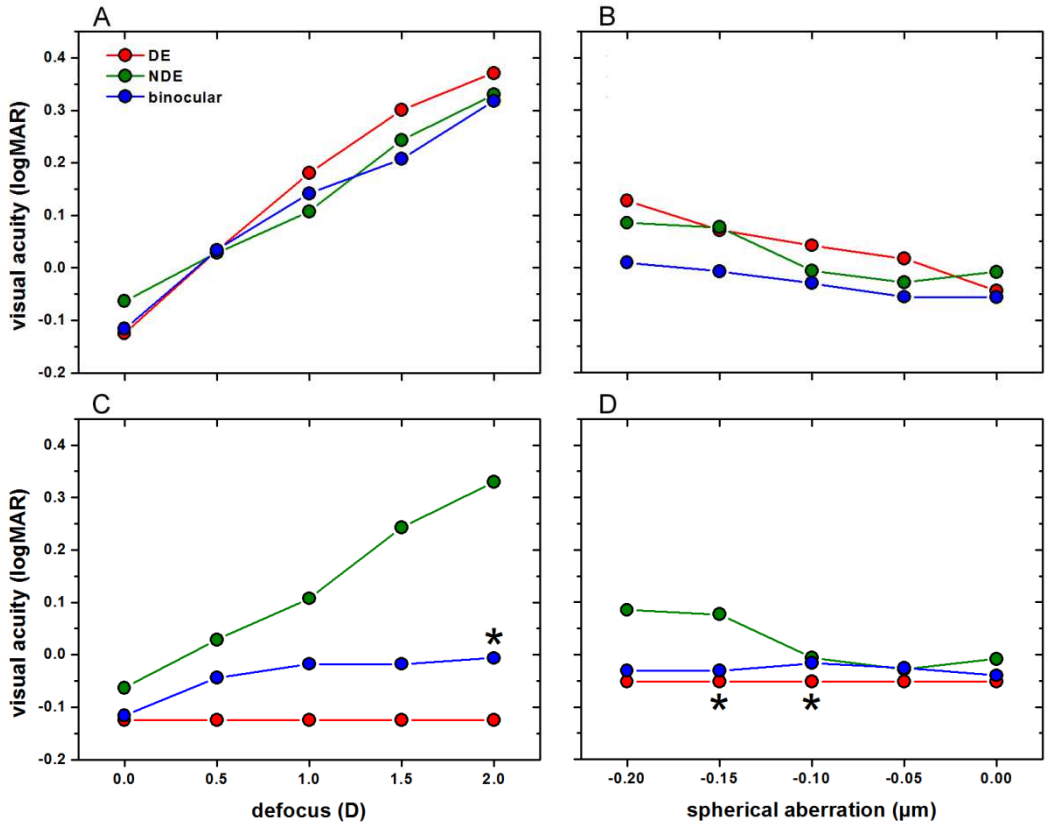

Figure 3.1: Monocular visual acuity for the dominant eye (DE) and the non-dominant eye (NDE) and binocular visual acuity when inducing aberrations bilaterally (A and B) or unilaterally (C and D). Asterisk mark statistically significant differences between binocular and best monocular performance.

3.4 Binocular summation

Average binocular summation ratios (BSRs) for induced defocus and SA are shown in Figure 3.2. The dashed line marks a BSR of 1 which means that binocular visual performance is equal to best monocular performance. As defocus was induced bilaterally, BSR showed an initial decrease but recovered then. Bilaterally induced SA had in general a positive effect on BSR. When SA was induced in equal measure in both eyes, BSR increased proportionally.

Unilaterally induced aberrations, however, had a detrimental effect on BSR. For both unilaterally induced defocus and unilaterally induced SA, BSR decreased first and leveled off for greater aberration inductions. Yet, BSR was only significantly reduced for unilaterally induced SA of -0.10 µm.

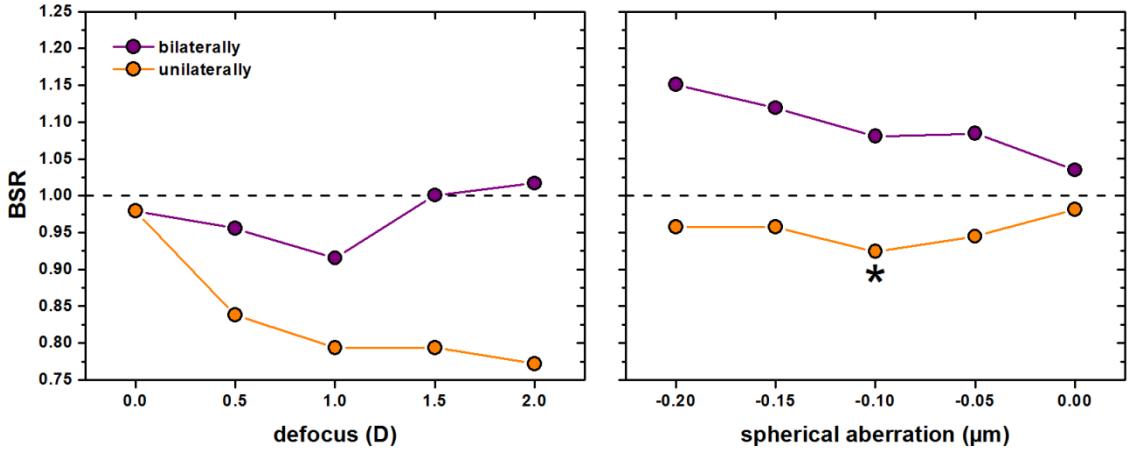

Figure 3.2: Binocular summation ratio (BSR) for bilaterally and unilaterally induced aberrations. The dashed line marks a BSR of 1, i.e. equality between binocular and best monocular performance and the asterisk a BSR statistically significant different from 1.

For unilaterally induced aberrations, BSR is shown against the interocular difference in visual acuities in Figure 3.3. The dashed line marks a BSR of 1. Measurements for individual subjects are coded with different symbols. For small IOD_VAs, BSR is close to 1 but as IOD_VA increases, BSR decreases approximately exponentially.

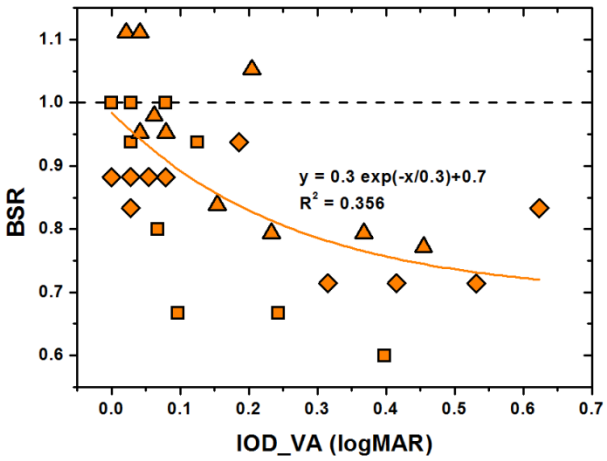

Figure 3.3: Binocular summation ratio (BSR) as a function of interocular difference in visual acuities (IOD_VA). The dashed line marks a BSR of 1 and different symbols stand for individual subjects.

3.5 Discussion

Previous studies have found that BSR depends on optical aberrations, i.e. the IOD between both eyes, and also on visual quality. Consideration of this behavior is of particular importance for the aging eye where optical aberrations increase whereas visual quality decreases, and in clinical practice, where the interocular difference in visual quality is increased externally to generate monovision-type presbyopia correction. In this chapter, we reported the effect of unilaterally and bilaterally induced defocus and

SA on binocular visual performance and summation with fixed artificial pupils. Here, only refraction and SA were corrected although AO visual simulators are capable to correct other HOA as well. We opted for this procedure to relate results to the two examples mentioned above of natural bilateral SA increase with age and external anisometropization with unilateral defocus and SA to overcome presbyopia. The pupil size of 4 mm in diameter was chosen to match a realistic adult pupil size in photopic light conditions (Winn *et al.*, 1994). Although this experiment was performed in monochromatic light, results should be valid in almost the same manner for polychromatic light. In a previous study, no difference in monochromatic and polychromatic CS was detected for the pupil size used here (Campbell & Gubisch, 1967).

Although both types of aberrations that were investigated in this study had rotationally symmetric phase profiles, essential differences in their effect on binocular visual acuity and summation were observed when induction was performed bilaterally.

As for bilaterally induced defocus, we found that the BSR decreases first but recovers for higher amounts. Thereby, BSR was lowest for 1 D of induced defocus. For 1.5 and 2 D of bilaterally induced defocus, however, BSR was greater than for distance. The general findings support thus a recent study by other authors where a positive correlation between BS and bilaterally induced defocus was found (Plainis *et al.*, 2011). The authors concluded that BS had the potential to mitigate the blurring effects of bilaterally induced defocus. In their study, BS was determined from binocular and monocular (dominant eye) VA measurements after inducing defocus with positive powered lenses of up to 2.5 D. As a result, VA decreased with induced defocus of 0.24 and 0.36 logMAR/D in case of binocular and monocular viewing, respectively. While binocular VA decline of 0.21 logMAR/D found in this study coincided rather well, monocular VA declines of 0.20 and 0.25 logMAR/D were found to be weaker here. In part, this could be due to a fixed artificial pupil size of 4 mm, whereas patients in the previous study performed visual testing through their natural pupils measuring about 4.2 and 4.7 mm for binocular and monocular conditions, respectively. With a larger pupil diameter under monocular visual conditions, vision is affected by a greater amount of aberrations which reduced the DOF of the eye. This should have a measureable influence on VA decrease. The authors of the previous study, however, estimated the effect to be small. Here, the defocus value of 1 D for which the smallest BSR was measured, corresponds to refractive correction for distance and an object located at 1 m. Interestingly, this was also the distance to the test chart in Plainis' study for which subjects were refracted. It remains to investigation whether BSR versus induced defocus would show another course if the test chart was located farther away.

Bilateral induction of SA had a clearly positive effect on binocular visual performance and summation. Binocular VA decrease was with 0.36 logMAR/µm about half the size compared with average monocular VA decrease. BSR increased from 1.03 to 1.15 when

0.2 µm of negative SA were induced in both eyes, while best monocular VA decreased by one line from -0.04 to 0.06 logMAR. The dependence of BSR on SA is probably the reason, why BSRs were reduced here. For best refractive correction with corrected SA, the average BSR was measured between 0.98 and 1.03 for different VA/induced aberration curves. This value is lower than the BSR of 1.1 reported elsewhere for natural SA (Cagenello *et al.*, 1993). However, for bilaterally induced SA of -0.05 µm, the average BSR agrees with the previously reported value. Although the sign of the aberration is inversed compared with the average SA for this pupil size (Salmon & van de Pol, 2006), magnitudes are largely in line. Comparing the effect of Zernike SA to defocus for the employed pupil size of 4 mm, 1 µm of induced SA resulted only thrice as detrimental as 1 µm of induced defocus under binocular viewing conditions but more than 5 times as detrimental under monocular viewing conditions.

For unilateral induction of both defocus and SA, binocular VA was worse than best monocular performance and consequently the BSR was reduced compared to the value achieved at best corrected refraction. Some twenty years ago, experiments on induced anisometropia with positive trial lenses that were located in front of one eye of a group of subjects revealed, that binocular CS summation decreased with increasing lens power reaching a minimum between 2 and 2.5 D (Pardhan & Gilchrist, 1990). Here we found, that binocular VA decreases when inducing defocus unilaterally and plateaus at about 0 logMAR. This behavior translates to a continuous reduction in BSR which levels off for higher defocus values. The same observation can be made when SA is induced unilaterally though the effect is smaller. Previous studies found, that for natural ocular aberrations, binocular CS summation was inversely correlated with natural IOD in visual quality and especially with IOD in SA (Jiménez *et al.*, 2008; Castro *et al.*, 2009). Here, we could extend this detrimental effect also to induced aberrations. BSR shows an exponential decrease as IOD in visual performance is increased.

Our most striking finding is probably the positive effect of increased bilateral SA on BS. In this way, the binocular visual system could, at least to some extent, naturally mitigate the effect when BS becomes reduced with age (Pardhan, 1996). As a practical implication for presbyopia correction, binocular monovision performance and summation is likely to be substantially increased when anisometropia is generated by a combination of defocus and SA. However, these speculations require further investigation.

4 Binocular visual acuity for the combined correction of spherical and longitudinal chromatic aberration

The human eye is affected by both monochromatic and chromatic aberrations. Monocular correction of ocular aberrations leads, in general, to improved visual outcome (Yoon & Williams, 2002; Artal *et al.*, 2010). In recent years, monochromatic aberrations, especially SA, have been extensively studied. It has been shown that SA plays a dominant role in visual performance and is the only aberration mode that averages to a non-zero value for a large population (Porter *et al.*, 2001; Castejón-Mochón *et al.*, 2002). In addition, it increases with age since the aberration balancing between the cornea and the lens (Artal *et al.*, 2001) breaks down (Artal *et al.*, 2002). Cataract surgery with aspheric IOLs (Artal, 2009) successfully restores the SA balance in the average old eye and, thus, improves visual quality with respect to cataract surgery with spherical IOLs (Holladay *et al.*, 2002; Guirao *et al.*, 2002*b*; Mester *et al.*, 2003).

The LCA of the eye is caused by the wavelength dependent refractive index of the ocular media and manifests in image planes at different distances from the retina for different colors. In contrast to monochromatic aberrations, the LCA of the eye does not present any age-dependency and shows very low inter-subject variability (Howarth *et al.*, 1988). Due to these properties, standard LCA correction based on the population average LCA could be feasible.

Previous theoretical calculations (Weeber & Piers, 2012) and studies using AO (Artal *et al.*, 2010) showed that vision could be improved by simultaneously correcting LCA and SA under monocular conditions. In a recent study (Weeber *et al.*, 2013), subjects were implanted with an IOL correcting both LCA and SA in one eye and an IOL correcting only SA in the fellow eye. Although this study included a small number of subjects, it showed a tendency for better visual performance in the eyes where both aberrations were corrected.

Binocular visual quality is more complex and the amount of binocular gain or loss depends on many factors. In the case of young subjects, binocular vision is in general superior to monocular vision for well-corrected optics (Campbell & Green, 1965*b*; Cagenello *et al.*, 1993). For binocular VA, an improvement of 11% compared to the monocular VA in the best eye was reported by Cagenello et al. (Cagenello *et al.*, 1993). Binocular summation (BS) is known to increase with decreasing contrast (Bearse & Freeman, 1994) and is inversely correlated to the interocular difference in sensitivity (Pardhan & Gilchrist, 1991) and optical quality (Pardhan & Gilchrist, 1990). For older subjects, the binocular summation ratio (BSR) decreases (Pardhan, 1996), so that the

binocular performance is well described by the monocular performance of the best eye.

In recent years, binocular adaptive optics visual analyzers (BAOVAs) have been introduced, offering the possibility to study binocular vision under carefully controlled optical conditions (Fernández *et al.*, 2009*a*, 2010). These instruments have been used to evaluate different presbyopia solutions (Tabernero *et al.*, 2011), and to investigate the effect of correcting HOAs on binocular VA and CS (Sabesan *et al.*, 2012).

To the best of our knowledge, the effect of the combined correction of SA and LCA has not yet been investigated for binocular vision. In this chapter, the visual benefit of correcting both SA and LCA was assessed under binocular conditions. This was compared to the expected performance for the typical pseudophakic patient implanted with conventional spherical IOLs.

4.1 Subjects

The three subjects who participated in this experiment were the same three subjects who took part in the previous monocular study (Artal *et al.*, 2010). Ocular data for the subjects can be found in Table 4.1 where aberration data are listed for a 4.8 mm pupil and the DE is marked with an asterisk. Subject ages at the time of the current study were 51, 39 and 52 years. Subjects 1 and 2 are right-eye dominant, and Subject 3 is left-eye dominant. All subjects reported normal eye health. Subjects 1 and 2 are mild myopes while Subject 3 is a near emmetrope. Astigmatism ranged from 0.25 D to 1 D. The average SA was 0.04 ± 0.03 µm for a 4.8 mm pupil.

For Subjects 2 and 3, accommodation was paralyzed and pupils were dilated with 1% Tropicamide. Subject 1 is presbyopic and his natural pupils were sufficiently large to conduct this experiment.

Subject	Age (y)	Eye	S (D)	C (D)	RMS (µm)	HOA-RMS (µm)	SA (µm)
#1	51	OS	2.75	-0.5	0.31	0.14	0.09
		OD*	2.75	-1	0.64	0.13	0.05
#2	39	OS	2.75	-0.75	0.55	0.21	0.04
		OD*	3.00	-0.5	0.30	0.16	0.01
#3	52	OS*	0.00	-0.25	0.23	0.18	0.020
		OD	0.25	-0.25	0.22	0.17	0.039

Table 4.1 Data of the subjects participating in this study for 4.8 mm pupils. The dominant eye of each subject is marked with an asterisk.

4.2 Experimental procedure

Wavefront aberrations were measured for a 4.8 mm pupil up to fifth order. Subjects' natural defocus, astigmatism and SA were statically corrected throughout the experiment. All higher-order aberrations, except SA, were not modified. In the experimental cases where SA was present, the average SA of pseudophakic eyes after spherical IOL implantation was induced by means of the LCoS-SLM. Based on the literature reporting SA in a pseudophakic population implanted with spherical IOLs (Mester *et al.*, 2003) and corneal SA in older eyes (Guirao *et al.*, 2000), a value of 0.149 µm for a 4.8 mm pupil was used. LCA effects were removed by performing the testing in monochromatic conditions, placing a 40 nm FWHM band-pass filter centered at 550 nm in front of the microdisplay. In order to keep the same luminance level for both the monochromatic and polychromatic conditions, additional neutral density filters were used to measure in polychromatic conditions.

In the following experiment, the condition in which visual testing was performed in white light inducing 0.149 µm of SA will be considered to be the reference situation because it emulates the vision of a pseudophakic patient implanted with a conventional spherical IOL in a natural (polychromatic) environment.

4.3 Visual testing

Visual testing was performed binocularly for four different cases: A) LCA and SA uncorrected (reference condition); B) LCA corrected and SA present; C) LCA present and SA removed; and D) both LCA and SA corrected. For clarity, the different cases are illustrated in Figure 4.1. In order to study the impact of every condition on BS, all four cases were repeated monocularly for the DE. Once an optical condition was set, a target letter with a detail size corresponding to 1 arcmin was presented on the microdisplay and the subject was given control over the defocus induced with the wavefront modulator. By scrolling a mouse wheel, the subjective best-focus position could then be adjusted in steps of 0.05 D. This procedure was repeated three times and the average was taken to be the final best-focus position. For binocular measurements, the best-focus position was adjusted for each eye monocularly while the fellow eye was covered with an eye patch.

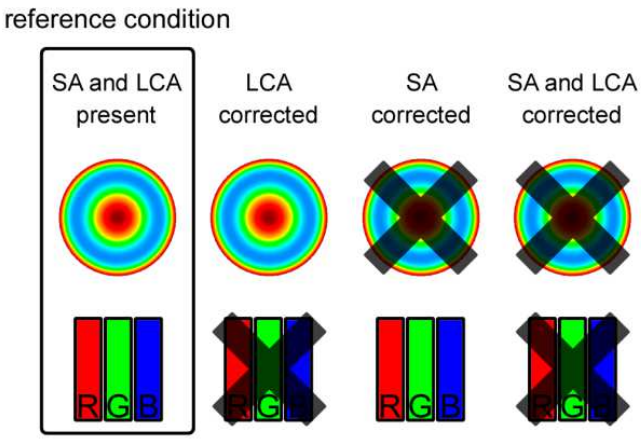

Figure 4.1: Illustration of the optical conditions which were simulated in this experiment.

VA measurements were performed using the illiterate E test presented at an intermediate contrast level of 30%. The subject adjusted the letter size to the approximate threshold and, subsequently, a tumbling E four-alternative forced-choice test was initiated. For each studied case, 7 letter sizes distributed in steps of 0.13 arcmin around the previously adjusted value were considered for the forced-choice test. Three runs were completed, each consisting of 42 presentations (6 per letter size) of a random-size randomly-oriented E letter for a duration of 300 ms. The subject was allowed to rest between runs but was given no feedback during the experiment. The averaged correct-response percentages were fit with a sigmoidal function. The acuity threshold was determined to be the letter size where the subject achieves 62.5% correct responses.

From the values obtained for VAs, three ratios were calculated: The BSR, defined as the ratio between binocular VA and monocular (DE) VA for the same visual condition; the binocular correction gain, defined as the ratio between binocular VAs before and after aberration correction; and the monocular correction gain, accordingly defined as the ratio between monocular VAs. Statistical significances were tested by performing paired student's t-tests.

4.4 Binocular performance and summation

Figure 4.2 shows the averaged monocular and binocular VAs for the four different cases of aberration correction. Monocular and binocular VAs tended to improve when aberrations were corrected. On average, for the cases in which LCA and SA were corrected separately, visual acuity was higher than for the reference case in which both types of aberration were present. The best VA for all individuals, both for monocular and binocular vision, was achieved when LCA, as well as SA, were corrected. In order to

quantify the improvement in VA due to aberration correction and BS, the ratio (correction gain) between different cases has been calculated.

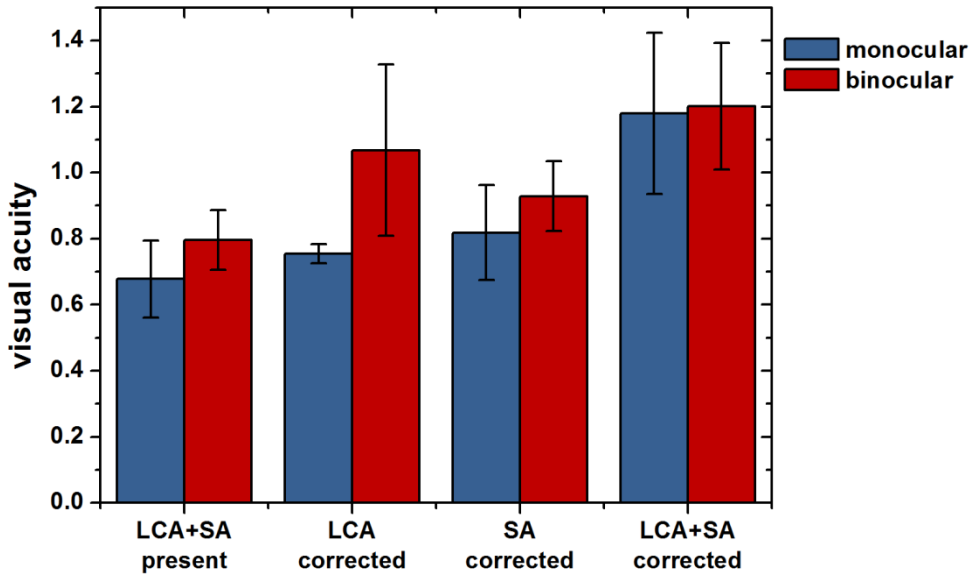

Figure 4.2: Average monocular and binocular visual acuity when correcting spherical aberration (SA) and longitudinal chromatic aberration (LCA) separately or in combination. Error bars represent standard deviations.

Figure 4.3 shows monocular and binocular correction gain. The blue bars represent the monocular correction gain. In agreement with previous data, individual correction of either LCA or SA produced an improvement in VA, while simultaneous correction of both aberration types further increased VA. The red bars in Figure 4.3 represent the binocular correction gain. Once again, correction of LCA or SA produced an increase in VA, both with the other aberration type present or corrected, with the greatest improvement occurring when both aberrations were corrected simultaneously. Table 4.2 gives statistical significance for differences between the individual levels of aberration correction. P-values for monocular VAs are shown in the left half of each cell, p-values for binocular VAs in the right half.

	correcting SA and LCA		**correcting SA**		**correcting LCA**	
SA and LCA present	0.001(***)	0.005(**)	0.017(*)	0.013(*)	0.206	0.045(*)
LCA corrected	0.060	0.065				
SA corrected	0.010(*)	0.007(**)				

Table 4.2: Statistical significance for the differences in visual acuity. The p-values for monocular VAs are shown in the left half of each cell, p-values for binocular VAs in the right half. Asterisks mark p-values if statistically significant (*: p-value<0.05, **: p-value<0.01, and ***: p-value<0.005).

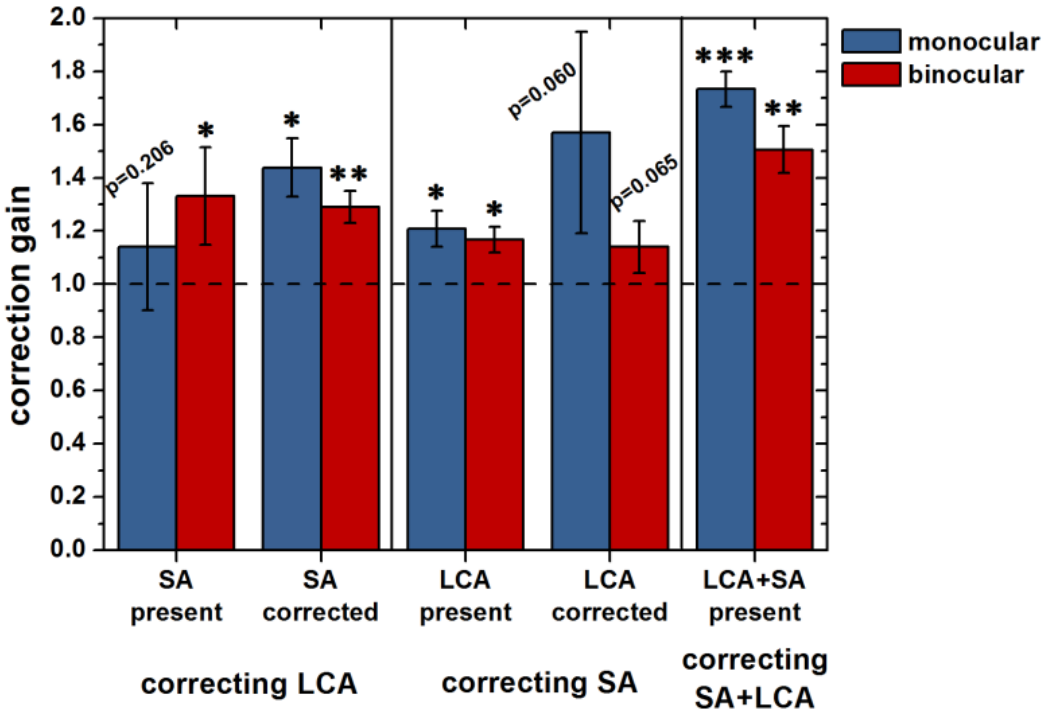

Figure 4.3: Mean correction gain (i.e., ratio between VAs) for different cases of aberration correction: LCA correction with SA present or previously corrected, SA correction with LCA present or previously corrected, and simultaneous correction of LCA and SA. Each value corresponds to the average across subject of the individual VA gains. Error bars represent standard deviations. VA gains are tagged with asterisks if statistically significant (*: p-value<0.05, **: p-value<0.01, and ***: p-value<0.005) or with the p-value otherwise. P-values are given in Table 4.2.

We also determined BS for each aberration correction condition. Figure 4.4 shows the BSR for each case. When LCA and SA are present, there is a statistically significant increase in VA. When either LCA or SA is corrected, the mean value of BS remains greater than 1 but shows higher variability across subjects. Due to this fact, the improvement in VA is not statistically significant in either case (p-value = 0.104 and p-value = 0.096, respectively). When LCA and SA are corrected in combination, BS is very close to one, both on average and for every subject individually. Table 4.3 gives the statistical significance for differences between binocular and monocular VAs.

LCA and SA present	LCA corrected	SA corrected	SA and LCA corrected
0.025(*)	0.104	0.096	0.286

Table 4.3: Statistical significance for the differences between monocular and binocular visual acuities at the same optical condition. The asterisk marks p-values smaller than 0.05.

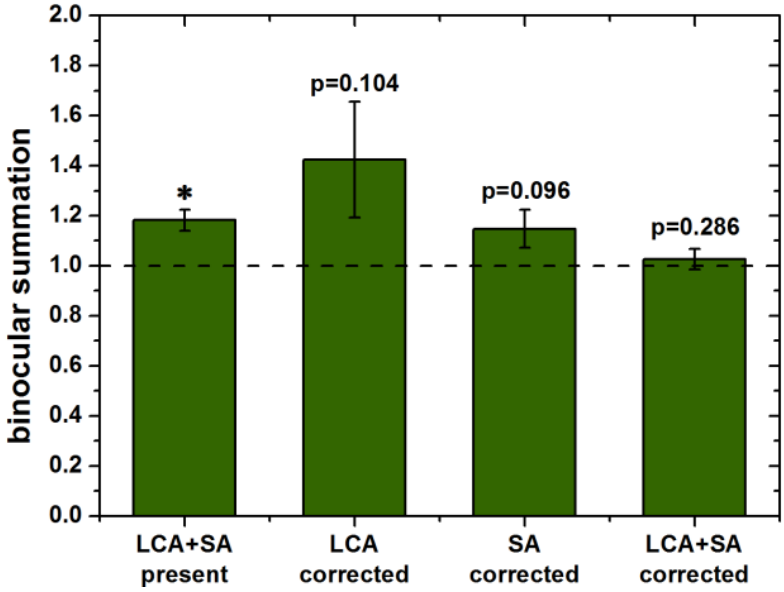

Figure 4.4: Binocular summation ratio for different levels of aberration correction, i.e. longitudinal chromatic aberration (LCA) and spherical aberration (SA) present, only LCA corrected, only SA corrected, and combined correction of LCA and SA. Error bars are standard deviations.

To further illustrate this point, Figure 4.5 shows binocular VA versus monocular VA for each subject and aberration condition. The black diagonal marks equality for monocular and binocular VA. In the uncorrected case (blue), the dots are located above the diagonal, indicating an improvement in VA due to BS. After correction of either LCA (green) or SA (yellow), the dots are still above the diagonal but there is a larger variability, especially in the LCA-corrected case. Finally, when both aberrations are simultaneously corrected, the orange dots approach the diagonal line, suggesting reduced BS.

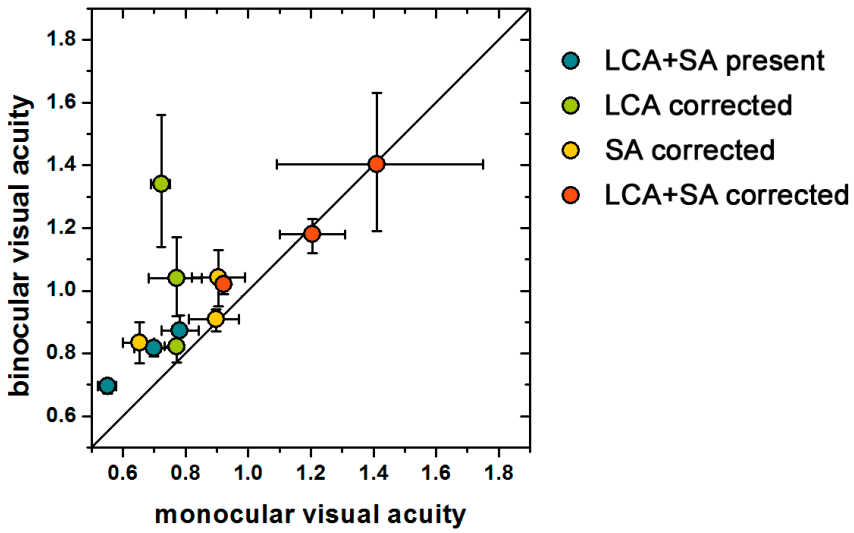

Figure 4.5: Binocular visual acuity versus monocular visual acuity. Each data point corresponds to an individual measurement for one of the subjects under a certain aberration correction condition indentified by color. Error bars correspond to one standard deviation. The black diagonal line marks equality for monocular and binocular data.

Figure 4.6 compares the three factors, that is, monocular correction gain (blue), binocular correction gain (red), and BS, averaged across subjects for three optical conditions: the reference condition, the case when only SA is corrected, and the condition for the combined correction of SA and LCA.

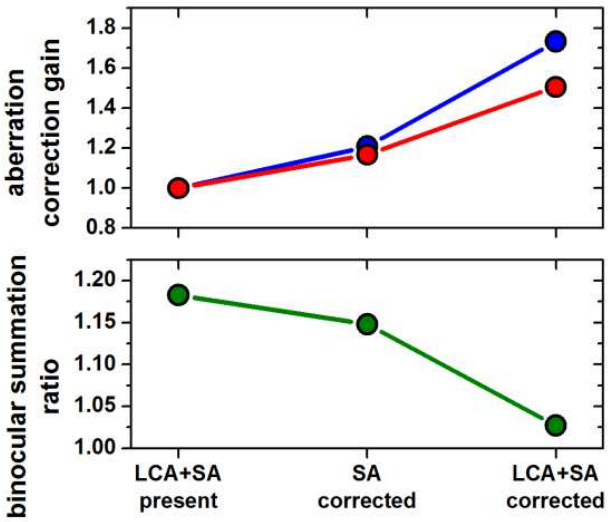

Figure 4.6: Average advantage factors for the reference case and the two aberration correction stages that are of interest for IOL design. The blue line represents the VA correction gain under monocular conditions, the red line represents the VA correction gain under binocular conditions and the green line represents the binocular summation factor for each case.

4.5 Discussion

The main goal of this study was to investigate the effect of the combined correction of spherical and longitudinal chromatic aberrations on binocular vision and to estimate the benefit of bilateral correction. In addition to performing a fundamental vision science study of these effects, we were interested in the potential results of a practical implementation of these types of corrections applied in cataract patients by implanting aspheric-achromatic IOLs. The average SA of pseudophakic eyes implanted with spherical IOLs was induced or corrected in both eyes with a binocular AO instrument. The LCA effects were removed by performing measurements in near-monochromatic conditions and comparing this to polychromatic conditions.

The experiment was performed with an artificial pupil diameter of 4.8 mm. This is considered to be a realistic pupil size for cataract patients under mesopic luminance conditions (Winn *et al.*, 1994). While for 4 mm pupils the effect of spherical and chromatic aberration is approximately equal (Campbell & Gubisch, 1967), monochromatic aberrations have a larger effect for large pupils. Monocular VA measurements averaged

across subjects confirm this finding. In the monocular case, the effect of correcting SA only was greater than the effect for correcting LCA only. However, under binocular viewing conditions, the behavior was reversed: the effect of correcting SA only was considerably smaller than for correcting LCA only. This finding may be due to the large differences between subjects and has to be further investigated.

VA was higher when aberrations were corrected than when aberrations were present when these cases were averaged across subjects. For binocular as well as for monocular measurements, the highest VA was achieved when both SA and LCA where corrected in combination. The VAs measured in this study were lower than those measured in the previous monocular study (Artal *et al.*, 2010) (0.7 versus 1 for the baseline case). However, the monocular aberration correction gain for the combined correction case was greater than in the previous study (1.73 versus 1.4). This difference may be explained by the decreased luminance of the vision test and the intermediate contrast letters that were employed in the current study.

While it is common practice to define the BSR as the ratio between binocular performance and monocular performance of the better eye, we calculated the ratio between the binocular performance and the monocular performance of the dominant eye. Although the BSR may be overestimated using this method, the difference should be considered to be small, due to the fact that all subjects had similar amounts of aberrations and comparable VA in both eyes as can be seen in Table 4.1.

BS is expected to be greater for sub-threshold than for threshold tasks. In particular, Sabesan et al. (Sabesan *et al.*, 2012) measured a decrease in binocular CS summation for the baseline aberration correction compared to additionally correcting SA and HOA correction, respectively (1.4 versus 1.3 and 1.3). However, they did not detect a difference in BS when measuring high contrast VA for the aberration correction states mentioned above and found a binocular VA summation ratio of 1.1 for all the cases. In order to investigate the effect of aberration correction, and to increase possible differences in BS, we employed intermediate contrast letters.

The average binocular VA was found to be higher than monocular VA for all correction states. The degree of improvement for binocular vision with regard to monocular vision depended on the optical condition. Binocular VA summation averaged across subjects decreased when increasing the level of aberration correction which is in accordance with findings for CS (Sabesan *et al.*, 2012).

For simultaneous correction of LCA and SA, binocular VA summation averaged across subjects was very close to 1, suggesting reduced BS compared to the reference condition. Plainis et al. (Plainis *et al.*, 2011) reported a BS of 13% for the case of best spherical correction. When inducing blur by means of spherical lenses, they observed an increase in binocular VA summation. Thinking of aberration correction in terms of im-

proving retinal image contrast and aberration induction in terms of deteriorating image contrast, these experiments are in line with the findings of Banton and Levi's study (Banton & Levi, 1991) and their theory of response saturation for high-energy, low-noise stimuli.

In our experiment, we removed chromatic effects by narrowing the spectral range of the test. This rather drastic method not only eliminates LCA but also transverse chromatic aberration (TCA). For pseudophakic patients, LCA may be corrected with IOLs by the use of refractive-diffractive designs. Natural foveal TCA is small in value (Rynders *et al.*, 1995) and should have small effects on visual quality for most subjects (Simonet & Campbell, 1990). However, induced TCA due to corrector misalignment or chromatic parallax (Zhang *et al.*, 1991) may reduce the advantage of this compensation of the eye's LCA if the IOL is not properly positioned (Tabernero *et al.*, 2006). Theoretical performance and limits of decentration have been computed based on realistic eye models (Weeber & Piers, 2012) and the results indicate that correction of SA and LCA with IOLs is a realistic option with some degree of tolerance.

Another relevant issue is the possible reduction in DOF after correction of these aberrations. Although, some level of DOF could be beneficial, it should be noted that in the real case of cataract patients, even an optimum correction of the aberrations studied herein would leave the rest of monochromatic aberrations uncorrected and thus provide some tolerance to defocus.

The subjects who participated in this study were relatively young compared to cataract patients. However, for older patients, VA is known to decrease due to age-related changes in the eye. In addition, BS decreases with age which is attributed to the loss of neurons and receptors in the visual pathway (Pardhan, 1996), and binocular visual performance tends to become closer to the monocular visual performance of the better eye (Rubin *et al.*, 2000). Therefore, the binocular VA gains found in this study may be reduced in older subjects studied as well as in cataract patients.

5 Binocular depth of focus with induced coma at different orientations

Once the eye is affected by cataract, the crystalline lens has to be removed and replaced by an IOL. Implantation of IOLs that extend monocular DOF by using an additional phase profile onto the refractive phase is thereby common practice. While it has been shown for monocular vision that HOA have a positive effect DOF (Guirao *et al.*, 2002*a*), they also reduce visual performance at best focus. In order to extend DOF without sacrificing visual performance at best focus, there is a continuous search for appropriate phase profiles. Fourth-order SA has proven to successfully extend DOF and is the traditional aberration term to be used. Besides, recent studies suggest combinations of fourth- and sixth-order SA (Yi *et al.*, 2011). However, other aberrations such as coma could also serve this purpose.

Like SA, coma belongs to the predominant aberration terms in a healthy population (Salmon & van de Pol, 2006). Thereby, corneal horizontal coma is balanced by the internal media of the normal eye (Kelly *et al.*, 2004; Artal *et al.*, 2006; Berrio *et al.*, 2010) probably by the angle between visual and optical axis of the eye itself. Absolute horizontal coma of the complete eye increases in peripheral vision (Lundström *et al.*, 2009) showing different signs for nasal and peripheral directions (Jaeken & Artal, 2012). The amount of natural coma can be altered due to several reasons. In diseased keratoconic eyes, vertical coma aberration is significantly larger than in healthy eyes (Maeda *et al.*, 2002) and increases progressively. Furthermore, cataract surgery modifies the natural aberration structure of the eye (Bellucci *et al.*, 2007) and in case of decentered or tilted IOLs coma is increased (Taketani *et al.*, 2004).

In recent studies, the interaction of coma with other aberrations has been investigated. AO studies revealed that certain combinations of induced coma and astigmatism can improve retinal image quality with respect to the condition of astigmatism alone (de Gracia *et al.*, 2010).

While VA did not improve for natural astigmats with the combination of coma and astigmatism, a visual benefit was detected for non-astigmatic subjects (de Gracia *et al.*, 2011). This beneficial effect was, however, reduced by the presence of other HOA. Furthermore, population studies showed a correlation between vertical trefoil and vertical coma aberration (Porter *et al.*, 2001; Thibos *et al.*, 2002). Villegas et al. found that subjects with a comparatively high amount of natural aberrations who exhibited coma and trefoil with opposite signs as predominant aberration terms, presented, in general, good VA (Villegas *et al.*, 2012). However, coma alone did not seem to be correlated with VA (Villegas *et al.*, 2008).

Results from other studies investigating the effect of coma on monocular DOF are largely in line with the beneficial interaction between coma and other aberrations. Cheng et al. observed DOF extension when presenting computationally coma-aberrated stimuli to observers with spectacle correction (Cheng *et al.*, 2004), whereas Rocha et al. found that induced coma did not significantly increase DOF when other HOA were corrected by AO (Rocha *et al.*, 2009).

As mentioned in chapter 3, for similar visual performance of both eyes and best corrected refraction, binocular summation (BS) occurs. However, BS not only depends on interocular performance difference but is also influenced in case retinal images do not fall on corresponding retinal areas. For artificially created fixation eso- and exo-disparities, binocular VA summation was found to be diminished (Jenkins *et al.*, 1992). In case coma is apparent in the visual system, the aberration gives rise to horizontal and vertical disparity in the retinal images. Therefore, BS is likely to suffer and induced coma might actually have a detrimental effect on binocular DOF.

In this chapter, we tested the potential influence of coma induced at different orientations on monocular and binocular VA and DOF. Additionally, the binocular situation was also evaluated.

5.1 Optical quality simulations

The PSF was calculated for a system affected by vertical coma. Wave aberrations, PSFs and rMTFs are shown in Figure 5.1. Inducing 0.22 µm of vertical coma over an otherwise aberration free 4.8 mm pupil, shifted the point where the PSF took its maximum by about 0.95 arcmin. Clipping the pupil to a smaller diameter of 3.5 mm, improved the Strehl ratio by a factor of 3 but maintained the PSF's vertical shift.

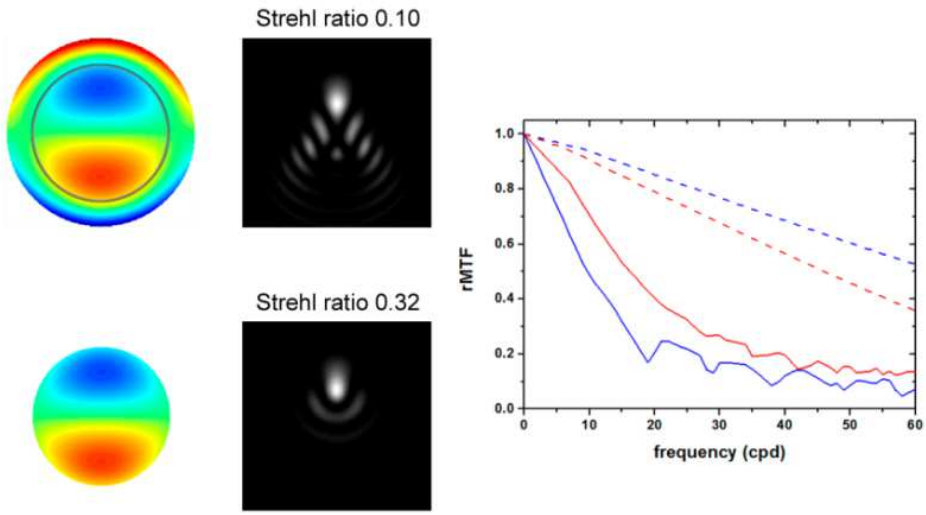

Figure 5.1: Wave aberration, point spread function, and radial modulation transfer function for the 4.8-mm pupil affected by coma (blue) and the according clipped pupil of 3.5 mm in diameter (red). Dashed lines represent diffraction limited performance.

A letter E of 10 x 10 arcmin was convolved with the PSFs for the cases of clipped coma with added defocus. Figure 5.2 shows simulated images. The vertical shift increased quadratically with defocus. Defocus values of 0.5 D and 1 D, no matter the sign, shift the images by 1.8 and 3.4 arcmin, respectively. Inverse signs of induced coma resulted in image shifts in inversed directions.

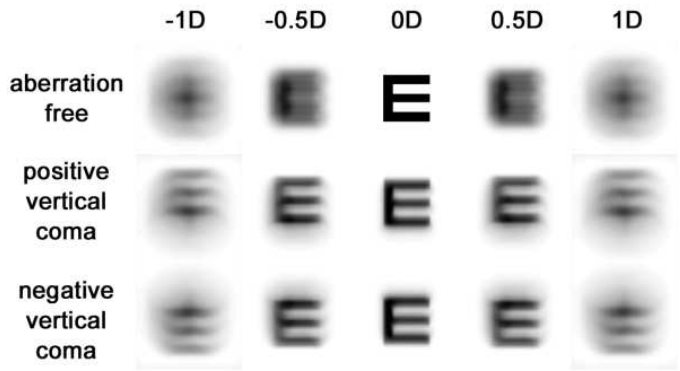

Figure 5.2: Simulation of retinal images of a letter E subtending 10 x 10 arcmin for defocus values ranging from -1 D to +1 D. The upper row represents images for an aberration free system. The two lower rows show images when the optical system is affected by positive and negative vertical coma (0.22 µm for a 4.8 mm pupil) and the pupil is clipped to 3.5 mm.

5.2 Subjects

Four trained male subjects participated in the experiment. Table 5.1 shows the refraction and aberration values of every subject. Ages were ranging from 33 to 52 years with a mean age of 40 ± 8 years. Inclusion criterion was a habitually uncorrected astigmatism of no more than 0.75 D. Two subjects are left eye dominant, the other two

subjects are right eye dominant. During the experiment, accommodation was paralyzed and pupils were dilated with 1% tropicamide. RMS values ranged from 0.09 µm to 0.22 µm for a 3.5 mm pupil. Coma RMS values obtained from the square root of both coma terms (Z(3,-1) and Z(3,1)) squared, ranged from 0.01 µm to 0.14 µm (average 0.06 ± 0.04 µm).

Subject	Age (y)	Eye	Subjective refraction (D)	RMS (µm)	HOA-RMS (µm)	Coma RMS (µm)
#1	52	OS*	-0.10 -0.53 x 119°	0.20	0.11	0.064
		OD	-0.46 -0.23 x 28°	0.17	0.15	0.14
#2	38	OS	-2.60 -0.57 x 66°	0.21	0.11	0.08
		OD*	-2.93 -0.26 x 120°	0.11	0.07	0.03
#3	38	OS*	-0.22 -0.61 x 92°	0.22	0.10	0.058
		OD	-0.22 -0.72 x 100°	0.24	0.07	0.01
#4	33	OS	-2.84 -0.26 x 159°	0.14	0.11	0.08
		OD*	-2.67 -0.12 x 73°	0.09	0.09	0.05

Table 5.1: Aberration profiles of the four subjects for 3.5 mm pupils after induced cycloplegia. The asterisk marks the dominant eye of the test person.

5.3 Through-focus visual acuity testing

After the full effect of cycloplegia and mydriasis was reached, wavefront aberrations were measured for both eyes. Subjects were then instructed to search for their monocular best focus for either eye while the fellow eye was occluded. The step size for best-focus search was set to 0.25 D. The subjects repeated the procedure three times and the average was calculated. The multiple of 0.25 D closest to the average was taken as preferred defocus correction. Astigmatism was left unmodified throughout the study.

Through-focus VA was measured for 37 conditions: 10 monocular conditions testing the dominant eye (DE), 10 monocular conditions testing the non-dominant eye (NDE), and 17 binocular conditions. To have a clear overview, all the conditions are illustrated in Figure 5.3. Monocular conditions corresponded to the case when 1) higher order aberrations remained unmodified, 2) natural coma was corrected, 3)-10) and 0.22 µm of coma was induced over a pupil of 4.8 mm at 8 different orientations, i.e. 0°, 45°, 90°, 135°, 180°, 225°, 270°, and 315° respectively. Binocular conditions comprised the cases when 1) aberrations remained unmodified in both eyes, 2) natural coma was corrected in both eyes, and 3)-18) 0.22 µm of positive vertical coma (0°) was induced in one eye and the same amount of coma but at different orientations in the fellow eye.

For the conditions when natural coma was corrected or induced, this was done statically, taking into account the aberrations that were taken at the beginning of the experiment. However, in between two through-focus series, we checked that aberrations

and in particular coma did not vary significantly (more than 0.05 µm over a 4.8-mm pupil). All other HOA were left unmodified. Although aberrations were induced and corrected over a 4.8 mm pupil, artificial pupils were set to 3.5 mm in diameter which lead to pupil clipping of the induced aberrations similar to the situation for which optical quality was simulated.

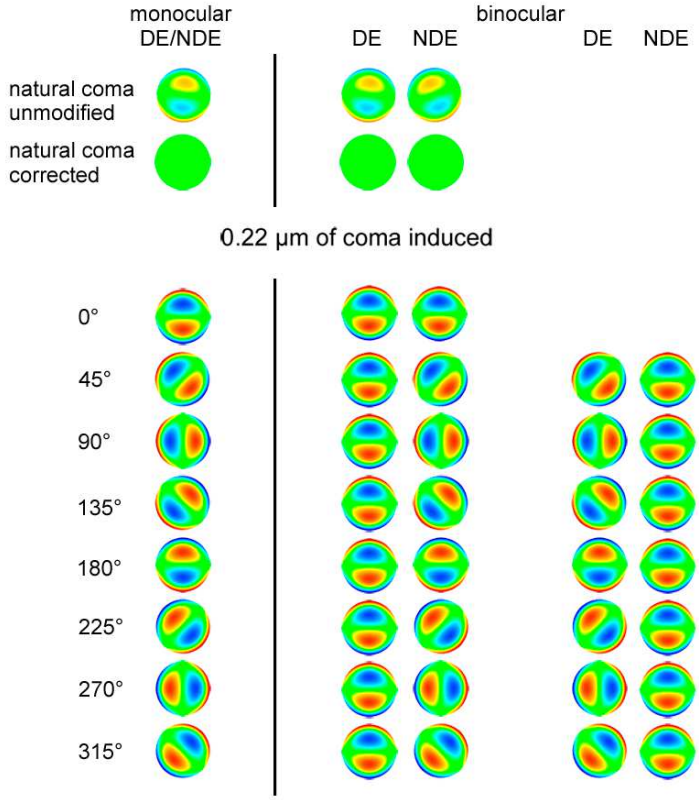

Figure 5.3: Monocular and binocular optical conditions for which through-focus visual acuity was measured. The modal amount of coma of 0.22 µm was induced over a 4.8 mm pupil.

Subjects were unaware of the order of testing conditions which was chosen randomly by the operators. However, neighboring points on through-focus curves were consecutive measurements. The test was a tumbling E test in green light presented on the microdisplay. During monocular testing, the fellow eye was occluded by an eye patch.

In general, VA was tested for a minimum range from -1.5 D to 1.5 D in increments of 0.5 D. However, if decimal VA was still better than 0.8, we extended this range until reaching this threshold. VA was taken 3 times at every defocus value by the method of adjustment. Through-focus performance was measured for the DE, the NDE and binocular. The whole experiment for one subject took about 4 hours organized in two separate sessions, including various breaks to rest and to refresh cycloplegia.

DOF was estimated by linearly interpolating the measured through-focus curves and determining the defocus interval over which decimal VA exceeded 0.8. Binocular VA

summation was calculated as the ratio between binocular decimal VA and best monocular VA.

As illustrated in Figure 5.4, data is presented in nasal-temporal coordinates of the DE and NDE since the aberrations of both eyes in general show mirror symmetry (Porter *et al.*, 2001). Positive horizontal coma is therefore referred to as nasal coma in OD and temporal coma in OS. Accordingly, negative horizontal coma is temporal coma in OD and nasal coma in OS.

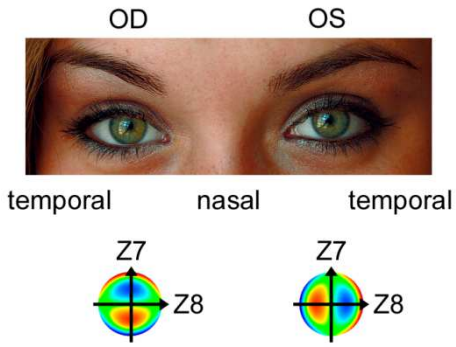

Figure 5.4: Due to mirror symmetry between both eyes and their aberration patterns, data is presented in nasal-temporal coordinates.

5.4 Monocular visual acuity and depth of focus

Figure 5.5 presents through-focus VAs averaged across subjects. Data for the subjects' DE is shown on the left and data for the NDEs is shown on the right. In the upper row, through-focus performance is illustrated for natural HOA and when coma aberration was corrected. Average best monocular VA with natural HOA unmodified of 1.3 ± 0.1 and 1.1 ± 0.2 in the DE and the NDE, respectively, was not altered significantly when the subjects' native coma aberration was corrected (1.24 ± 0.06 in the DE and 1.2 ± 0.2 in the NDE). In case of the reference condition of unmodified HOA, average DOF was 1.6 ± 0.2 D and 1.8 ± 0.3 D in the DE and the NDE, respectively. Correcting natural coma did not have significant influence on monocular DOF (1.8 ± 0.1 D and 1.6 ± 0.4 D, respectively). In the lower row, through-focus VA for induced coma is shown. For purpose of clarity, error bars were omitted. In most cases, induced coma had no influence on best focus position. Best through-focus VA slightly decreased when coma was induced, but remained on average greater than 1. For natural aberrations decimal VA decreased by about 0.53 ± 0.06 and 0.43 ± 0.04 per induced diopter of defocus in the DE and NDE, respectively. When coma was induced, slopes were noticeably shallower, especially in the DE. On average, decimal VA decreased by less than 0.33 ± 0.05 and 0.39 ± 0.01 per induced diopter of defocus.

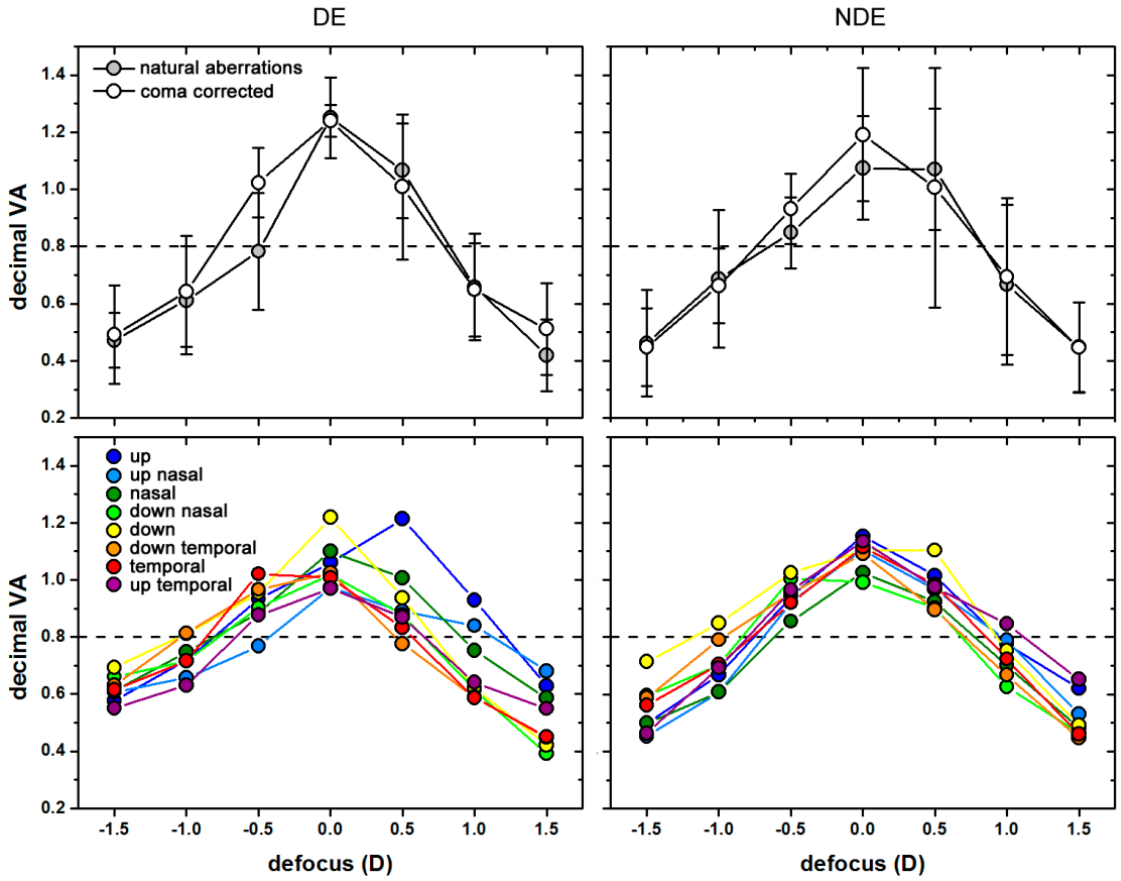

Figure 5.5: Through-focus visual acuity (VA) for the dominant eye (DE) and the non-dominant eye (NDE) averaged across subjects. The dashed line marks the threshold VA of 0.8 which was used to determine depth of focus. Error bars represent standard deviations.

Figure 5.6 shows the average monocular DOF for the subjects' DE on the left and for the NDE on the right extracted from through-focus VA curves. DOF for the reference condition of unmodified aberrations is illustrated in black and DOF for induced coma aberration is shown in blue. In most cases of induced coma, a DOF extension was observed, although the most beneficial effect appeared when induced in vertical direction. Positive vertical coma (up) extended DOF to 2.0 ± 0.3 D and 2.1 ± 0.6 D, and negative vertical coma (down) to 1.9 ± 0.5 D and 2.4 ± 0.2 D in the DE and NDE, respectively.

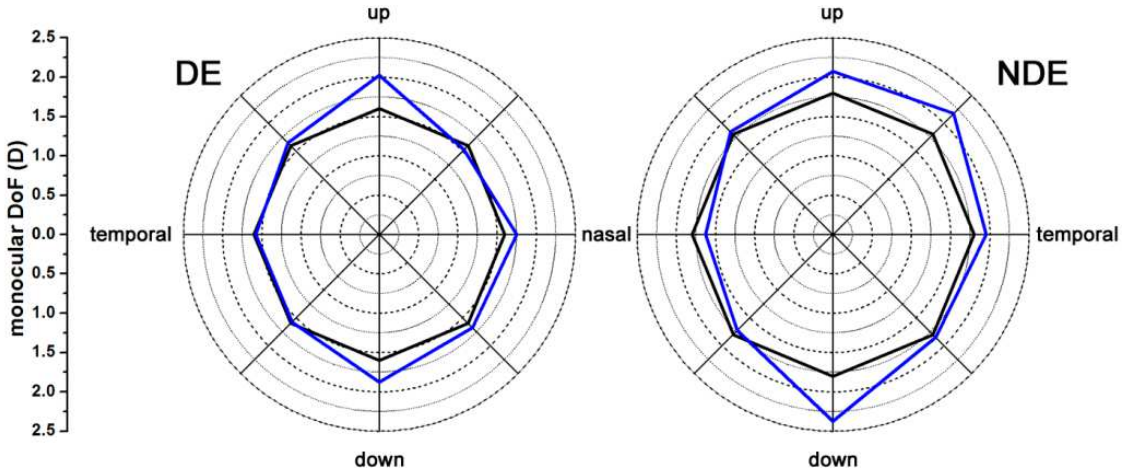

Figure 5.6: Average monocular depth of focus (DOF) in the dominant eye (DE) on the left and in the non-dominant eye (NDE) on the right. DOF for the reference condition of natural coma is illustrated in black, whereas DOF with induced coma aberration at different orientations is shown in blue.

Figure 5.7 compares monocular best through-focus VAs and DOF averaged across both eyes and all subjects. Inducing positive and negative vertical coma had no effect on best through-focus VA (1.2 ± 0.2 with natural aberrations versus 1.2 ± 0.1 for both orientations of induced vertical coma) but extended DOF by 0.4 D to 2.1 ± 0.4 D and 2.1 ± 0.5 D. DOF extensions with both types of vertical coma were found to be statistically significant (p=0.023 and p=0.036 for positive and negative vertical coma, respectively).

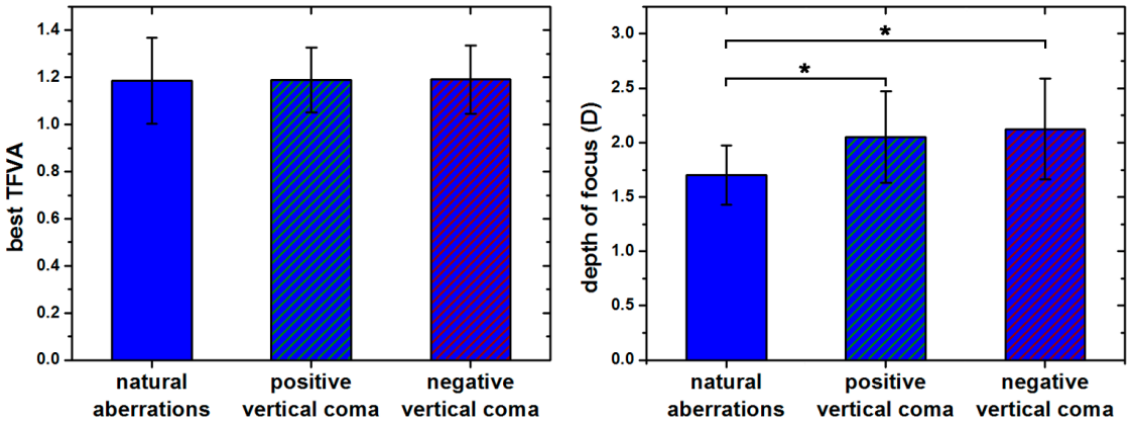

Figure 5.7: Monocular best through-focus visual acuity (TFVA) and depth of focus (DOF) for natural aberrations in comparison to data with induced positive and negative vertical coma. Error bars are standard deviations. Asterisks mark statistically significant differences between data (p<0.05).

5.5 Binocular visual acuity and depth of focus

Binocular through-focus VAs are shown in Figure 5.8. In the upper row, binocular through-focus performance is illustrated for natural HOA and when coma aberrations were corrected. Average best binocular VA with natural HOA was not altered signifi-

cantly when the subjects' native coma aberration was corrected (1.32 ± 0.09 versus 1.3 ± 0.1). In case of the reference condition of unmodified HOA, average binocular DOF was 2.0 ± 0.5 D. Correcting natural coma did not have significant influence on binocular DOF (1.9 ± 0.5 D). In the lower row, through-focus VA for induced coma is shown. For purpose of clarity, error bars were omitted. The left panel gives data when coma aberration was rotated in the DE and coma was induced in up-direction in NDE. The right panel gives data for rotated coma in the NDE and fixed coma in up-direction in the DE. In most cases, induced coma had no influence on best-focus position but decimal VA leveled off around the best focus position. Best binocular VA with induced coma ranged between 1.1 and 1.2. Decimal VA measured under binocular vision decreased with the same amount per induced diopter of defocus like under monocular vision (0.53 ± 0.01/D with natural aberrations and 0.39 ± 0.03/D with induced coma).

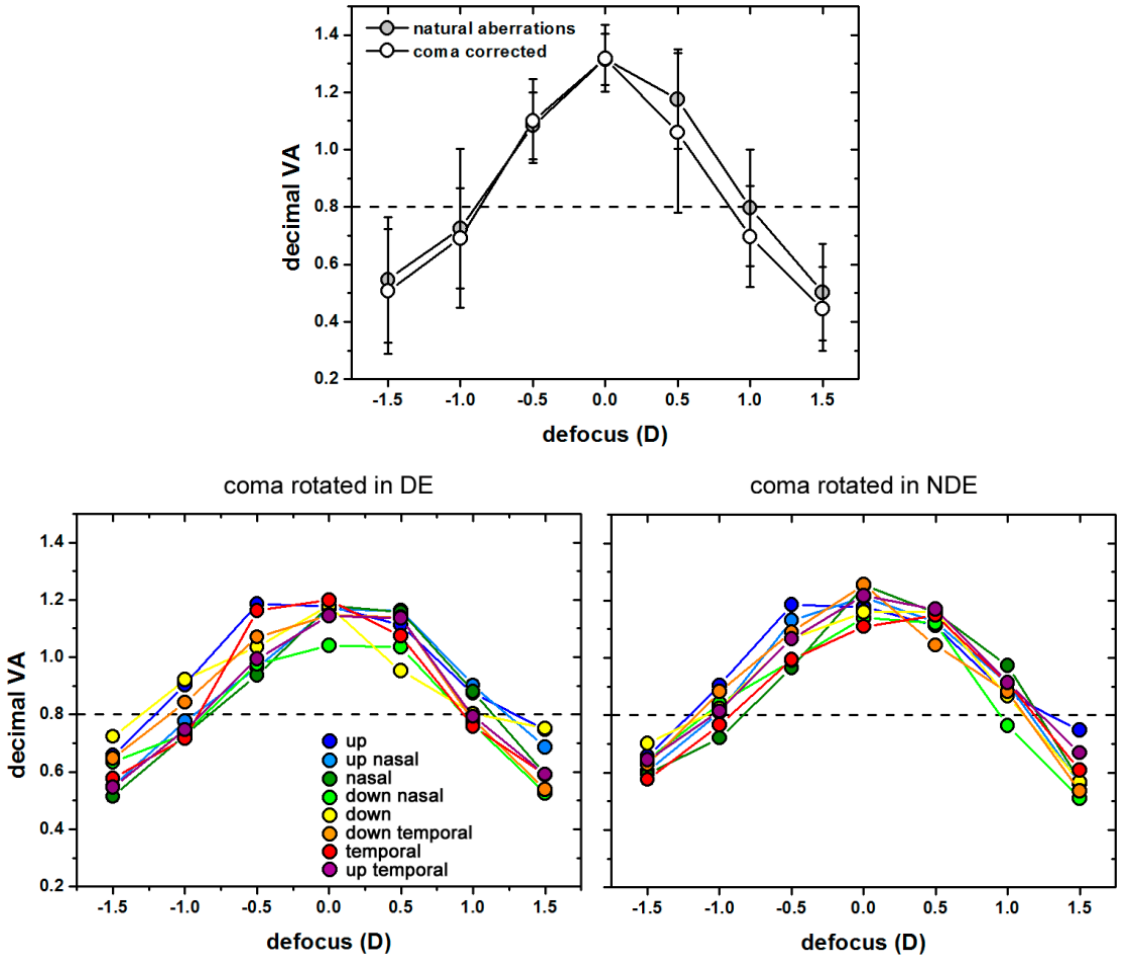

Figure 5.8: Binocular through-focus visual acuities (VA) averaged across subjects. The reference condition of natural aberrations and when coma aberrations were corrected are shown in the upper panel. The lower row shows VAs when coma was rotated in one eye (in the dominant eye (DE) on the left and in the non-dominant eye (NDE) on the right, respectively) and positive vertical coma was induced in the fellow eye. The dashed line marks the threshold VA that was used to determine depth of focus. Error bars represent standard deviations.

In Figure 5.9, binocular DOF is shown in blue, when coma was induced at different orientations in one eye (in the DE on the left and in the NDE on the right, respectively) and positive vertical coma was induced in the fellow eye. Binocular DOF for the reference case of unmodified natural aberrations is illustrated in black. Binocular DOF with induced coma was observed to be extended for most orientations with respect to DOF with natural aberrations. The smallest gain (<0.1 D) was found when inducing coma in nasal direction. In contrast, DOF was extended by more than 0.5 D when the following combinations of coma were: up-direction in both eyes and down-direction in the DE with up-direction in the NDE.

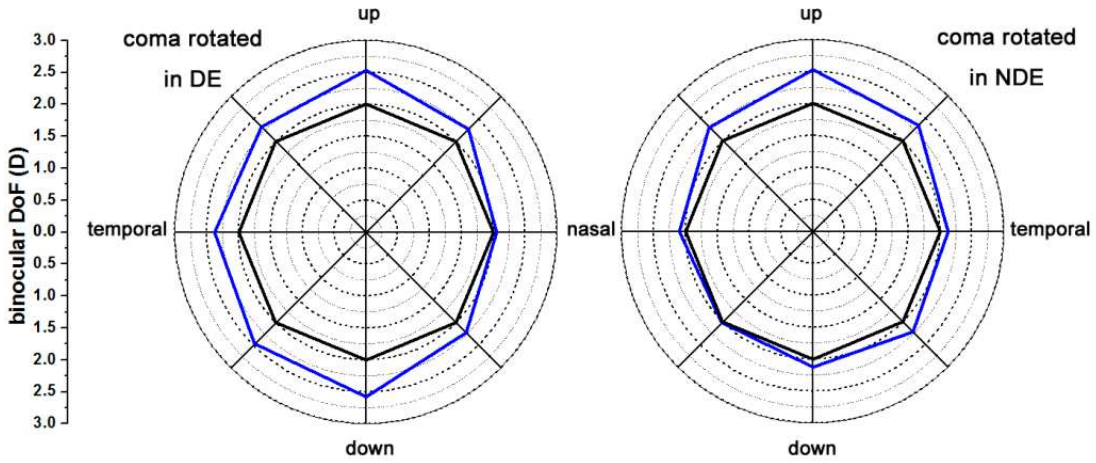

Figure 5.9: Average binocular depth of focus (DOF) when coma at different orientations was induced in the dominant eye (DE) on the left and in the non-dominant eye on the right, while positive vertical coma was induced in the fellow eye. The reference DOF for unmodified aberrations is illustrated in black.

Figure 5.10 shows binocular best through-focus VA in the left panel and DOF in the right panel for the cases when aberrations remained unmodified, when both eyes were induced with positive vertical coma and when one eye was induced with positive and the fellow eye with negative vertical coma. Data was averaged across both eyes and all subjects. Although best through-focus VA hardly changed with induced coma (1.2 ± 0.2 versus 1.2 ± 0.1 for induced positive and negative vertical coma), coma had a positive effect on DOF (2.0 ± 0.5 D versus 2.5 ± 0.7 D and 2.4 ± 0.8 D).

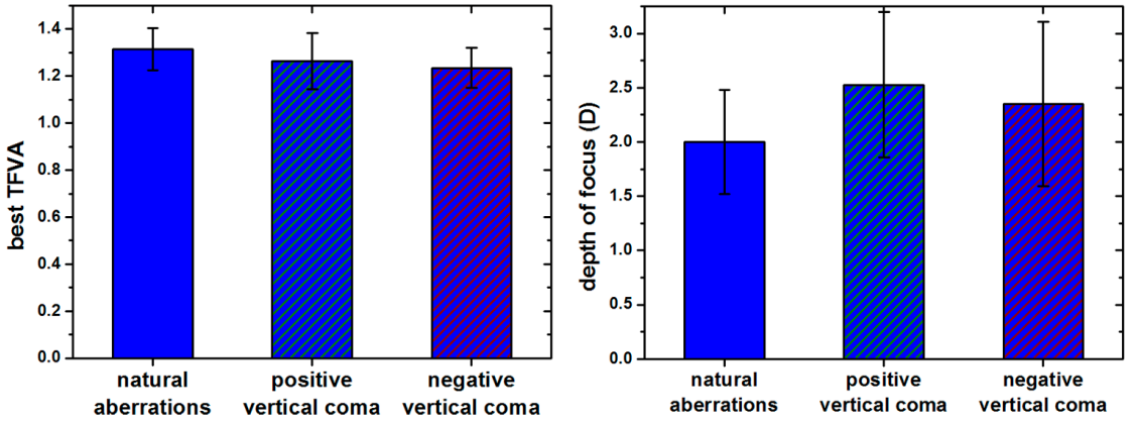

Figure 5.10: Binocular best through-focus visual acuity (TFVA) and depth of focus for natural aberrations compared to the cases when positive or negative vertical coma was induced in one eye while the fellow eye had positive vertical coma. Error bars represent standard deviations.

5.6 Binocular summation advantages

Due to summation, binocular performance is expected to exceed best monocular performance. In Figure 5.11 average through-focus VA and DOF with unmodified natural aberrations for both monocular visual conditions (NDE and DE) and under binocular conditions are illustrated. Binocular through-focus VA envelopes both monocular curves and consequently shows greater DOF than either eye alone (2.0 ± 0.5 D versus 1.6 ± 0.2 D and 1.8 ± 0.3 D).

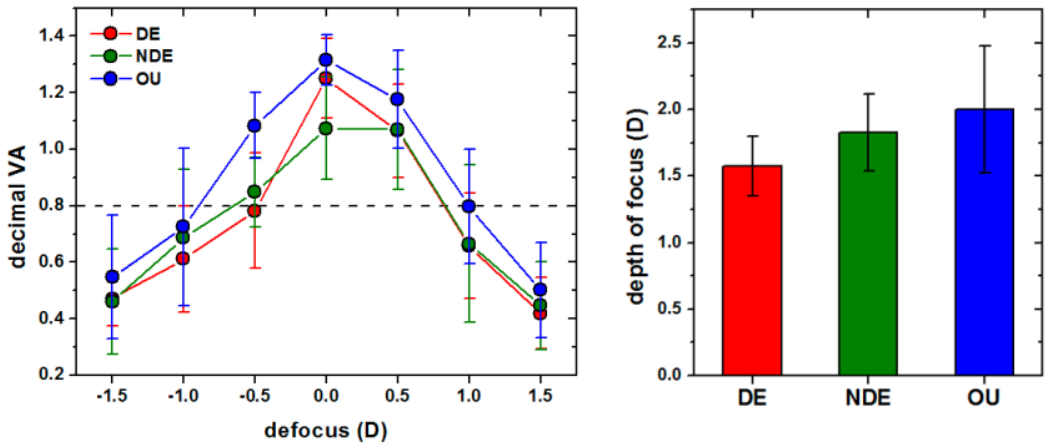

Figure 5.11: Average through focus visual acuity (VA) of the dominant eye (DE), the non-dominant eye (NDE) and binocular (OU) on the left and average depth of focus on the right. Error bars represent standard deviations

Binocular and monocular DOF are shown in Figure 5.12. Binocular DOF exceeded monocular DOF in nearly all cases. Binocular vision was most advantageous with positive vertical coma induced in both eyes. No advantage was observed when one eye was induced with coma in nasal direction. Combinations of positive and negative vertical

coma aberration induced in both eyes showed contradictory results. For negative vertical coma induced in the DE and positive vertical coma in the NDE, binocular vision was advantageous. The same types of coma but induced in contralateral eyes resulted in reduced binocular DOF with respect to monocular DOF of the NDE.

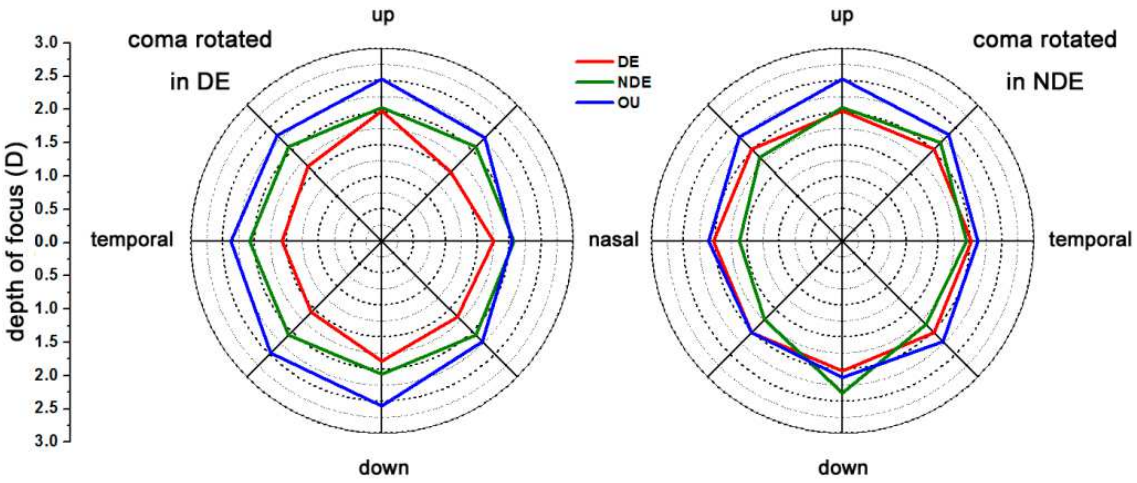

Figure 5.12: Binocular (OU) depth of focus when inducing positive vertical coma in one eye and rotating coma in the fellow eye compared to according monocular depth of focus of the dominant eye (DE) and the non-dominant eye (NDE) averaged across subjects.

Due to the relationship between binocular DOF extension and induced coma orientation, binocular VA summation seems to be affected. Binocular summation ratios were computed and averaged across subjects and defocus values. Results are shown in the left panel of Figure 5.13. The best average BSR was achieved with natural aberrations (1.09 ± 0.08) which is marked by the black dashed line. Binocular summation with positive vertical coma in both eyes was 1.03 ± 0.07. For all other cases, binocular summation ratios were lower. Except for two conditions (NDE up and DE up-nasal and up-temporal), this difference was significant ($p<0.05$). Since defocus increases retinal disparity when coma is induced at different orientations in both eyes, binocular summation suffers when defocus is added. In the right panel of Figure 5.13, BSRs versus defocus are given. Data is averaged across different combinations of disparity inducing comas. A second order polynomial fit results in good agreement with the data ($R^2=0.94$). The fit curve's maximum is reached at a myopic shift of about 0.25 D. In case of 1.5 D of hyperopic defocus, BSR is significantly smaller than 1.

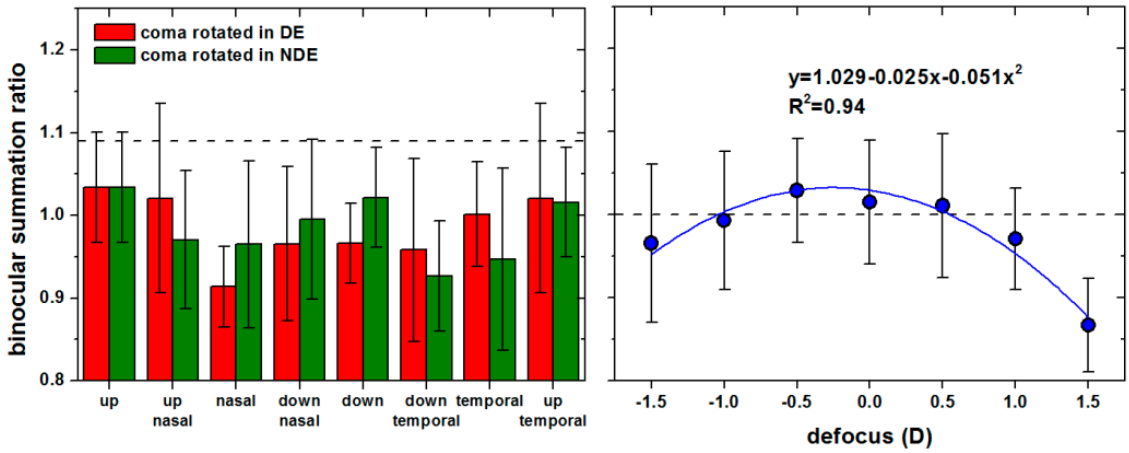

Figure 5.13: Left panel: Binocular summation ratio (BSR) averaged across subjects and defocus. The dashed line marks BSR for natural aberrations. Right panel: Binocular summation ratio versus defocus values averaged across all disparity-inducing conditions of added coma. The dashed line marks a BSR of one, that is, points lying under the line represent that binocular vision is of disadvantage compared with best monocular vision in terms of visual acuity. Error bars represent standard deviations.

5.7 Discussion

We investigated whether induced coma extends binocular DOF and to what extent relative coma orientation in both eyes plays a role thereby.

Apart from natural coma, aberrations remained uncorrected throughout the experiment. This procedure was agreed upon to permit possible beneficial interactions between induced coma and other aberrations. The amount of coma of 0.22 µm that was induced over a 4.8 mm pupil is about twice as big as the average coma in a healthy population (Salmon & van de Pol, 2006) and about 1.5 times bigger than the average natural coma for subjects involved in the study. Villegas et al. found a similar value to the one that was induced here in subjects with normal and excellent visual acuity (Villegas *et al.*, 2008).

Visual acuity was tested with the subjects viewing through an artificial pupil of 3.5 mm in diameter, so that the residual aberration was a combination of coma and a shift in direction of the induced coma. Although very good monocular VA can be achieved, tilts induce retinal disparity under binocular vision which is known to have a detrimental effect on binocular vision (Jenkins *et al.*, 1992). This situation actually does occur for a part of the population, however vertical coma is more frequent.

On average, VA was better in the DE of the subject group (1.3 ± 0.1 versus 1.1 ± 0.2) and DOF was greater in the NDEs (1.6 ± 0.2 D versus 1.8 ± 0.3 D) for unmodified natural aberrations. RMS values were also found to be slightly higher in NDEs than in DEs (0.19 ± 0.04 µm versus 0.16 ± 0.06 µm). Best through-focus VA was not affected signifi-

cantly by induced coma when visual tests were performed with high-contrast letters, neither monocular nor binocular. For all but one direction of induced coma, average best through-focus VA ranged between 1.1 and 1.2. However, to what extent performance with low-contrast letters is constrained, remains to be investigated.

We found that inducing negative and positive vertical coma in eyes of healthy subjects with uncorrected subclinical astigmatism and HOA had a positive effect on monocular DOF. For a 3.5 mm pupil, average monocular DOF was extended by 0.4 D. Astigmatism angles for participating subjects whose natural astigmatism exceeded 0.5 D were without exception close to the vertical axis, being in line with previous findings of a beneficial combination between astigmatism and coma with same or opposite orientation (de Gracia *et al.*, 2010, 2011). However, on average, increased DOF for vertical coma was observed to a similar extent in eyes without astigmatism. Inducing coma in diagonal directions, in contrast, had no effect on DOF. In consideration of the tumbling E letter having been presented in horizontal and vertical directions, this could occur due to the employed test itself. Repeating the experiment with Sloan letters might smooth the effect.

Although retinal disparity must have occurred under binocular vision due to the clipped pupil affected by coma, the amount was within Panum's fusional area and at no time subjects reported diplopia. As a result, binocular DOF also benefitted from coma induction. The effect seemed to be stronger when positive vertical coma was induced in the NDE and coma was rotated in the DE than for the reversed case. Probably this is due to the naturally larger DOF of the NDE compared to the DE for subjects included in this study. Furthermore, combinations with induced coma in nasal direction, proofed less gainful than induced coma in temporal direction, no matter the eye it was induced in. Although the experimenters did not detect vergence eye movements by means of the pupil camera, subjects could have unconsciously tried to compensate to some extent for induced horizontal disparities. However, entrance pupils of the system are fixed, and such attempts should only yield limited results.

Binocular summation was found to be significantly reduced with induced coma in both eyes compared with binocular summation for natural aberrations, except when coma was induced in both eyes at the same direction. Considering that rotated coma induces horizontal and vertical image shifts, the drop off can be attributed to retinal disparity between both eyes. Added defocus significantly increased shifts in retinal images and thus retinal disparity for binocular vision. Averaged across all orientation of induced coma and both eyes, binocular summation decreased quadratically with induced defocus.

6 Binocular visual performance with aberration correction as a function of light level

From our daily experience we know that visual performance decreases under low luminance conditions. A considerable amount of literature has been published on this topic. A complete study of visual performance over a large range of luminance levels was provided by Koenig as early as 1897 (Koenig, 1897). Results show that VA increases as a sigmoidal function of the logarithm of luminance, with a steep linear increase for intermediate light levels between -2.5 and 0.5 log cd/m^2. In this range, the relationship between VA and stimulus luminance is mainly due to two reasons. On the one hand, neural performance falls off when retinal illuminance is reduced (van Nes & Bouman, 1967). On the other hand, pupil diameters (Leibowitz, 1952), and with them aberrations (Campbell & Green, 1965*b*), increase for lower light levels and reduce the optical quality of the eye.

With the availability of AO instruments several studies investigated the benefit of monocular HOA correction at differing light levels. Yoon and Williams found a significant increase in VA when correcting monochromatic aberrations for a fixed pupil size of 6 mm in a group of subjects (Yoon & Williams, 2002). Thereby, the AO benefit was higher for a low luminance stimulus (2 cd/m^2) than for a bright stimulus (20 cd/m^2). A later study confirmed this behavior over a wider luminance range of 2 log-scales for VA (Marcos *et al.*, 2008). However, for AO benefits derived from CSs, an inversed dependency was reported for similar light levels and the same pupil size (Dalimier *et al.*, 2008). Moreover, Dalimier et al. extended the study for several fixed pupil diameters and found that the slope of AO benefit versus light levels became shallower with decreasing pupil diameters. From their measurements, they could estimate the AO benefit for a natural light-adapted pupil size.

While the studies mentioned above were performed with induced cycloplegic-mydriatic drugs and fixed artificial pupil sizes, pupil diameters increase with decreasing ambient luminance under normal conditions (Winn *et al.*, 1994). Furthermore, the research to date has tended to focus on monocular vision. In binocular viewing, natural pupil sizes are smaller than in monocular viewing under the same luminance conditions (Doesschate & Alpern, 1967). While smaller pupil sizes reduce the amount of aberrations of the eye but extend DOF (Guirao *et al.*, 2002*a*), retinal illuminance is reduced. Leibowitz and Walker observed a minor non-significant effect on binocular summation of suprathreshold stimuli when reducing retinal illuminance by three log scales (Leibowitz & Walker, 1956). However, stimuli viewed binocularly appear brighter than stimuli viewed monocularly. Binocular brightness summation was shown to

depend on the stimulus size. Ganzfeld conditions caused a summation of 2, whereas a 2°-field failed from evoking binocular summation (Bolanowski, 1987). In what way binocular summation of threshold stimuli is affected by reduced stimulus luminance and whether this can be influenced by aberration correction, still remains to investigation.

In an effort to better understand natural binocular vision under varying luminance conditions, this study investigates monocular and binocular visual performance with or without AO correction over a range of light levels. AO benefits and BSRs are deduced and interpreted.

6.1 Experimental procedure

Throughout the experiment, artificial pupils were set to 7 mm due to a limited area in conjugate pupil planes. The subjects' pupils were not dilated and the subjects were able to accommodate normally. Astigmatism and HOA of the subjects were corrected statically according to HSS measurements. Aberration measurement was performed for the largest available pupil size of individual subjects during illumination with the 780 nm laser diode. In case a subject did not reach a pupil diameter of 7 mm and aberrations had to be measured for a smaller pupil size, the wavefront modulator software expanded the wavefront map by extending the normalized pupil radius to the ratio between 7 mm and the pupil diameter during aberration measurement. In this way, the wavefront map was not altered for the measured pupil and did not suffer abrupt changes in case the pupil dilated to a diameter larger than the one during aberration measurement. To ensure the success of this method, the criterion was that all subjects had to reach a minimum pupil diameter of 5 mm during aberration measurement and that the difference between the pupil diameter for aberration measurement and the maximum effective pupil at the lowest luminance level could not exceed 1 mm.

The experiment involved high contrast VA testing in quasi-monochromatic (green) light for four different stimulus luminances in an otherwise dark room. The maximum stimulus luminance measured through the AO system was 2 cd/m^2. Stimulus luminance was then reduced by placing neutral density filters with optical density 1, 2, and 3 in front of the microdisplay, so that the effective stimulus luminances were 0.2 cd/m^2, 0.02 cd/m^2, and 0.002 cd/m^2, respectively. Visual testing was performed with best corrected refraction, with or without additional static HOA correction. Subjects adjusted their best-focus position themselves in increments of 0.1 D. This procedure was performed monocularly for either eye while the fellow eye was occluded with an eye patch. The average of three adjustments was taken as final value. The subjects' task was to conduct four-alternative forced-choice tumbling E tests under monocular and binocular viewing. Stimuli were presented during 300 ms. A psychometric

function was obtained for 3 series of 30 trials each. VA was defined as the letter size for which 62.5% of the orientations were correctly detected. For binocular viewing conditions, in addition, CS was measured for vertical Gabor patches with a carrier frequency of 6 cpd. The averages of three consecutive adjustments were taken as final CSs.

Subsequently, the binocular AO benefit was calculated as ratio between binocular visual performance (VA and CS) with AO correction and binocular performance without AO correction. Monocular AO benefits were derived accordingly as ratios between monocular VA with AO correction and monocular VA without AO correction. The BSR was determined by dividing binocular VA by monocular VA

6.2 Subjects

Three experienced subjects, aged 51, 41, and 28, participated in the study. They had normal binocular vision and no history of ocular disease. All the subjects are mild myopes with spherical errors between 1 and 3 D; Subject 1 is presbyopic. Table 6.1 provides the subjects' aberration data for a 5 mm pupil and the DE is marked with an asterisk.

Subject	Age [y]	Eye	Objective refraction [D]	RMS [µm]	HOA-RMS [µm]
#1	51	OS	-2.46 -0.57 x 68°	0.39	0.15
		OD*	-2.40 -1.01 x 92°	0.68	0.22
#2	41	OS	-2.40 -0.90 x 63°	0.62	0.24
		OD*	-3.02 -0.38 x 86°	0.32	0.20
#3	28	OS*	-0.93 -0.45 x 110	0.30	0.10
		OD	-1.01 -0.30 x 59	0.22	0.12

Table 6.1: Ocular data and aberrations for 5 mm pupils of subjects involved in the study. The asterisk marks the dominant eye.

6.3 Visual performance at low luminance

Figure 6.1 shows visual performance as a function of light level. In the left panel, VA data is illustrated. Typical standard deviations were about 15% of the average VA. Monocular VAs were omitted for the lowest stimulus luminance without HOA correction, since for two of the subjects, the stimulus luminance was too faint to search for the best-focus position. Average VA decreased with decreasing luminance, no matter if measured monocular, binocular, with baseline correction (noAO) or HOA correction (AO). For all luminance conditions, binocular VA was greater than monocular VA. Moreover, VA assessed during AO correction was always greater than VA with baseline

correction only. VA versus log luminance curves leveled off for the highest stimulus luminance. Curves for which average VAs were obtained over all stimulus luminances, were fit with linear regressions. For monocular AO corrected VAs a slope of 0.45 (R^2=0.99) was found. In case of binocular VAs, a slope of 0.44 (R^2=0.98) was found when HOA were not corrected. When HOA were corrected, the slope was 0.53 (R^2=0.98). For the lowest luminance, monocular and binocular performance with or without AO correction was similar.

In the right panel of Figure 6.1, binocular CS versus log luminance is shown. CS measurements for the lowest stimulus luminance without AO correction were omitted. Average CS decreased with decreasing luminance for both aberration correction conditions. For all luminance levels, CS with AO correction was greater than CS without HOA correction.

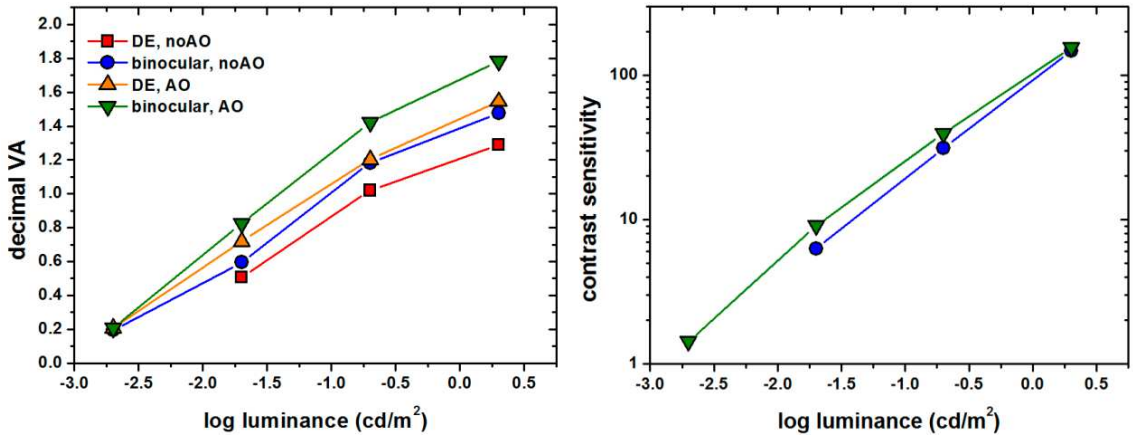

Figure 6.1: Average decimal visual acuity (VA) and contrast sensitivity measured for the dominant eye (DE) or binocular with or without adaptive optics correction (AO and noAO, respectively) versus log luminance.

Figure 6.2 shows average AO benefits versus stimulus light levels. Typical standard deviations measured about 0.15. Ratios derived from monocular and binocular VAs are presented on the left, whereas ratios derived from binocular CS are illustrated on the right. AO benefits increased significantly with decreasing luminance and were similar under monocular and binocular visual conditions.

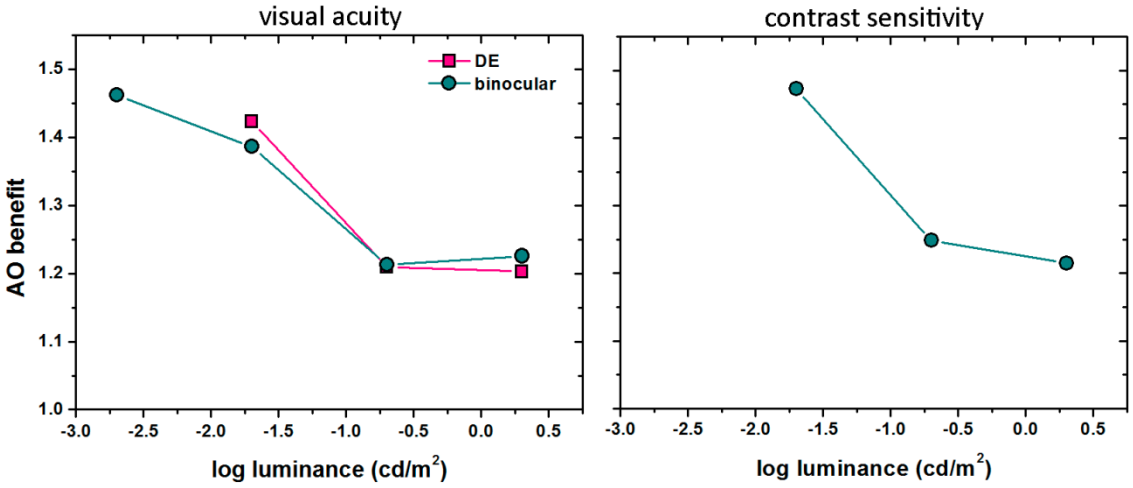

Figure 6.2: Average adaptive optics (AO) visual benefit derived from visual acuities (VA) on the left and contrast sensitivities (CS) on the right.

The left panel of Figure 6.3 shows BSR derived from VAs as a function of luminance. Standard deviations measured about 0.05. Without AO correction, the curve shows a slight, though not significant increase. With AO correction, the BSR was significantly greater for the lowest light level compared to the brightest stimulus luminance ($p=0.04$). Over the three highest luminances, in contrast, BSRs with and without AO correction were similar with an average value of 1.16 ± 0.02. In the right panel, BSR versus monocular VA is shown for individual subjects. For two subjects, BSR increased as monocular performance became worse. Linear regressions to the data provided slopes of -0.14 for Subject 1 ($R^2=0.99$) and -0.17 for Subject 3 ($R^2=0.91$), when the data point for the highest AO corrected monocular VA was neglected.

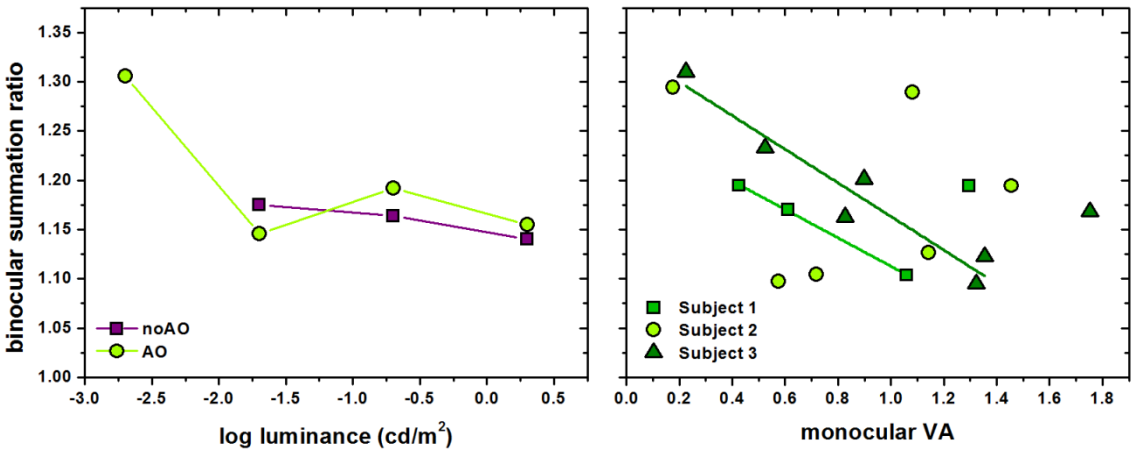

Figure 6.3: Average binocular summation ratio derived from visual acuities versus log luminance on the left and binocular summation ratio for individual subjects as a function of monocular visual acuity (VA) on the right. Colored solid lines in the right panel represent linear regression fits to the data.

6.4 Discussion

In the current study, we measured binocular and monocular visual performance over the range of luminances for which changes in performance are known to be greatest (Koenig, 1897). In accordance with this, VA versus log luminance curves flatten noticeably for the highest luminance measured in this experiment, and slopes of linear regressions fit to the data were found to be steeper than reported elsewhere for higher light levels (Marcos *et al.*, 2008). To the best of our knowledge, this is the first study that reports visual performance with AO correction at a stimulus luminance as low as -2.5 log cd/m2. Comparisons to other studies can therefore only be made for the highest stimulus luminance measured here of 0.5 log cd/m^2.

We found that AO correction improves binocular VA over a range of luminance conditions with vision through natural pupil diameters. The monocular AO benefit derived from VAs for the highest stimulus luminance of 1.2 is broadly in line with previous studies (Yoon & Williams, 2002; Marcos *et al.*, 2008). Monocular AO benefits measured with natural pupil diameters increase with decreasing light levels from 1.2 to 1.4. Dalimier et al. predicted a similar range of AO benefits with natural light-adapted pupils for CSs (Dalimier *et al.*, 2008). The binocular AO benefit shows a similar course and increases for the lowest luminance to about 1.5. Since at this luminance the natural pupil diameters were similar to the limiting artificial pupil diameters, the binocular AO benefit found here, can be taken as benefit occurring under natural pupil conditions for our group of subjects. Thereby, the factor depends on both the amount of aberrations and the natural light-adapted pupil diameters of the subjects.

In a previous experiment with fixed artificial pupils and intermediate contrast letters presented in Chapter 4, the monocular aberration correction benefit was found to be greater than the binocular correction benefit. In the current experiment, one might expect to observe a similar or even stronger effect considering the reduced pupil size and thus a smaller amount of aberrations when viewing a stimulus of equal brightness under binocular instead of monocular conditions. However, a negligible difference in monocular and binocular AO was found, not revealing a consistent trend. There are several possible explanation for this result. For the small visual test field used here, monocular and binocular pupil diameters are assumed to differ little (Watson & Yellott, 2012). Additionally, visual tests employed high contrast letters which are less affected by HOA as is generally known. For a vision test employing a larger visual test field and low contrast letters, probably a greater difference in monocular and binocular AO benefit can be observed.

BSR was calculated here as the ratio between binocular VA and monocular VA of the dominant eye. In other studies, BSR is defined as the ratio between binocular VA and monocular VA of the better performing eye. Although our definition could result in

higher BSRs, the difference should be minor, since monocular VA acuities and the amount of HOA were similar between both eyes of individual subjects. Average BSR for the highest stimulus luminance was calculated as 1.14 ± 0.05 when HOA were present and 1.16 ± 0.05 when HOA were corrected. Both values accord with earlier reports for BSRs derived from VAs (Cagenello *et al.*, 1993; Plainis *et al.*, 2011; Sabesan *et al.*, 2012).

With respect to dependence on luminance, we found that binocular summation averaged across subjects increased with decreasing light levels. However, BSRs were similar for both aberration correction conditions. The BSRs of individual subjects showed a linear correlation with monocular VA which is consistent with the findings of previous studies (Plainis *et al.*, 2011; Sabesan *et al.*, 2012) where BSR averaged across subjects decreased as the level of aberration correction increased. The correlation between BSR and monocular VA is interesting as it implies that binocular VA is a quadratic function of monocular VA. It is possible to hypothesize that this behavior might be related to receptive field sizes responsible for vision at a certain optical condition and due to activation of a larger number of neurons as Plainis et al. speculated (Plainis *et al.*, 2011). Further research needs to be done to establish whether this correlation exists also between the BSR derived from CSs and monocular CS.

The current study estimates the visual benefit when HOA are corrected under natural binocular visual conditions. Successful HOA correction presents a major advantage under low luminance conditions in monocular and binocular viewing. The study provides additional evidence to the ameliorating effect of binocular compared to monocular vision when optical quality is reduced.

7 Refractive changes at low luminance under monocular and binocular vision

With the transition from the photopic to the scotopic luminance ranges, the visual system undergoes significant changes, including modifications of optical as well as neural factors (Leibowitz, 1952; van Nes & Bouman, 1967). An interesting trend regarding refraction is that with decreasing luminances the human eye becomes more myopic. This phenomenon, referred to as night myopia, was first mentioned by Maskelyne in the late XVIII century (Levene, 1965) and was widely studied during WWII to improve night-vision instruments (Otero & Durán, 1941; Wald & Griffin, 1947; Koomen *et al.*, 1951). Although night myopia has been known about for such a long time, it still lacks complete understanding due to the number of contributing and probably subject-dependent factors. The large number of conducted experiments thus produced conflicting results.

From the beginning SA was thought to be the main reason for the relative myopic shift (Koomen *et al.*, 1949, 1951). The overall SA of the unaccommodated human eye is positive on average. That means that the outer zones are more myopic with respect to the central zone. As the pupil size increases for lower luminances, the amount of SA grows and can therefore cause a myopic shift. Certainly, the Purkinje shift plays a role for night myopia (Wald & Griffin, 1947). However, already Wald and Griffin concluded that the Purkinje shift in combination with the chromatic aberration of the eye causes a moderate change in refractive power of about 0.4 D. The strength of the effect depends thereby on the subject and the spectrum of the light source used for visual testing. Further, it is known that the eyes take up their states of rest in case of no apparent stimulus (Schober, 1954; Leibowitz & Owens, 1978). Although dark vergence and dark accommodation seem to be independent from each other, both can contribute to the relative myopic shift. When the eyes are not fixated on some object, they are converged to a point about 0.89 meters away (Owens & Leibowitz, 1980). Then, the peripheral retina is involved in the visual process for which the eye is known to be relatively more myopic by some tenths of a diopter (Jaeken & Artal, 2012). Besides, subjects involuntarily accommodate in the dark. While this was already investigated by Otero and Duran (Otero & Durán, 1941) and later on by Wald and Griffin (Wald & Griffin, 1947), the effect could not be separated from that arising from ocular SA.

Recently, current state-of-the-art technology permitted to revisit the phenomenon of night myopia under largely controlled optical conditions (Artal *et al.*, 2012). Using an invisible infrared laser for wavefront sensing and a remote controlled AO system, a monocular AO visual simulator was adapted to operate under extremely low lumi-

nance conditions. The aim of the study was to quantify the contribution of the different factors described above to the relative myopic shift occurring with low luminance in a group of subjects. Results proofed a limited role of SA and the combination of the Purkinje-effect with the LCA of the eye in night myopia and identified the accommodative error in dim light as the main contributing factor.

Having found in a previous experiment that binocular summation is greater at low light levels (see Chapter 6), the intention of the study described in this chapter was to find out if there was a detectable difference in the relative myopic shift with lower luminances under monocular and binocular visual conditions. Additionally, the effect of SA in combination with the natural light-adapted pupil size was investigated.

7.1 Experimental procedure

Artificial pupils were set to 7 mm, but since no cycloplegic-mydriatic drugs were used, the subjects' pupils could adapt normally in size to given lighting conditions and accommodation was not impeded. Astigmatism and HOA of the subjects were corrected statically according to HSS measurements. Aberration measurement was performed for the largest available pupil size of individual subjects during illumination with the 780 nm laser diode. In case a subject did not reach a pupil diameter of 7 mm (dmax), aberration coefficients for astigmatism and SA were scaled to this pupil size according the following formulas:

$$C(2,\pm2)_{7mm} = C(2,\pm2)_{dmax} \cdot \left(\frac{7}{dmax}\right)^2 \quad \text{and} \quad C(4,0)_{7mm} = C(4,0)_{dmax} \cdot \left(\frac{7}{dmax}\right)^4$$

In this experiment, we determined defocus shifts for low luminances (0.6 cd/m^2, 0.06 cd/m^2, 0.006 cd/m^2, 0.002 cd/m^2) with respect to the baseline condition of the highest stimulus luminance (0.6 cd/m^2) when the ceiling light was on. Stimuli were polychromatic (white) and presented on the OLED display. The subjects' task was to adjust their best-focus position subjectively, starting at a hyperopic defocus. For the baseline luminance condition, best focus was adjusted for the left and right eye separately. Henceforth, for binocular measurements the interocular defocus difference was kept constant and defocus could only be added in equal measure for both eyes when the luminance level was reduced. Defocus adjustment was performed three times and the average rounded to one decimal place was taken as value. For every luminance condition, the subjects' natural light-adapted pupil diameters were measured by means of the pupil camera after adjustment of the best-focus position. Subjects performed the defocus adjustment monocularly and binocularly with natural HOA, and corrected or induced SA. In particular, three magnitudes of SA were induced over a 7 mm pupil: 0.3 µm, 0.6 µm and 0.9 µm.

7.2 Subjects

Five experienced subjects aged between 27 and 51 years (average 37 ± 9 years) participated in the experiments. The 51-year-old subject is presbyopic; the remaining subjects were either nearly emmetropes or mild myopes (< 3 D). Table 7.1 gives their ocular data and aberrations obtained through HSS measurements and evaluated for a 5 mm pupil. The subjects' average SA for a 5 mm pupil is 0.06 µm (corresponding to 0.23 µm for a 7 mm pupil). Visual testing was performed with natural pupil sizes and normal accommodation.

Subject	Age (y)	Eye	Objective refraction (D)	RMS (µm)	HOA-RMS (µm)	SA (µm)
#1	34	OS	-0.48 -0.42 x 5°	0.30	0.15	0.08
		OD*	-0.41 -0.27 x 163°	0.23	0.15	0.08
#2	31	OS	-0.31 -1.24 x 35°	0.84	0.28	0.05
		OD*	-1.67 -0.54 x 87°	0.42	0.24	-0.01
#3	27	OS	-0.29 -0.40 x 2°	0.31	0.17	0.08
		OD*	-0.60 -0.02 x 135°	0.25	0.25	0.14
#4	51	OS	-2.46 -0.57 x 68°	0.39	0.15	0.10
		OD*	-2.40 -1.01 x 92°	0.68	0.22	0.10
#5	40	OS	-2.55 -1.15 x 63°	0.62	0.24	0.02
		OD*	-3.26 -0.31 x 90°	0.32	0.20	-0.06

Table 7.1: Ocular data and aberrations for 5 mm pupils of subjects involved in the study. The asterisk marks the dominant eye.

7.3 Optical quality simulations

As an optical quality metric, the area under the radially averaged monochromatic MTF between 0 and 60 cpd was computed. Since we wanted to estimate the position subjects would judge as best-focus, the metric was calculated for defocus values from 0 to 2 D in increments of 0.1 D for different optical conditions. The maximum rMTF was assumed to occur at the defocus, a subject would choose as best-focus position. The metric was computed for perfect optics and a 7 mm pupil or for optics affected by SA of different amounts, i.e. 0.3 µm, 0.6 µm, and 0.9 µm. The pupil was then clipped to a series of diameters between 4 and 6.5 mm and the metric was computed again through-focus.

The left panel of Figure 7.1 shows the area under the rMTF as a function of defocus for a 7 mm pupil. Best-focus position was at 0 D, 0.3 D, 0.9 D and 1.4 D for induced amounts of SA from 0 µm to 0.9 µm in increments of 0.3 µm. Linear regressions determined a slope of 1.60 D per µm of induced SA (R^2=0.98). In the right panel, the simulated relative best-focus shift versus the clipped pupil diameter is shown in case the full 7 mm pupil is affected by positive SA of 0.3 µm, 0.6 µm, and 0.9 µm. The graph

shows that mainly the best focus position for 0.3 µm of SA is affected when the pupil is clipped. The remaining best-focus positions are largely the same as for the larger 7 mm pupil. As a consequence, best-focus versus induced SA slopes are but slightly shallower with a minimum value of 1.53 D/µm for a pupil diameter of 4 mm (R^2>0.99).

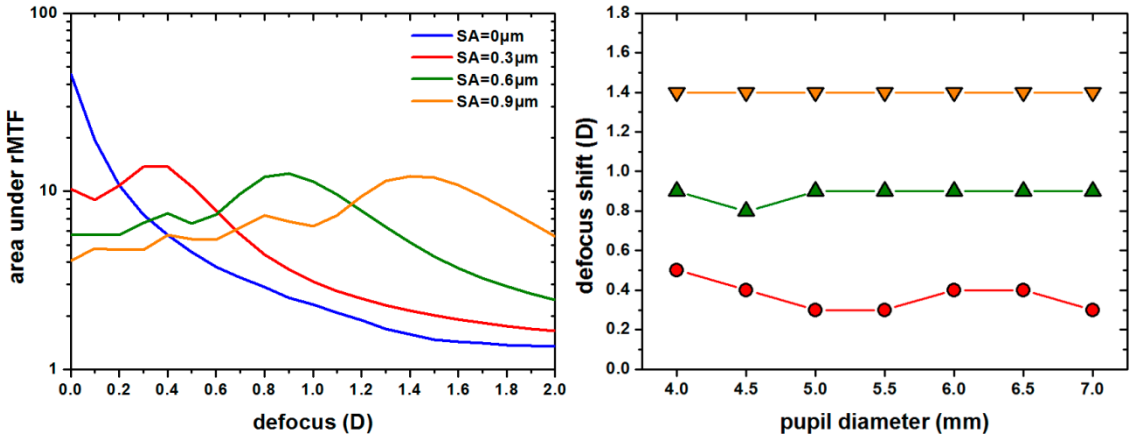

Figure 7.1: Area under the radially averaged MTF computed through-focus for a 7 mm pupil affected by different amounts of SA on the left, and defocus shift versus clipped pupil diameters when the full 7 mm pupil is affected by different amounts of SA (color coded).

7.4 Best focus shift for reduced light levels

Figure 7.2 shows average light-adapted pupil diameters as a function of background luminance under monocular and binocular visual conditions. The dashed line marks the limiting artificial pupil diameter of 7 mm. Monocular and binocular pupil diameters increased from 4.5 to 7.4 mm and from 3.9 to 7.2 mm over the whole luminance range. For all luminance conditions, monocular pupil diameters were larger than binocular pupil diameters. However, a statistically significant difference of 0.6 mm was only found for the highest stimulus luminance when the ceiling light was on (p=0.031). For lower luminance levels, monocular and binocular pupil diameters differed by about 0.2 mm.

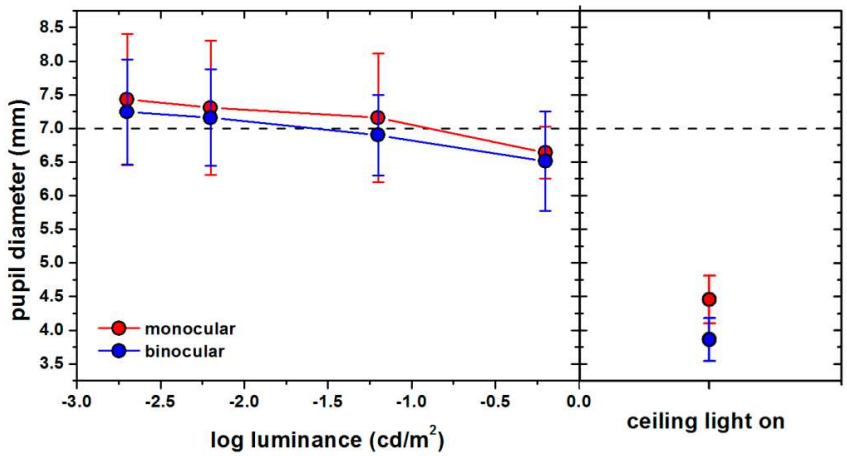

Figure 7.2: Pupil diameter as a function of stimulus luminance when the ceiling light was off compared with pupil diameters for the highest stimulus luminance when the ceiling light was on. The dashed line marks the limiting artificial pupil diameter of 7 mm.

Figure 7.3 gives the average relative defocus shift versus induced SA for different background luminances. In the following, defocus shifts are intended as relative values and zero diopters of defocus refer to the best focus position that was determined for the reference condition of high ambient luminance and corrected spherical aberration. For all luminances, a hyperopic defocus shift between 0.4 and 0.6 D per 0.3 µm of induced SA was observed. Under monocular visual conditions, the hyperopic shift tended to be smaller for lower luminances.

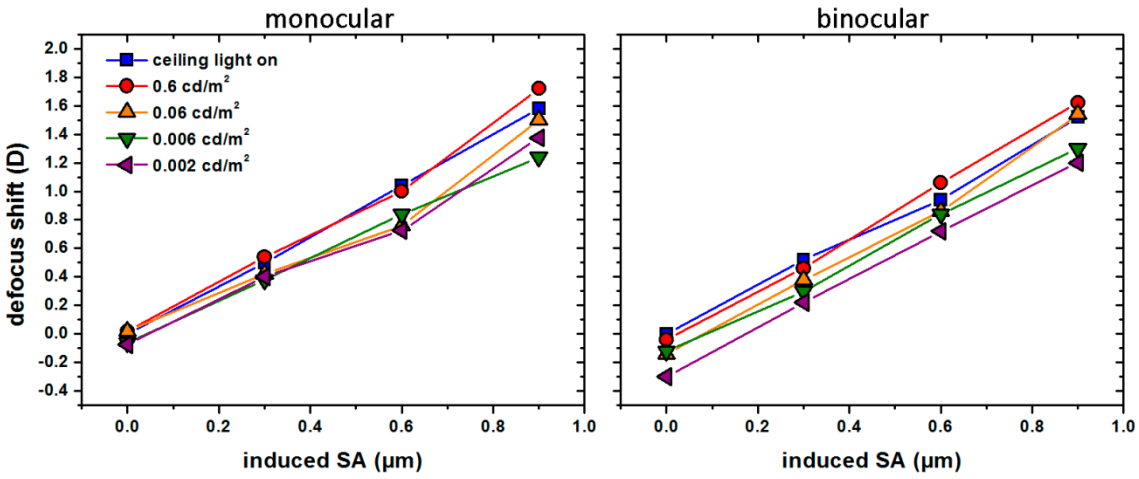

Figure 7.3: Relative defocus shift as a function of induced SA for monocular and binocular vision.

Linear regressions were fit to the data for individual subjects. Averaged slopes are presented in Table 7.2. Monocular slopes showed a small decrease with decreasing stimulus luminance. Also standard deviations decreased with decreasing stimulus luminance. Monocular and binocular slopes were similar for the same luminance. However, for the three lowest stimulus light levels, standard deviations under binocular conditions were only half the standard deviation found under monocular conditions.

	monocular slope (D/µm)	binocular slope (D/µm)
Ceiling light on	1.8 ± 0.7	1.7 ± 0.6
0.6 cd/m^2	1.9 ± 0.7	1.9 ± 0.6
0.06 cd/m^2	1.6 ± 0.5	1.8 ± 0.3
0.006 cd/m^2	1.5 ± 0.5	1.6 ± 0.2
0.002 cd/m^2	1.6 ± 0.4	1.7 ± 0.2

Table 7.2: Average slopes of linear regressions fit to the defocus shift versus induced spherical aberration (SA) data of individual subjects.

Figure 7.4 represents the relative defocus shift averaged across subjects under monocular and binocular visual conditions when stimulus luminance is reduced. On average, subjects became more myopic with decreasing luminance, no matter whether SA was modified or not. When SA remained unmodified (red squares), this myopic shift was statistically significant only for the lowest luminance condition under monocular viewing (-0.22 D, p=0.005). However, under binocular vision a statistically significant difference of -0.18, -0.17, and -0.22 D was detected for the three lowest luminance conditions (p=0.010, p=0.006, and p=0.003, respectively).

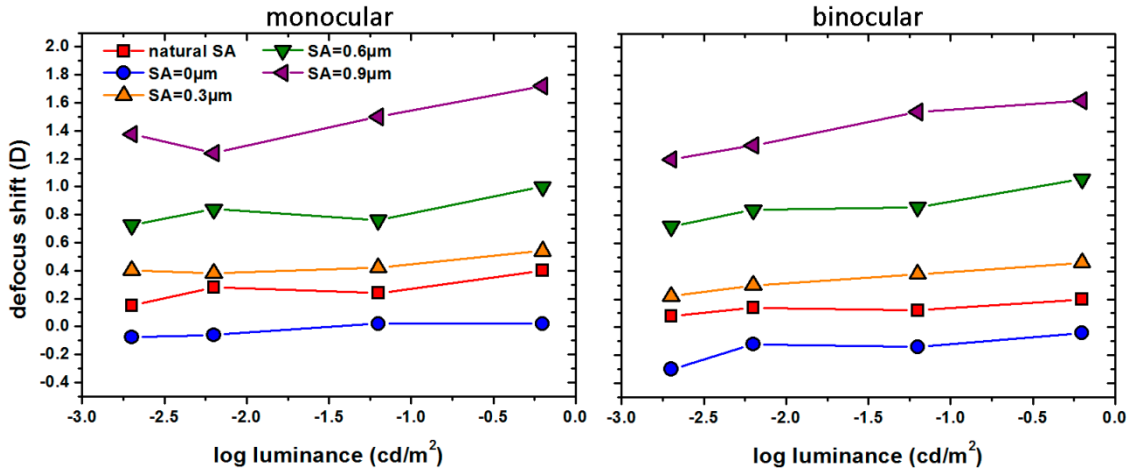

Figure 7.4: Relative defocus shift as a function of stimulus luminance for monocular vision on the left and binocular vision on the right.

Linear regressions were fit to the defocus shift versus log luminance data for individual subjects. Table 7.3 gives averaged slopes and standard deviations. In general, monocular and binocular slopes were similar and both tended to increase with the amount of induced SA. The increase was however not statistically significant. Comparatively smaller average slopes and particularly small standard deviations were found for unmodified natural SA.

	monocular slope ($D/(cd/m^2)$)	binocular slope ($D/(cd/m^2)$)
natural SA	0.07 ± 0.09	0.04 ± 0.06
SA = 0 µm	0.07 ± 0.17	0.08 ± 0.09
SA = 0.3 µm	0.06 ± 0.11	0.09 ± 0.11
SA = 0.6 µm	0.09 ± 0.17	0.12 ± 0.21
SA = 0.9 µm	0.22 ± 0.12	0.17 ± 0.19

Table 7.3: Average slopes of linear regressions fit to the defocus shift versus log luminance data of individual subjects.

7.5 Discussion

Pupil sizes were found to be comparatively large and to differ little under monocular and binocular visual conditions, except when the ceiling light was additionally switched on. This can be attributed to the small visual test field of 0.95° which was limited by the optical system. A larger test field might lead to different results. For low luminance stimuli, subjects might have involuntarily tried to use their peripheral retina by adjusting their vergence to the background luminance. Due to the fixed entrance pupils of the AO instrument, however, the success of the attempt should be limited. In particular, in the images taken with the pupil camera no significant vergence differences could be observed.

Average slopes for defocus shift versus induced SA data are in accordance with the previous simulations for all luminances. For lower luminances, average monocular slopes gained by experimental data approach the simulated value and standard deviations become clearly smaller. A similar behavior was observed for average binocular slopes and related standard deviations. These findings reflect the small inter-subject variability and objectively confirm the subjects' general perception to be able to judge best-focus positions easier and with enhanced certainty for lower stimulus luminances and binocular vision.

Interestingly, average slopes of defocus shift versus log stimulus luminance data and standard deviations were minimal when natural SA was not modified. Average slopes increased though not significantly with the amount of induced SA. Optical quality simulations estimating the effect of pupil clipping when a 7 mm pupil is affected by SA showed that best-focus is not shifted for 0, 0.6 and 0.9 µm of induced SA. For 0.3 µm of induced SA which is close to the average SA across the group of subjects rescaled to a 7 mm pupil, the best-focus position shifted very little (0.2 D). In our measurements, the effective average pupil diameter varied from 4.5 to 7 mm and from 3.9 to 7 mm under monocular and binocular viewing, respectively. When the ceiling light was off, average pupils were always greater than 6.5 mm. Therefore, it is very unlikely that pupil clipping accounts for the best-focus shift.

The defocus shift that occurs at lower luminance levels is small, i.e. 0.22 D, but statistically significant for unmodified SA and can be fully explained by the Purkinje-shift in combination with the LCA of the eye which was estimated as 0.4 D for the microdisplays' spectrum. However, the Purkinje-shift can neither explain the change in monocular slopes of defocus shift/induced SA curves nor the increase in slopes of defocus shift/log luminance curves with increasing amounts of induced SA. It can be speculated that the combined effect of an extended DOF and the accommodative lag could account for these changes (Gambra *et al.*, 2009). However, more research on this topic needs to be undertaken.

A consistent though moderate relative myopic shift for decreased light levels could be observed under monocular and binocular visual conditions. With increased SA the relative shift increased, probably due to the extended DOF.

8 Visual simulation of a corneal small aperture inlay

As the eye ages, it becomes affected by presbyopia. Since the percentage of the elderly population is steadily growing, a constant search for the best solution to meet visual needs of presbyopic patients is going on. Although vision correction with synthetic intrastromal implants was already suggested in 1949 (Barraquer, 1949), it has only become a procedure of increased interest within the last years. Progress in refractive surgery techniques reduced complexity of its implementation and advances in the development of biocompatible materials reduced postoperative complications. A currently available corneal inlay to overcome presbyopia is the AcuFocus Corneal Inlay 7000 (ACI 7000, AcuFocus Inc., Irvine, CA). Based on small-aperture monovision, it extends DOF of the eye it is implanted in. Clinical studies support efficacy and safety of the device for presbyopia treatment with published data of up to 3 years (Seyeddain *et al.*, 2010, 2012; Dexl *et al.*, 2012).

The intrastromal corneal inlay is a 5 µm thick polyvinylidene fluoride ring opacified by carbon nanoparticles. Its outer diameter measures 3.8 mm and the central aperture 1.6 mm. The inlay is perforated with 5-11 µm holes, which are randomly arranged allowing nutritional flow through the inlay to sustain stromal tissue. Average light transmission with an 8400-hole pattern is approximately 5%. The two left images of Figure 8.1 show the appearance of the inlay and compare the dimension of the inlay to that of a conventional contact lens. Its microperforations are clearly visible. On the right an AcuFocus Corneal Inlay 7000 in a patient's eye is shown. Meant to be a binocular solution to presbyopia, the inlay is usually implanted in the patient's non-dominant eye and centered on the line of sight.

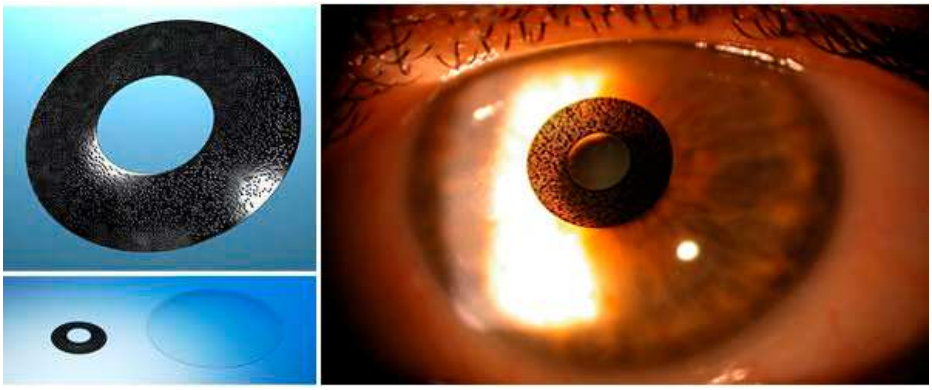

Figure 8.1: Aspect of the Acufocus Corneal Inlay 7000, its dimension in comparison to that of a conventional contact lens and an inlay in a patient's eye.

While the inlay is approved in Europe since 2005, some limitations and maximum potential benefits of the corneal small aperture approach are still unknown. Although

computer-based optical simulations with eye models can estimate monocular outcomes, it is unclear how the mechanism of binocular summation behaves in such an unnatural condition of unequal pupils and retinal illuminance. The use of a BAOVA as a pre-screening device could customize the inlay implantation and optimize postoperative outcomes. Furthermore, the instrument could provide general information about critical limits for reduced light levels or inlay-decentrations. These studies should thereby be understood as complementary to the clinical works mentioned above.

While the advantages of the inlay are its simple operating principle, one of the possible disadvantages could be the reduction in the amount of light reaching the retina. Other downsides might be possible misalignments during implantation of the corneal inlay regarding the intended location. Another critical point is the outer diameter of the implant which was selected to permit fundus imaging (Casas-LLera *et al.*, 2011) and due to cosmetic reasons but could cause a problem in very low light conditions when the patients' natural pupil diameter increases beyond the outer diameter of the implant. In this chapter, the above-mentioned possible issues are addressed. In addition, visual performance with the small aperture inlay was compared to the performance with traditional monovision for the same subjects.

Previous initial experiments (Tabernero *et al.*, 2011) with a similar instrument, together with a related study comparing stereoacuity with the inlay to monovision (Fernández *et al.*, 2013) were reported.

8.1 Optical quality predictions

The area under the radially averaged monochromatic MTF between 0 and 60 cpd was used as optical quality metric. The metric was calculated for the small aperture pupil measuring 1.6 mm in diameter, a natural photopic pupil diameter of 4 mm, a natural scotopic pupil diameter of 5 mm, and an annulus pupil with an outer diameter of 5 mm. Relative sizes and shapes of these pupils are illustrated in Figure 8.2. Calculations were performed for an unaberrated eye and object vergences ranging from 0 to 3 D in 0.5 D increments.

Figure 8.2: Pupils for which optical quality through-focus was predicted. The small aperture pupil of 1.6 mm, a natural photopic pupil of 4 mm, a natural scotopic pupil of 5 mm, and the annulus pupil of 5 mm (inner inlay diameter 1.6 mm, outer inlay diameter 3.8 mm).

8.2 Subjects

Four experienced male subjects with normal vision and eye health participated in the study. Their mean age at the time of the study was 43 ± 6 years. For two subjects, accommodation was paralyzed with 1% tropicamide. The other two subjects are presbyopes. Three subjects are right-eye dominant and one subject is left-eye dominant. Natural defocus and astigmatism was corrected throughout the study, whereas HOA were not modified. The subjects' refractive profiles and aberration data for 4 mm pupils can be found in Table 8.1.

Subjects 1-3 participated in measurements studying the effect of an annulus pupil and inlay centration (section 8.5). Subjects 1-4 participated in the part of the study investigating binocular performance in photopic light (section 8.6) and Subjects 2-4 also took part in the measurements under mesopic lighting conditions (section 8.7).

Subject	Age (y)	Eye	Objective refraction	RMS (µm)	HOA-RMS (µm)
#1	37	OS	-0.18 -0.30 x 140°	0.24	0.20
		OD*	0.10 -0.73 x 180°	0.37	0.22
#2	50	OS	-2.55 -0.55 x 68°	0.24	0.07
		OD*	-2.40 -1.02 x 95°	0.44	0.14
#3	38	OS	-2.36 -0.90 x 68°	0.41	0.18
		OD*	-3.09 -0.47 x 93°	0.22	0.10
#4	47	OS*	-4.14 -0.39 x 68°	0.20	0.13
		OD	-3.79 -0.56 x 166°	0.24	0.09

Table 8.1: Refractive profiles and aberration data for 4 mm pupils of subjects involved in the study. The asterisk marks the dominant eye.

8.3 Experimental procedure and data evaluation

Measurements were organized in several sessions lasting between one and two hours each. One session was dedicated to perform monocular VA measurements in order to study the effect of the annulus pupil and inlay centration on visual performance and another one to measure binocular performance in photopic and mesopic light.

VA was assessed using the method of adjustment with a *Tumbling E test*. Monocular performance was assessed in the NDE of the subjects by means of VA measurements. As a first reference, the inlay was centered on the pupil center. Monocular through-focus performance was tested for the small aperture pupil, the 4 mm pupil and 5 mm annulus pupil from distance to 3 D vergence in steps of 0.5 D under monochromatic light conditions. Optimum inlay centration was then tested at distance in polychromatic light. Therefore, the inlay was displaced with respect to the pupil center in hori-

zontal direction. Increments of 0.5 mm were chosen and maximum decentration was 2 mm.

Binocular performance was tested for natural vision and three different types of monovision. For clarity, Figure 8.3 illustrates amplitude and phase of the pupil functions for unaberrated eyes at distance when individual binocular optical conditions were simulated. Henceforth, these conditions are referred to as *natural vision*, *traditional monovision, small aperture monovision*, and *ACI monovision*. *Natural vision* was simulated with artificial pupils of 4 mm in diameter and without any added phase. *Traditional monovision* was simulated with artificial pupils of 4 mm in both eyes and inducing 1.25 D of pure defocus in the NDE. In case of simulating *small aperture monovision*, the artificial pupil conjugate to the NDE's pupil plane was reduced to 1.6 mm in diameter. *ACI monovision* was simulated by reducing the artificial pupil to 1.6 mm in diameter and additionally inducing 0.75 D of defocus in the NDE.

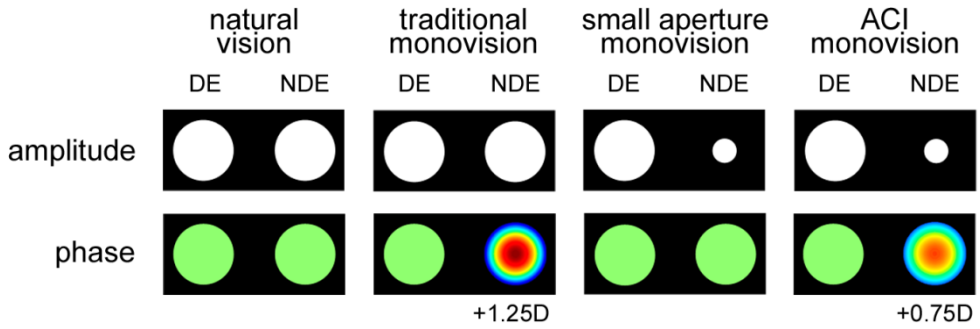

Figure 8.3: Binocular optical conditions for which through-focus visual acuity was assessed.

Binocular through-focus performance was assessed under photopic and mesopic luminance conditions in quasi-monochromatic light. In photopic light, monocular through-focus VA was measured in both the DE and the NDE, additionally. VA decrease was determined by fitting linear regressions to the averaged through-focus VAs. Coefficients of determination are given as R^2-values.

DOF was derived from linearly interpolating through-focus curves for individual subjects. In photopic light a VA threshold of Jaeger score J2 (0.18 logMAR) was chosen, whereas in mesopic light the threshold was lowered to J3 (0.3 logMAR). The BSR was obtained as the ratio between binocular decimal VA and monocular decimal VA of the better performing eye for according optical conditions.

8.4 Optical quality computer simulations

The left panel of Figure 8.4 shows the area under the rMTF as a function of objects vergence calculated for an unaberrated eye for the pupil intensity profiles illustrated in Figure 8.2. Data for natural pupils is illustrated in red, whereas data for inlay pupils is

shown in green. Optical quality simulations predict that the inlay reduces distance performance with respect to vision with 4 mm pupils. For closer objects (greater object vergences), however, performance with the inlay is better than with the 4 mm pupil. Through-focus performance with a 5 mm pupil is predicted to be very similar to that with a 4 mm pupil. Optical quality with the 5 mm annulus pupil is similar to that with the small aperture pupil for distance and near. However, for intermediate object vergences, performance is similar to that with the 5 mm pupil.

In the right panel, optical performance is shown for the left eye of Subject 3 to demonstrate the expected effect when HOA are present. While performance with the small aperture pupil is hardly affected, distance performance is reduced for larger pupils but the decrease of performance with greater object vergences is attenuated due to HOA. At near, performance with the 5 mm annulus pupil is still better than with the same sized natural pupil.

The optimum centration of a small aperture corneal inlay and the effect of residual defocus to maximize depth of focus were determined by means of Strehl ratio calculation for personalized eye model by Tabernero et al. (Tabernero & Artal, 2012).

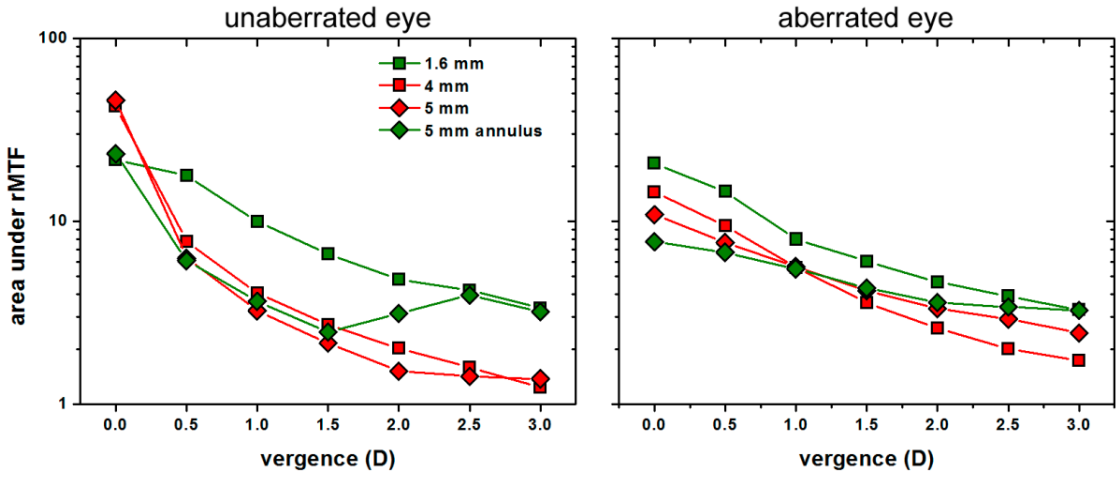

Figure 8.4: Optical quality predictions for an unaberrated eye (left) and an eye affected by HOA (right) with different pupil diameters and with the annulus pupil.

8.5 Monocular through-focus performance and inlay centration

Monocular through-focus VA measurements for the different pupils simulated with the BAOVS are shown in Figure 8.5. For the small aperture pupil and the larger 4 mm pupil, distance VA is similar. However, with the small aperture inlay, VA decrease is considerably reduced from 0.20 logMAR/D (R^2=0.99) to 0.12 logMAR/D (R^2=0.93). The through-focus curve measured with the 5 mm annulus pupil runs approximately parallel to that measured with the small aperture pupil (R^2=0.96), though average performance is re-

duced by about 0.07 logMAR. For greater vergences than 0.5 D, performance with the annulus pupils is noticeably better than with the 4 mm reference pupil.

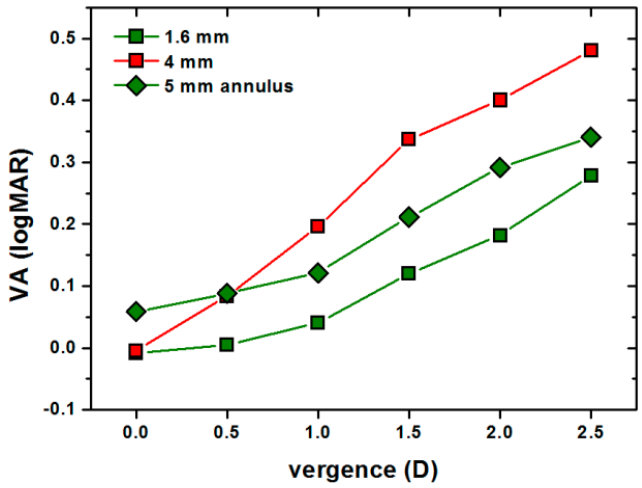

Figure 8.5: Monocular through-focus visual acuity (VA) for different pupils.

VA with the small aperture depended strongly on the centration of the inlay. Figure 8.6 shows the average VA as a function of inlay decentration with respect to the natural pupil center. Positive decentrations mean that the inlay was displaced in nasal direction whereas negative decentrations stand for temporal displacements. Standard deviations were around 0.2 logMAR. On average, best VA was achieved when the inlay was located between 0 and 0.5 mm nasally and VA decrease was greater nasally than temporally, however the course varied strongly among subjects.

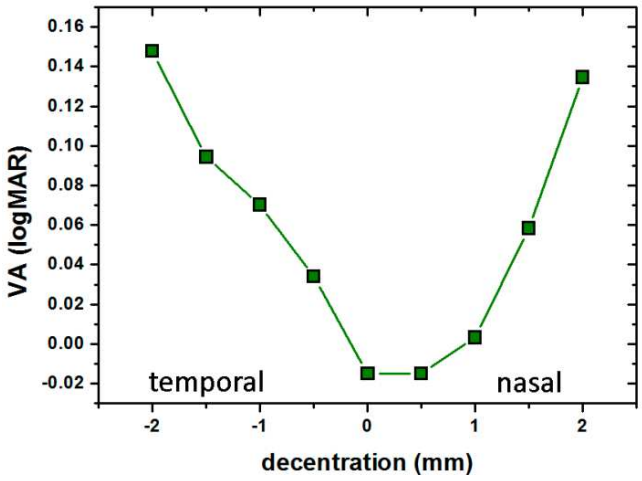

Figure 8.6: Visual acuity as a function of inlay centration.

8.6 Binocular performance and summation

Figure 8.7 shows monocular VAs for DE and NDE, and binocular VAs as a function of object vergence averaged across subjects. Standard errors were in the range of 0.1 logMAR. Each panel stands for one binocular optical condition. In the upper row, conditions with equal sized pupils are shown, whereas in the lower row, conditions with different pupil dimensions are illustrated. In the left and right column, results for conditions without and with unilaterally induced defocus are given.

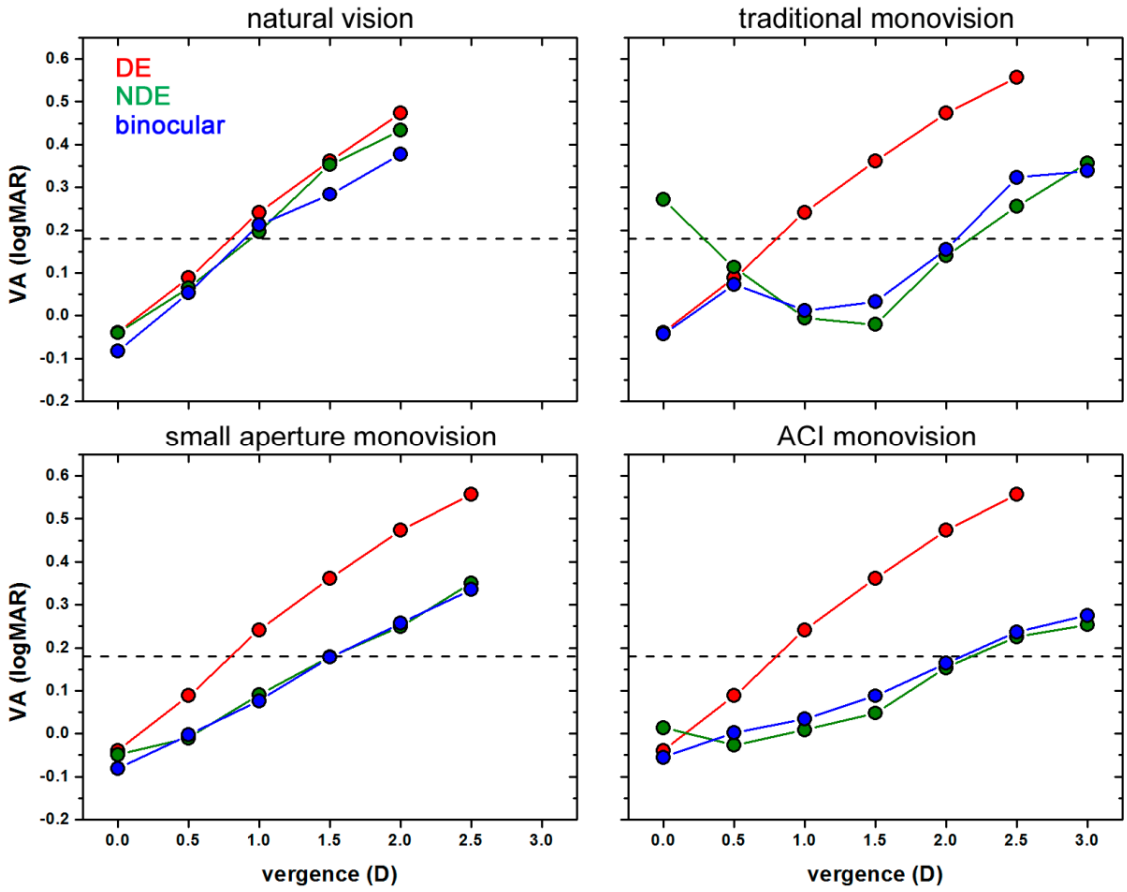

Figure 8.7: Monocular (dominant eye: DE; non-dominant eye: NDE) and binocular visual acuity (VA) in dependence of object vergence. Dashed lines mark the J2-line (0.18 logMAR). For purpose of clarity, error bars were omitted. Typical standard deviations were in the range of 0.1 logMAR.

For all simulated conditions, binocular VA closely followed monocular VA of the better performing eye. However, when defocus was induced unilaterally, binocular performance was slightly worse than best monocular performance at some vergences. For *natural vision*, binocular VA decreased with increasing object vergence according 0.23 logMAR/D (R^2=0.97). For *traditional monovision*, the slope of binocular through-focus VA was similar when considering vergences greater than 1 D (0.22 logMAR/D; R^2=0.89).

The small aperture approach in the NDE had no significant effect on monocular distance VA. However, it reduced binocular VA decrease with object vergence to 0.169 logMAR/D (R^2=0.99). Binocular through-focus VA with *ACI monovision* did not show the typical double peak for unilaterally induced defocus. Instead, a linear regression resulted in accurate fitting (R^2=0.99). *ACI monovision* further reduced binocular VA decrease to 0.113 logMAR/D.

Figure 8.8 directly compares binocular through-focus VA for the four simulated cases on the left. Distance VA of -0.08 logMAR with *natural vision* dropped to -0.04 logMAR with *traditional monovision*. Yet, according to a one-sided, paired student's t-test this difference was not statistically significant (p=0.055). Binocular distance VA was not sacrificed with the small aperture pupil. With *ACI monovision*, distance performance decreased slightly less than with *traditional monovision* to -0.06 logMAR (p=0.069). At vergences greater than 0.5 D, binocular VA was significantly better with *traditional monovision* and *ACI monovision* than with *natural vision*.

Binocular DOF is presented in the right panel of Figure 8.8. The threshold was set to J2 (0.18 logMAR). All types of monovision extended binocular DOF. Small aperture monovision increased binocular DOF from 0.9 D to 1.5 D (p=0.046). The greatest DOF of 2.1 D, however, was achieved with *ACI monovision* and *traditional monovision*. Both increases with respect to *natural vision* were highly statistically significant (p=0.003 and p<0.001).

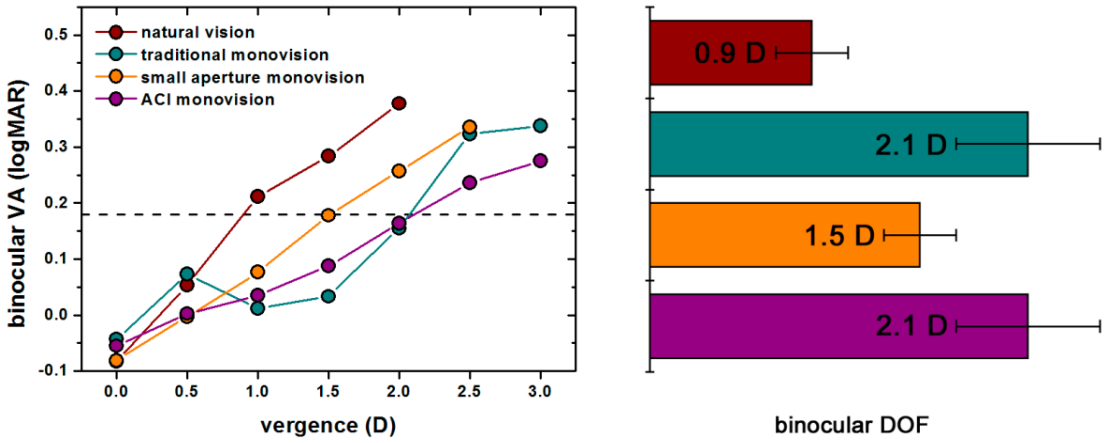

Figure 8.8: Comparison of binocular through-focus visual acuities (VA) and binocular depth of focus (DOF) when a threshold of 0.18 logMAR (J2) is set for the four optical conditions in photopic light.

BSR was calculated for the four cases. Figure 8.9 shows the ratio versus object vergence. For natural vision, BSR versus vergence showed a decrease first, but recovered to the original value then. It was significantly greater than 1 at distance (BSR=1.09 ± 0.05; p=0.015) and at an object vergence of 2 D (BSR=1.10 ± 0.07; p=0.032). For all types of monovision, BSR at distance was decreased, however, inhibition (BSR<1) was not observed.

Averaged across subjects and object vergences, the ratio was 1.05 ± 0.06 for *natural vision*. While BSR with *small aperture monovision* was still slightly greater than 1 on average (1.01 ± 0.02), the ratio was significantly reduced both with *ACI monovision* and *traditional monovision* to 0.96 ± 0.04 and 0.97 ± 0.05 (p=0.010 and p=0.049), respectively. BSR with *traditional monovision* reached its minimum close to a vergence where the image was in focus in the NDE.

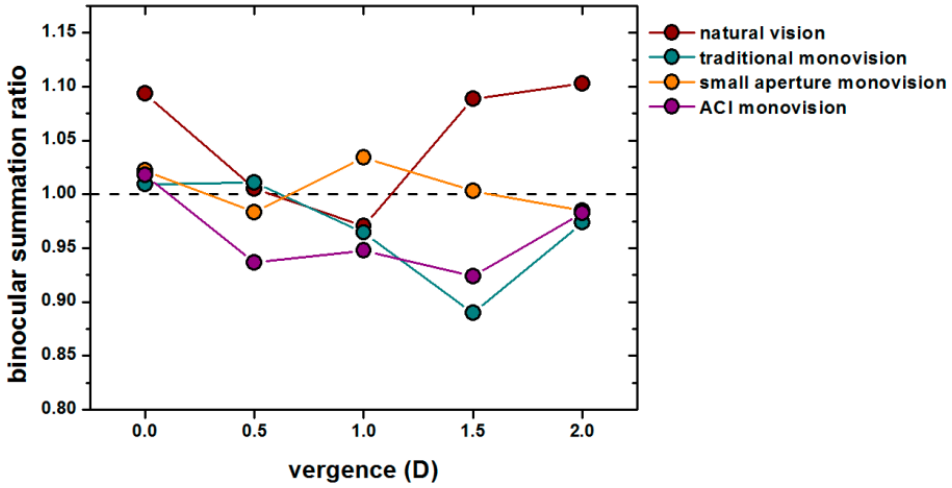

Figure 8.9: Binocular summation ratio versus object vergence for the four optical conditions. The black dashed line marks a binocular summation ratio of one.

8.7 Performance in mesopic light

Figure 8.10 shows average binocular through-focus VAs for the four optical conditions in mesopic (solid colored lines) and photopic light (dashed colored lines). Dashed black lines mark the J3-line (0.3 logMAR). Visual performance in mesopic light was reduced with respect to performance in photopic light, however, mesopic and photopic curves showed very similar decreases for the same optical conditions.

Averaged across vergences, VA with *natural vision* was 0.15 logMAR worse than in photopic luminance conditions. With monovision, no matter of what type, mesopic VA was reduced more drastically. Binocular VA with *traditional monovision*, *small aperture monovision*, and *ACI monovision* resulted 0.23, 0.26, and 0.25 logMAR worse than when measured under photopic luminance conditions.

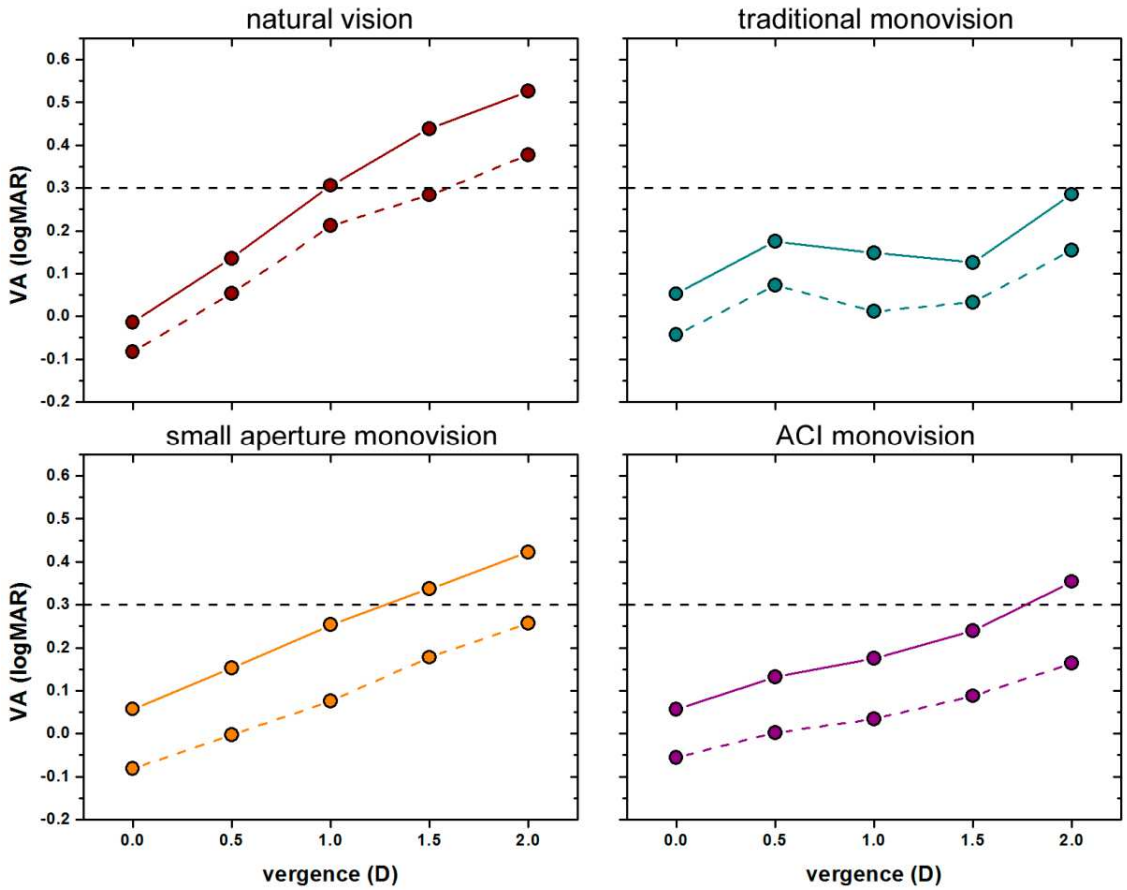

Figure 8.10: Binocular visual acuity (VA) in dependence of object vergence for mesopic (colored solid lines) and photopic (colored dashed lines). Black dashed lines mark the J3-line (0.3 logMAR). For purpose of clarity, error bars were omitted. Typical standard deviations were in the range of 0.1 logMAR.

In the left panel of Figure 8.11, binocular VA in mesopic light versus object vergence is compared for the four optical conditions. For *natural vision*, distance VA was -0.01 logMAR. With all types of monovision, distance VA was significantly reduced. *Traditional monovision* caused a distance VA of 0.05 logMAR (p=0.026), whereas simulating *small aperture monovision* and *ACI monovision*, decreased distance VA to 0.06 logMAR (p=0.003 and p=0.047). However, for object vergence of 1.5 D and 2 D, binocular VA with monovision, no matter which type, was significantly better than for *natural vision*. Binocular VA for *traditional monovision* and *ACI monovision* only differed significantly at an object vergence of 1.5 D (p=0.038).

The right panel of Figure 8.11 compares binocular DOF for *natural vision* with binocular DOF with monovision. Binocular DOF with *natural vision* averaged across the three subjects was 1.0 ± 0.2 D. Binocular DOF resulted largest for *traditional monovision* (2.0 ± 0.2 D). With *small aperture monovision* and *ACI monovision*, average binocular DOF was 1.2 ± 0.4 D and 1.4 ± 0.9 D. Error bars were comparatively large here, because the small aperture inlay had no effect in mesopic light for Subject 3. When only considering Subject 1 and 2, binocular DOF averaged 1.4 ± 0.1 D with *small aperture monovision* and 2.0 ± 0.1 D with *ACI monovision*.

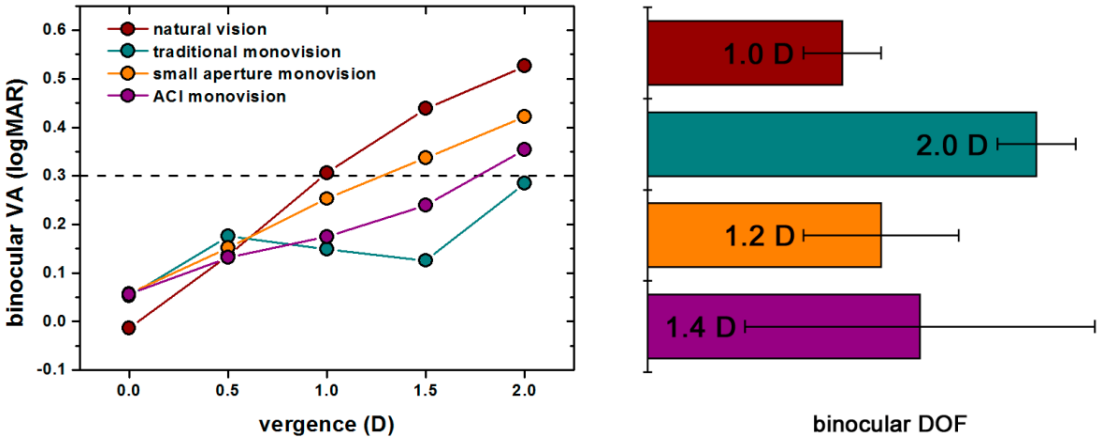

Figure 8.11: Comparison of binocular through-focus visual acuities (VA) and binocular depth of focus (DOF) when a threshold of 0.3 logMAR (J3) is set for the four optical conditions in mesopic light.

8.8 Discussion

The study demonstrated that the BAOVA is appropriate to explore potential and limitations of presbyopia correction methods. Without the need of a real implantation, the instrument realistically simulates different aspects of monocular and binocular visual conditions with the small aperture approach. In particular, artificial pupil generation with liquid-crystal spatial light modulators reveals a great advantage (Schwarz *et al.*, 2011). The current setup makes it possible to control artificial pupils with a spatial resolution difficult to obtain with physical apertures (~1/30 mm). In particular, the impact of pinhole decentrations and annular pupils on real monocular or even binocular vision can be explored. Although it is possible to estimate optical outcomes with customized ray tracing, satisfactory results are more likely to be achieved if patients are given an active role in the decision on a particular method for presbyopia correction. Visual simulators similar to the one used here could be used in screenings prior to presbyopia surgery in order to customize and optimize visual outcomes.

Efficacy of a small aperture pupil has been demonstrated with an AO instrument for monocular vision in photopic conditions (Hickenbotham *et al.*, 2012). Although distance VA with corrected HOA decreased when visual testing was performed through an artificial pupil of 2 mm compared with vision through 5 mm pupils, average through-focus VA was improved with the smaller pupil. In our measurements, monocular distance VA with the small aperture was not found to differ from that with the larger 4 mm pupil, but was comparable to small aperture distance VA in the study named above. This can be attributed to the fact that, in contrast to the previous study, HOA were not corrected here. While HOA correction should have a minor impact on visual performance at best focus with small pupils, visual performance with larger pupils would improve noticeably (Yoon & Williams, 2002). A second consequence would be a

eper slope in through-focus curves measured with equal pupil diameters due to reduced DOF (Guirao *et al.*, 2002*a*). However, hardly any difference could be observed when comparing our measurements for the small aperture with results from Hickenbotham et al. Probably this is due to the larger vergence range that was chosen here. In contrast to the small aperture pupil, the 5 mm annulus pupil reduced visual performance at distance. For closer objects, however, VA was better with the annulus pupil than with the natural 4 mm pupil like predicted with optical quality simulations. Yet, how subjects perform in lower light levels where the annulus pupil actually occurs still lacks investigation.

Distance VA was found to be strongly dependent on inlay centration and the course of the curve was in turn strongly subject-dependent. Here, maximum VA was measured when the small aperture was located between 0 and 0.5 mm nasal to the pupil center. Tabernero and Artal determined the average optimum position of the inlay to maximize Strehl ratios for personalized eye models to be located 0.4 mm nasal from the center of the pupil (Tabernero & Artal, 2012) which agrees well with our measurements.

Monocular DOF extension with small aperture pupils does not necessarily implicate that binocular DOF will be extended in case only one of the pupils is reduced. In case of keeping a constant light-source level, the smaller pupil investigated here reduces retinal illuminance about 6-fold. Unequal monocular illuminances are known to have a detrimental effect on BSR (Gilchrist & Pardhan, 1987). Our measurements showed that although binocular summation is sacrificed to a comparable extent both with the small aperture in one eye and with induced anisometropia when compared to *natural vision*, the ratio is not significantly different from one. As a consequence of this, both types of monovision produce the same extension of binocular DOF to 2.1 D which is highly significant.

Comparing visual performance with the simulated small aperture with clinical results (Seyeddain *et al.*, 2010; Dexl *et al.*, 2012), both monocular and binocular distance VA agree well. However, near VAs differ by about 1-2 lines. Possible reasons could be neural adaptation of the subjects who underwent surgery or the lower luminance that was employed for visual testing here.

In contrast to visual performance in photopic light, performance in mesopic light was highly subject-dependent. For the two younger subjects the small aperture was just as effective as in photopic light when lowering the DOF threshold from J2 to J3. The oldest subject presented the comparatively lowest VA under photopic lighting conditions and VA was reduced more than for the other subjects in mesopic light. These results suggest that preliminary VA measurements in reduced light levels are important prior to implantation of the inlay.

CONCLUSIONS

9 Conclusions

The aim of this thesis was to achieve a better understanding of the influence of aberrations on binocular vision. In this final chapter the main results and conclusions of this research are summarized.

1. A binocular adaptive optics visual simulator fully capable to control the two complex pupil functions was successfully designed and constructed. The system is based on liquid crystal spatial light modulators offering high resolution in pupil conjugate planes to manipulate amplitude and phase of both eyes independently. This allows to noninvasively modify optical factors such as aberrations and pupil shapes while subjects undergo visual testing. The instrument was used in a variety of experiments to investigate in what way the optics of the eye influence binocular vision.

2. Bilateral defocus has a detrimental effect on binocular summation, with the minimum occurring at an intermediate vergence. Binocular summation recovers to values obtained at best focus for greater vergences, mitigating the reduction in optical quality. For bilaterally induced spherical aberration, in contrast, a beneficial effect on binocular summation was observed. However, when optical quality is different between both eyes, both defocus and spherical aberration have a negative influence on the binocular advantage.

3. The potential visual benefit of bilateral implantation of the average pseudophakic patient with aspheric-achromatic intraocular lenses was studied. In case of a combined correction of spherical and longitudinal chromatic aberration, significant increase in binocular visual acuity can be expected, albeit the improvement under binocular conditions is lower compared to that under monocular conditions. As the level of aberration correction increases, the binocular summation declines.

4. Inducing coma has the potential to extend monocular and binocular depth of focus, without significantly affecting visual acuity at best focus. Due to the generated retinal disparity, this effect is however orientation dependent. The greatest depth of focus extension is achieved when coma occurs vertically in the same direction.

5. Binocular aberration correction and binocular summation presents a special benefit under low luminance conditions for natural light-adapted pupils. Binocular summation seems to be inversely correlated with monocular VA under natural viewing conditions, thus, mitigating reduced visual performance.

6. Binocular viewing increases the subjects' precision to judge best-focus positions under reduced luminance conditions. A small but consistent relative myopic shift can be observed as light levels are reduced which can be fully explained by the Purkinje shift in combination with the longitudinal chromatic aberration of the human eye. The shift increases when spherical aberration is induced, probably due to the extended depth of focus in combination with the accommodative lag.

7. Visual simulations of a corneal small aperture inlay proves that this device extends depth of focus just as effectively as traditional monovision in photopic light. Under mesopic luminance conditions, performance is more subject-dependent. For two subjects, performance was still comparable to traditional monovision. However, centration of the device is critical and also the annulus pupil could reduce visual performance with the corneal inlay.

8. Successful simulation of different monovision-types for presbyopia correction demonstrates the potential of the binocular adaptive optics visual simulator as a pre-screening device. The instrument could be used to find the appropriate vision correction for a large number of patients, so that they could take an active role in the treatment process.

References

ANSI (2010). *ANSI Z.80.28 2010 - Methods for reporting optical aberrations of eyes*.

Artal P (2009). History of IOLs that correct spherical aberration. *J Cataract Refract Surg* **35,** 962–963.

Artal P, Benito A & Tabernero J (2006). The human eye is an example of robust optical design. *J Vis* **6,** 1–7.

Artal P, Berrio E, Guirao A & Piers P (2002). Contribution of the cornea and internal surfaces to the change of ocular aberrations with age. *J Opt Soc Am A* **19,** 137–143.

Artal P, Chen L, Fernández EJ, Singer B, Manzanera S & Williams DR (2004). Neural compensation for the eye's optical aberrations. *J Vis* **4,** 281–287.

Artal P, Guirao A, Berrio E & Williams DR (2001). Compensation of corneal aberrations by the internal optics in the human eye. *J Vis* **1,** 1–8.

Artal P, Manzanera S, Piers P & Weeber H (2010). Visual effect of the combined correction of spherical and longitudinal chromatic aberrations. *Opt Express* **18,** 1637–1648.

Artal P, Schwarz C, Cánovas C & Mira-Agudelo A (2012). Night myopia studied with an adaptive optics visual analyzer. *PLoS One* **7,** e40239.

Artal P & Tabernero J (2008). The eye's aplanatic answer. *Nat Photonics* **2,** 586–589.

Atchison DA & Smith G (2000). *Optics of the Human Eye*. Butterworth Heinemann.

Banks M, Ghose T & Hillis J (2004). Relative image size, not eye position, determines eye dominance switches. *Vision Res* **44,** 229–234.

Banton T & Levi DM (1991). Binocular summation in vernier acuity. *J Opt Soc Am A* **8,** 673–680.

Barlow HB, Blakemore C & Pettigrew JD (1967). The neural mechanism if bincoular depth discrimination. *J Physiol* **193,** 327–342.

Barraquer J (1949). Queratoplastia refractiva. *Estud e Inf oftalmológicas* **2,** 10–30.

Bearse MA & Freeman RD (1994). Binocular summation in orientation discrimination depends on stimulus contrast and duration. *Vision Res* **34,** 19–29.

Bedford R & Wyszecki G (1957). Axial chromatic aberration of the human eye. *J Opt Soc Am* **47,** 2–3.

Bellucci R, Morselli S & Pucci V (2007). Spherical aberration and coma with an aspherical and a spherical intraocular lens in normal age-matched eyes. *J Cataract Refract Surg* **33,** 203–209.

Benjamin W (2006). *Borish's Clinical Refraction*. Butterworth Heinemann.

Berrio E, Tabernero J & Artal P (2010). Optical aberrations and alignment of the eye with age. *J Vis* **10,** 1–17.

Blake R & Fox R (1973). The psychophysical inquiry into binocular summation. *Attention, Perception, Psychophys* **14,** 161–185.

Born M & Wolf E (1999). *Principles of Optics*. Cambridge University Press.

Brainard DH (1997). The Psychophysics Toolbox. *Spat Vis* **10,** 433–436.

Cagenello R, Arditi A & Halpern DL (1993). Binocular enhancement of visual acuity. *J Opt Soc Am A* **10,** 1841–1848.

Campbell FW & Green DG (1965*a*). Monocular versus binocular visual acuity. *Nature* **208,** 191–192.

Campbell FW & Green DG (1965*b*). Optical and retinal factors affecting visual resolution. *J Physiol* **181,** 576–593.

Campbell FW & Gubisch RW (1967). The effect of chromatic aberration on visual acuity. *J Physiol* **192,** 345–358.

Cánovas C, Prieto PM, Manzanera S, Mira A & Artal P (2010). Hybrid adaptive-optics visual simulator. *Opt Lett* **35,** 196–198.

Casas-LLera P, Ruiz-Moreno JM & Alió JL (2011). Retinal imaging after corneal inlay implantation. *J Cataract Refract Surg* **37,** 1729–1731.

Castejón-Mochón JF, López-Gil N, Benito A & Artal P (2002). Ocular wave-front aberration statistics in a normal young population. *Vision Res* **42,** 1611–1617.

Castro JJ, Jiménez JR, Hita E & Ortiz C (2009). Influence of interocular differences in the Strehl ratio on binocular summation. *Ophthalmic Physiol Opt* **29,** 370–374.

Cheng X, Bradley A & Thibos LN (2004). Predicting subjective judgment of best focus with objective image quality metrics. *J Vis* **4,** 310–321.

Chin SS, Hampson KM & Mallen EAH (2008). Binocular correlation of ocular aberration dynamics. *Opt Express* **16,** 14731–14745.

Dalimier E, Dainty C & Barbur J (2008). Effects of higher-order aberrations on contrast acuity as a function of light level. *J Mod Opt* **55,** 791–803.

Dexl AK, Seyeddain O, Riha W, Rückl T, Bachernegg A, Emesz M, Ruckhofer J & Grabner G (2012). Reading performance and patient satisfaction after corneal inlay implantation for presbyopia correction: two-year follow-up. *J Cataract Refract Surg* **38,** 1808–1816.

Dodgson N (2004). Variation and extrema of human interpupillary distance. *Proc SPIE* **5291,** 36–46.

Doesschate J & Alpern M (1967). Effect of photoexcitation of the two retinas on pupil size. *J Neurophysiol* **30,** 562–576.

Donders FC (1864). *On the anomalies of accommodation and refraction of the eye*. New Sydenham Society.

Dreher AW, Bille JF & Weinreb RN (1989). Active optical depth resolution improvement of the laser tomographic scanner. *Appl Opt* **28,** 804–808.

Duane A (1912). Normal Values of the Accommodation at all Ages. *J Amercian Med Assoc* **59,** 1010–1013.

Ehrenstein WH & Ehrenstein A (1966). Pschophysical Methods. In *Modern techniques in Neuroscience*, p. 1325.

Evans BJW (2007). Monovision: a review. *Ophthalmic Physiol Opt* **27,** 417–439.

Fernández EJ, Iglesias I & Artal P (2001). Closed-loop adaptive optics in the human eye. *Opt Lett* **26,** 746–748.

Fernández EJ, Manzanera S, Piers P & Artal P (2002). Adaptive optics visual simulator. *J Refract Surg* **18,** 634–638.

Fernández EJ, Prieto PM & Artal P (2009*a*). Binocular adaptive optics visual simulator. *Opt Lett* **34,** 2628–2630.

Fernández EJ, Prieto PM & Artal P (2009*b*). Wave-aberration control with a liquid crystal on silicon (LCOS) spatial phase modulator. *Opt Express* **17,** 11013–11025.

Fernández EJ, Prieto PM & Artal P (2010). Adaptive optics binocular visual simulator to study stereopsis in the presence of aberrations. *J Opt Soc Am A* **27,** 48–55.

Fernández EJ, Prieto PM & Artal P (2012). Adaptive optics visual analyzer under white-light illumination using liquid crystal on silicon (LCOS) technology. In *SPIE Photonics West*, pp. 1–3.

Fernández EJ, Schwarz C, Prieto PM, Manzanera S & Artal P (2013). Impact on stereo-acuity of two presbyopia correction approaches: monovision and small aperture inlay. *Biomed Opt Express* **4,** 822–830.

Fernández EJ, Unterhuber A, Povazay B, Hermann B, Artal P & Drexler W (2006). Chromatic aberration correction of the human eye for retinal imaging in the near infrared. *Opt Express* **14,** 6213–6225.

Fielder AR & Moseley MJ (1996). Does stereopsis matter in humans? *Eye* **10,** 233–238.

Gambra E, Sawides L, Dorronsoro C & Marcos S (2009). Accommodative lag and fluctuations when optical aberrations are manipulated. *J Vis* **9,** 1–15.

Gilchrist J & Pardhan S (1987). Binocular contrast detection with unequal monocular illuminance. *Ophthalmic Physiol Opt* **7,** 373–377.

Glasser A (2008). Restoration of accommodation: surgical options for correction of presbyopia. *Clin Exp Optom* **91,** 279–295.

Glasser A & Campbell M (1998). Presbyopia and the optical changes in the human crystalline lens with age. *Vision Res* **38,** 209–229.

Glasser A & Campbell MC (1999). Biometric, optical and physical changes in the isolated human crystalline lens with age in relation to presbyopia. *Vision Res* **39,** 1991–2015.

Goodman JW (2005). *Introduction to Fourier Optics*. Roberts and Company Publishers.

De Gracia P, Dorronsoro C, Gambra E, Marin G, Hernández M & Marcos S (2010). Combining coma with astigmatism can improve retinal image over astigmatism alone. *Vision Res* **50,** 2008–2014.

De Gracia P, Dorronsoro C, Marin G, Hernández M & Marcos S (2011). Visual acuity under combined astigmatism and coma: Optical and neural adaptation effects. *J Vis* **11,** 1–11.

Guirao A, Porter J, Williams DR & Cox IG (2002*a*). Calculated impact of higher-order monochromatic aberrations on retinal image quality in a population of human eyes: erratum. *J Opt Soc Am A* **19,** 620–627.

Guirao A, Redondo M & Artal P (2000). Optical aberrations of the human cornea as a function of age. *J Opt Soc Am A* **17,** 1697–1702.

Guirao A, Redondo M, Geraghty E, Piers P, Norrby S & Artal P (2002*b*). Corneal optical aberrations and retinal image quality in patients in whom monofocal intraocular lenses were implanted. *Arch Ophthalmol* **120,** 1143–1151.

Guirao A & Williams DR (2003). A Method to Predict Refractive Errors from Wave Aberration Data. *Optom Vis Sci* **80,** 36–42.

Hartmann J (1900). Bemerkungen über den Bau und die Justierung von Spektrographen. *Zeitschrift für Instrumentenkd* **20,** 47–64.

Haynes J-D, Deichmann R & Rees G (2005). Eye-specific effects of binocular rivalry in the human lateral geniculate nucleus. *Nature* **438,** 496–499.

Hecht S (1928). The relation between visual acuity and illumination. *J Gen Physiol* **11,** 255–281.

Helmholtz H (1909). *Handbuch der physiologischen optik*. Leopold Voss.

Hickenbotham A, Tiruveedhula P & Roorda A (2012). Comparison of spherical aberration and small-pupil profiles in improving depth of focus for presbyopic corrections. *J Cataract Refract Surg*1–9.

Hofer H, Artal P, Singer B, Aragón JL & Williams DR (2001). Dynamics of the eye's wave aberration. *J Opt Soc Am A* **18,** 497–506.

Hofer H, Carroll J, Neitz J, Neitz M & Williams DR (2005). Organization of the human trichromatic cone mosaic. *J Neurosci* **25,** 9669–9679.

Holladay JT, Piers P a, Koranyi G, van der Mooren M & Norrby NES (2002). A new intraocular lens design to reduce spherical aberration of pseudophakic eyes. *J Refract Surg* **18,** 683–691.

Horowitz MW (1949). An analysis of the superiority of binocular over monocular visual acuity. *J Exp Psychol* **39,** 581–596.

Howard I & Rogers B (1995). *Binocular Vision and Stereopsis*.

Howarth PA, Zhang XX, Bradley A, Still DL & Thibos LN (1988). Does the chromatic aberration of the eye vary with age? *J Opt Soc Am A* **5,** 2087–2092.

Hubel DH & Wiesel TN (1962). Receptive fields, binocular interaction and functional architecture in the cat's visual cortex. *J Physiol* **160,** 106–154.

Jaeken B & Artal P (2012). Optical quality of emmetropic and myopic eyes in the periphery measured with high-angular resolution. *Invest Ophthalmol Vis Sci* **53,** 3405–3413.

Jenkins TC, Pickwell LD & Abd-Manan F (1992). Effect of induced fixation disparity on binocular visual acuity. *Ophthalmic Physiol Opt* **12,** 299–301.

Jiménez JR, Castro JJ, Jiménez R & Hita E (2008). Interocular differences in higher-order aberrations on binocular visual performance. *Optom Vis Sci* **85,** 174–179.

Kelly JE, Mihashi T & Howland HC (2004). Compensation of corneal horizontal/vertical astigmatism, lateral coma, and spherical aberration by internal optics of the eye. *J Vis* **4,** 262–271.

Khan A & Crawford J (2001). Ocular dominance reverses as a function of horizontal gaze angle. *Vision Res* **41,** 1743–1748.

Kobayashi M, Nakazawa N, Yamaguchi T, Otaki T, Hirohara Y & Mihashi T (2008). Binocular open-view Shack-Hartmann wavefront sensor with consecutive measurements of near triad and spherical aberration. *Appl Opt* **47,** 4619–4626.

Koenig A (1897). Die Abhängigkeit der Sehschärfe von der Beleuchtungsintensität. *Sitzungsberichte der Königlichen Preuss Akad der Wissenschaften zu Berlin* **26,** 559–575.

Koomen M, Scolnik R & Tousey R (1951). A study of night myopia. *J Opt Soc Am* **259,** 80–90.

Koomen M, Tousey R & Scolnik R (1949). The spherical aberration of the eye. *J Opt Soc Am* **39,** 370–376.

Krueger RR, Kuszak J, Lubatschowski H, Myers RI, Ripken T & Heisterkamp A (2005). First safety study of femtosecond laser photodisruption in animal lenses: tissue morphology and cataractogenesis. *J Cataract Refract Surg* **31,** 2386–2394.

Leibowitz H (1952). The effect of pupil size on visual acuity for photometrically equated test fields at various levels of luminance. *J Opt Soc Am* **42,** 416–422.

Leibowitz H & Owens D (1978). New evidence for the intermediate position of relaxed accommodation. *Doc Ophthalmol* **46,** 133–147.

Leibowitz H & Walker L (1956). Effect of field size and luminance on the binocular summation of suprathreshold stimuli. *J Opt Soc Am* **46,** 171–172.

Levene J (1965). Nevil Maskelyne, FRS, and the discovery of night myopia. *Notes Rec R Soc Lond* **20,** 100–108.

Liang J, Grimm B, Goelz S & Bille JF (1994). Objective measurement of wave aberrations of the human eye with the use of a Hartmann-Shack wave-front sensor. *J Opt Soc Am A* **11,** 1949–1957.

Liang J & Williams DR (1997). Aberrations and retinal image quality of the normal human eye. *J Opt Soc Am A* **14,** 2873–2883.

Liang J, Williams DR & Miller DT (1997). Supernormal vision and high-resolution retinal imaging through adaptive optics. *J Opt Soc Am A* **14,** 2884–2892.

Lundström L, Gustafsson J & Unsbo P (2009). Population distribution of wavefront aberrations in the peripheral human eye. *J Opt Soc Am A* **26,** 2192–2198.

Maeda N, Fujikado T, Kuroda T, Mihashi T, Hirohara Y, Nishida K, Watanabe H & Tano Y (2002). Wavefront aberrations measured with Hartmann-Shack sensor in patients with keratoconus. *Ophthalmology* **109,** 1996–2003.

Manzanera S, Prieto PM, Ayala DB, Lindacher JM & Artal P (2007). Liquid crystal Adaptive Optics Visual Simulator: Application to testing and design of ophthalmic optical elements. *Opt Express* **15,** 16177–16188.

Mapp AP, Ono H & Barbeito R (2003). What does the dominant eye dominate? A brief and somewhat contentious review. *Percept Psychophys* **65,** 310–317.

Marcos S, Burns S, Moreno-Barriusop E & Navarro R (1999). A new approach to the study of ocular chromatic aberrations. *Vision Res* **39,** 4309–4323.

Marcos S, Sawides L, Gambra E & Dorronsoro C (2008). Influence of adaptive-optics ocular aberration correction on visual acuity at different luminances and contrast polarities. *J Vis* **8,** 1–12.

Mester U, Dillinger P & Anterist N (2003). Impact of a modified optic design on visual function: clinical comparative study. *J Cataract Refract Surg* **29,** 652–660.

Miles W (1929). Ocular dominance demonstrated by unconscious sighting. *J Exp Psychol* **12,** 113–126.

Van Nes FL & Bouman MA (1967). Spatial modulation transfer in the human eye. *J Opt Soc Am* **57,** 401–406.

Newton I (1730). *Opticks*. Dover Publications.

Ogle K (1952). On the limits of stereoscopic vision. *J Exp Psychol* **44,** 253–259.

Otero JM & Durán A (1941). Rendimiento fotométrico de sistemas ópticos a bajas luminosidades. *An Física y Quim* **37,** 459.

Owens DA & Leibowitz HW (1980). Accommodation, convergence, and distance perception in low illumination. *Am J Optom Physiol Opt* **57,** 540–550.

Panum PL (1858). *Physiologische Untersuchungen über das Sehen mit zwei Augen*. Schwer.

Pardhan S (1996). A comparison of binocular summation in young and older patients. *Curr Eye Res* **15,** 315–319.

Pardhan S & Gilchrist J (1990). The effect of monocular defocus on binocular contrast sensitivity. *Ophthalmic Physiol Opt* **10,** 33–36.

Pardhan S & Gilchrist J (1991). The importance of measuring binocular contrast sensitivity in unilateral cataract. *Eye* **5,** 31–35.

Pelli D, Robson J & Wilkins A (1988). The design of a new letter chart for measuring contrast sensitivity. *Clin Vis Sci* **2,** 187–199.

Pelli DG (1997). The VideoToolbox software for visual psychophysics: Transforming numbers into movies. *Spat Vis* **10,** 437–442.

Pelli DG (2013). Pelli Software. Available at: http://psych.nyu.edu/pelli/software.html [Accessed July 1, 2013].

Piers PA, Fernandez EJ, Manzanera S, Norrby S & Artal P (2004). Adaptive optics simulation of intraocular lenses with modified spherical aberration. *Invest Ophthalmol Vis Sci* **45,** 4601–4610.

Plainis S, Petratou D, Giannakopoulou T, Atchison D a & Tsilimbaris MK (2011). Binocular summation improves performance to defocus-induced blur. *Invest Ophthalmol Vis Sci* **52,** 2784–2789.

Porac C & Coren S (1976). The dominant eye. *Psychol Bull* **83,** 880–897.

Porter J, Guirao A, Cox IG & Williams DR (2001). Monochromatic aberrations of the human eye in a large population. *J Opt Soc Am A* **18,** 1793–1803.

Porter J, Queener H, Lin J, Thorn K & Awwal A (2006). *Adaptive optics for vision science: Principles, practices, design and applications*. Wiley Interscience.

Prieto PM, Fernández EJ, Manzanera S & Artal P (2004). Adaptive optics with a programmable phase modulator: applications in the human eye. *Opt Express* **12,** 4059–4071.

Prieto PM, Vargas-Martín F, McLellan JS & Burns SA (2002). Effect of the polarization on ocular wave aberration measurements. *J Opt Soc Am A* **19,** 809–814.

Prieto PMP, Vargas-Martín F, Goelz S, Artal P & Vargas-Martin F (2000). Analysis of the performance of the Hartmann-Shack sensor in the human eye. *J Opt Soc Am A* **17,** 1388–1398.

Rocha KM, Vabre L, Chateau N & Krueger RR (2009). Expanding depth of focus by modifying higher-order aberrations induced by an adaptive optics visual simulator. *J Cataract Refract Surg* **35,** 1885–1892.

Rubin GS, Muñoz B, Bandeen-Roche K & West SK (2000). Monocular versus binocular visual acuity as measures of vision impairment and predictors of visual disability. *Invest Ophthalmol Vis Sci* **41,** 3327–3334.

Rynders M, Lidkea B, Chisholm W & Thibos LN (1995). Statistical distribution of foveal transverse chromatic aberration, pupil centration, and angle psi in a population of young adult eyes. *J Opt Soc Am A* **12,** 2348–2357.

Rynders M, Navarro R & Losada M (1998). Objective measurement of the off-axis longitudinal chromatic aberration in the human eye. *Vision Res* **38,** 513–522.

Sabesan R, Zheleznyak L & Yoon G (2012). Binocular visual performance and summation after correcting higher order aberrations. *Biomed Opt Express* **3,** 3176–3189.

Saleh BEA, Teich MC & Saleh BE (1991). *Fundamentals of photonics*. Wiley.

Salmon TO & van de Pol C (2006). Normal-eye Zernike coefficients and root-mean-square wavefront errors. *J Cataract Refract Surg* **32,** 2064–2074.

Sanderson KJ, Bishop PO & Darian-Smith I (1969). Binocular corresponding receptive fields of single units in the cat dorsal lateral geniculate nucleus. *Exp Brain Res* **13,** 178–207.

Schober HAW (1954). Über die Akkommodationsruhelage. *Optik (Stuttg)* **11,** 282–290.

Schumacher S, Oberheide U, Fromm M, Ripken T, Ertmer W, Gerten G, Wegener A & Lubatschowski H (2009). Femtosecond laser induced flexibility change of human donor lenses. *Vision Res* **49,** 1853–1859.

Schwartz S (2009). *Visual Perception: A Clinical Orientation*. McGraw Hill Professional.

Schwarz C, Prieto PM, Fernández EJ & Artal P (2011). Binocular adaptive optics vision analyzer with full control over the complex pupil functions. *Opt Lett* **36,** 4779–4781.

Seyeddain O, Hohensinn M, Riha W, Nix G, Rückl T, Grabner G & Dexl AK (2012). Small-aperture corneal inlay for the correction of presbyopia: 3-year follow-up. *J Cataract Refract Surg* **38,** 35–45.

Seyeddain O, Riha W, Hohensinn M, Nix G, Dexl AK & Grabner G (2010). Refractive surgical correction of presbyopia with the AcuFocus small aperture corneal inlay: two-year follow-up. *J Refract Surg* **26,** 707–715.

Shack R & Platt BC (1971). Production and use of a lenticular Hartmann screen. *J Opt Soc Am A* **61,** 656–660.

Simonet P & Campbell MC (1990). The optical transverse chromatic aberration on the fovea of the human eye. *Vision Res* **30,** 187–206.

Sloane LL (1959). New test charts for the measurement of visual acuity at far and near distances. *Am J Ophthalmol* **48,** 807–813.

Snellen H (1862). *Probebuchstaben zur Bestimmung der Sehschärfe*. Van de Weijer.

Steinman SB, Steinman BA & Garzia R (2000). *Foundations of binocular vision: A clinical perspective*. McGraw Hill Professional.

Stockman A & Sharpe LT (2006). Into the twilight zone: the complexities of mesopic vision and luminous efficiency. *Ophthalmic Physiol Opt* **26,** 225–239.

Tabernero J & Artal P (2012). Optical modeling of a corneal inlay in real eyes to increase depth of focus: optimum centration and residual defocus. *J Cataract Refract Surg* **38,** 270–277.

Tabernero J, Piers P, Benito A, Redondo M & Artal P (2006). Predicting the optical performance of eyes implanted with IOLs to correct spherical aberration. *Invest Ophthalmol Vis Sci* **47,** 4651–4658.

Tabernero J, Schwarz C, Fernandez EJ & Artal P (2011). Binocular visual simulation of a corneal inlay to increase depth of focus. *Invest Ophthalmol Vis Sci* **52,** 5273–5277.

Taketani F, Matuura T, Yukawa E & Hara Y (2004). Influence of intraocular lens tilt and decentration on wavefront aberrations. *J Cataract Refract Surg* **30,** 2158–2162.

Thibos LN, Hong X, Bradley A & Cheng X (2002). Statistical variation of aberration structure and image quality in a normal population of healthy eyes. *J Opt Soc Am A* **19,** 2329–2348.

Thibos LN, Ye M, Zhang X & Bradley a (1992). The chromatic eye: a new reduced-eye model of ocular chromatic aberration in humans. *Appl Opt* **31,** 3594–3600.

Vargas-Martín F, Prieto PM & Artal P (1998). Correction of the aberrations in the human eye with a liquid-crystal spatial light modulator: limits to performance. *J Opt Soc Am A* **15,** 2552–2562.

Villegas EA, Alcón E & Artal P (2008). Optical quality of the eye in subjects with normal and excellent visual acuity. *Invest Ophthalmol Vis Sci* **49,** 4688–4696.

Villegas EA, Alcón E & Artal P (2012). Impact of positive coupling of the eye's trefoil and coma in retinal image quality and visual acuity. *J Opt Soc Am A* **29,** 1667–1672.

Wald G & Griffin DR (1947). The change in refractive power of the human eye in dim and bright light. *J Opt Soc Am* **37,** 321–336.

Wang J, Candy TR, Teel DFW & Jacobs RJ (2008). Longitudinal chromatic aberration of the human infant eye. *J Opt Soc Am A* **25,** 2263–2270.

Watson A & Yellott J (2012). A unified formula for light-adapted pupil size. *J Vis* **12,** 1–16.

Weeber HA & Piers PA (2012). Theoretical performance of intraocular lenses correcting both spherical and chromatic aberration. *J Refract Surg* **28,** 48–52.

Weeber HA, Pohl R, Mester U & Piers PA (2013). Visual performance of pseudophakic eyes corrected for spherical and chromatic aberrations with an achromatic intraocular lens. *Invest Ophthalmol Vis Sci* **54,** E–Abstract 808.

Westheimer G (1994). The Ferrier Lecture, 1992. Seeing depth with two eyes: stereopsis. *Proc Biol Sci* **257,** 205–214.

Wheatstone C (1838). On Some Remarkable, and Hitherto Unobserved, Phaenomena of Binocular Vision - Part I. *Contrib to Physiol Vis*1–22.

Wichmann FA & Hill NJ (2001*a*). The psychometric function: I. Fitting, sampling, and goodness of fit. *Percept Psychophys* **63,** 1314–1329.

Wichmann FA & Hill NJ (2001*b*). The psychometric function: II. Bootstrap-based confidence intervals and sampling. *Percept Psychophys* **63,** 1314–1329.

Winn B, Whitaker D, Elliott DB & Phillips NJ (1994). Factors affecting light-adapted pupil size in normal human subjects. *Invest Ophthalmol Vis Sci* **35,** 1132–1137.

Yi F, Iskander DR & Collins M (2011). Depth of focus and visual acuity with primary and secondary spherical aberration. *Vision Res* **51,** 1648–1658.

Yoon G-Y & Williams DR (2002). Visual performance after correcting the monochromatic and chromatic aberrations of the eye. *J Opt Soc Am A* **19,** 266–275.

Young T (1802). An account of some cases of the production of colours, not hitherto described. *Philos Trans R Soc London* **92,** 387–397.

Zernike F (1934). Beugungstheorie des Schneidenverfahrens und seiner verbesserten Form, der Phasenkontrastmethode. *Physica* **1,** 689–704.

Zhang XX, Bradley A & Thibos LN (1991). Achromatizing the human eye: the problem of chromatic parallax. *J Opt Soc Am A* **8,** 686–691.

Acknowledgments

Though only my name appears on the front cover of this thesis, many people have contributed to its completion. I am not only thankful for their help and support during my graduate experience, but also for turning it into a period I will always remember with pleasure.

First of all, I would like to express my sincere gratitude to my supervisor and mentor Pablo Artal. With the right mix of counsel and advice, but also space for my own ideas, he guided me through the years. I will always appreciate his support and encouragement which have contributed substantially to my growing as a scientist.

Obviously, a good leader is nothing without a great team and that is why the LOUM has to be mentioned. Special thanks goes to Silvestre Manzanera. His patience and accurateness make him probably one of the best teachers to learn from about optical system alignment and his even-tempered personality turns him into an even better colleague. Further, I am particularly grateful for the assistance given by Pedro Prieto. Plenty of times I was inspired by his analytical way of thinking and his enthusiasm for his work. I appreciate advice I received from Josua Fernández. His expert knowledge about optical system design was of great help to me many times.

I am also grateful to Juanma Bueno for his help with all the paperwork, especially in the past 2 months and when I first arrived in Murcia to get me enrolled in the Doctoral Program. Moreover, I am grateful to Luis Blanco for programming most of the software used in the binocular simulator and for continuously adjusting the vision tests to the different experiments and to Astrid Duque for her assistance with IT and paperwork whenever need was. Further, I would like to thank Esther Berrio for proofreading the Spanish part of this thesis.

The interesting discussions about spherical aberration and coma or economy and politics with Eloy Villegas and Antonio Benito during lunch are much appreciated. Thanks also goes to Bart Jaeken, Emmanuel Chirre, and Martin Skorsetz for the pleasant atmosphere in our shared “European” office. In addition, I would like to thank Juan Tabernero, Harilaos Ginis, Alexandros Pennos, Dimitrios Christaras, Augusto Arias, and Guillermo Perez together with the rest of the Voptica team for the good times we had during conferences, excursions, celebrations, long-lasting flights and the daily coffee break. Of course, this also includes past LOUM members such as Linda Lundström, Emilio Gualda, Ismael Kelly, Annie Giakoumaki, Encarna Alcón, Oscar del Barco, and Raquel Palacios, and frequent visitors like Eva Acosta, Carmen Cánovas and Alejandro Mira.

Most importantly, I owe a great debt of gratitude to all those who were willing to participate in the often long-lasting experiments with the binocular simulator. At the heart of this thesis lies the contribution of the subjects.

The months I spent at the Center for Visual Science in Rochester were very enriching. I am especially grateful to David Williams, Jesse Schallek, and Debbie Shannon and her family who treated me really well. I am looking forward to be back soon.

Furthermore, I am grateful to the Spanish “Ministerio de Ciencia e Innovación” for financial support in form of a FPI scholarship and grants FIS2010-14926 and CSD2007-00013, to the “Fundación Seneca”, Región de Murcia, Spain for grant 4524/GERM/06, and to the EU for EU-FEDER funds. Also, the companies AMO, Acufocus, and CIBA provided additional financing for parts of this thesis.

My gratitude to my family cannot be adequately expressed with words, so it remains to them to find the formula converting my simple ‘Thanks’ into what I feel. I would particularly like to thank my parents Gerda and Günther Schwarz for all the opportunities they provided me and their unconditional support throughout the years. Further, I would like to thank my sister and friend Nicole Schwarz for always lending an ear, an eye, or whatever is asked of her. Finally, I would like to offer special thanks to Hency Arévalo Silva for being a source of encouragement and support every single day.